Construction Scenes Point Cloud Acquisition, Object Finding and Clutter Removal in Real Time

by

Mohammad Mahdi Sharif

A thesis
presented to the University of Waterloo
in fulfillment of the
thesis requirement for the degree of
Master of Applied Science
in
Civil Engineering

Waterloo, Ontario, Canada, 2017

AUTHOR'S DECLARATION

This thesis consists of material all of which I authored or co-authored: see Statement of Contributions included in the thesis. This is a true copy of the thesis, including any required final revisions, as accepted by my examiners.

I understand that my thesis may be made electronically available to the public.

Statement of Contributions

This thesis is partially the product of collaborative research and co-authored publications as follows:

Chapter 2:

- Sharif, M., Nahangi, M., Haas, C., West, J., Ibrahim, M. (2016). "A preliminary investigation of the applicability of portable sensors for fabrication and installation control of industrial assemblies." Proc., Resilient Infrastructure, London, ON.

Chapter 3:

- Sharif, M., Nahangi, M. Haas, C. West, J. (2017), "Automated BIM-Based Finding of 3D Objects in Cluttered Construction Point Cloud Models", Journal of Computer-aided Civil and Infrastructure Engineering, under review.

Chapter 4:

- Sharif, M., Kwiatek, C. Jeanclos, N. Nahangi, M., Haas, C., West, J. (2017), "Optimal Nearest Neighbor Calculation for Automated Retrieval of Construction Elements from Cluttered Point Clouds." Proc., CSCE Resilient Infrastructure Conf., Vancouver, BC.

Abstract

Within industrial construction, piping can constitute up to 50% of the cost of a typical project. It has been shown that across the activities involved in pipe fabrication, pipe fitting has the highest impact on the critical path. The pipe fitter is responsible for interpreting the isometric drawing and then performing the tack welds on piping components so that the assembly complies with the design. Three main problems in doing this task are identified as: (1) reading and interpreting the isometric drawing is challenging and error prone for spatially complicated assemblies, (2) in assemblies with tight allowable tolerance, a number of iterations will take place to fit the pipes with compliance to the design. These iterations (rework) will remain unrecorded in the production process, and (3) no continuous measurement tool exists to let the fitter check his/her work in progress against the design information and acceptance specifications. Addressing these problems could substantially improve pipe fitters' productivity.

The objective of this research is to develop a software package integrating a threefold solution to simplify complex tasks involved in pipe fabrication: (1) making design information easier to understand, with the use of a tablet, 3D imaging device and an application software, (2) providing visual feedback on the correctness of fabrication between the design intent and the as-built state, and (3) providing frequent feedback on fabrication using a step-by-step assembly and control framework. The step-by-step framework will reduce the number of required iterations for the pipe fitter.

A number of challenges were encountered in order to provide a framework to make real time, visual and frequent feedback. For frequent and visual feedback, a real time 3D data acquisition tool with an acceptable level of accuracy should be adopted. This is due to the speed of fabrication in an industrial facility. The second challenge is to find the object of interest in real time, once a point cloud is acquired, and finally, once the object is found, to optimally remove points that are considered as clutter to improve the visual feedback for the pipe fitters.

To address the requirement for a reliable and real time acquisition tool, Chapter 3 explores the capabilities and limitations of low cost range cameras. A commercially available 3D imaging tool was utilized to measure its performance for real time point cloud acquisition. The device was used to inspect two pipe spools altered in size. The acquired point clouds were super-imposed on the BIM (Building Information Model) model of the pipe spools to measure the accuracy of the device. Chapter 4 adapts and examines a real time and automatic object finding algorithm to measure its performance with

respect to construction challenges. Then, a K-Nearest Neighbor (KNN) algorithm was employed to classify points as being clutter or corresponding to the object of interest. Chapter 5 investigates the effect of the threshold value “K” in the K-Nearest Neighbor algorithm and optimizing its value for an improved visual feedback.

As a result of the work described in this thesis, along with the work of two other master students and a co-op student, a software package was designed and developed. The software package takes advantage of the investigated real time point cloud acquisition device. While the object finding algorithm proved to be effective, a 3-point matching algorithm was used, as it was more intuitive for the users and took less time. The KNN algorithm was utilized to remove clutter points to provide more accurate visual feedback more accurate to the workers.

Acknowledgements

First and foremost, I would like to express my sincere appreciation to my advisors, Professors Carl Haas and Jeffrey West. I have been amazingly fortunate to have advisors who gave me the freedom to explore on my own and yet closely watching me in every step. Distinguished supervisors whose academic advice, encouragement, and unconditional support helped me step forward throughout my Master's.

I wish to express my sincere gratitude to Dr. Nahangi for all of his wonderful advice, support, and friendship, both academically and personally during my Masters. I would also like to thank Christopher Rausch, Thomas Czerniawski, Caroline Kwiatek, Nicolas Jeanclos and Shang Kun Li for their collaboration and helpful advice that improved my research.

It is my pleasure to thank members of our industrial partner Aecon Industrial, West, Scott Waters, Stacey Jenson Rose, Rob Bierman and Rick McEwen for their time and financial support.

My gratitude goes to all my dearest friends in Waterloo without whom my Master's journey would not have been filled with the wonderful times and enjoyable moments that we shared together. Last, but not least, my warmest gratitude goes to my family, and in particular to my wife, Fatemeh Keyvani. I would not be anywhere near where I am today without their love, support, sacrifice, guidance, and the opportunities they provided for me throughout my life.

Table of Contents

List of Figures

List of Tables

Chapter 1

1.1 Introduction

Industrial construction is categorized as one of the most expensive construction sectors and thus requiring rigorous project management tools and techniques. Industrial construction mostly refers to construction of petrochemical, oil and gas, power plants and manufacturing facilities. According to the U.S. Census Bureau (U.S Census Bureau News October 2014) $83 billion was spent in 2013 only on industrial power generation projects. All developed countries consider industrial construction as a primary sector in their economy. Across activities in industrial construction, piping can constitute up to 50% of the cost of a typical project. It has also been reported that rework costs between 2% and 20% of a construction project (CII 2011). In the context of piping, the 20% rework only accounts for the recorded rework and does not consider the iterations a pipe fitter or welder encounters in aligning the pipe with the design.

In order to reduce rework, rigorous and continuous inspections throughout the fabrication process have to be employed. Conventionally, pipe fitters and welders focus on doing good work. Once fabrication is completed, the quality control personnel are responsible to measure angular and translation errors to make sure the fabricated component is within tolerance. Development of a continuous measurement framework would have the potential to replace the current lagging process. Furthermore, manual direct contact measuring tools are currently being used, such as tapes and calipers. Utilization of such devices increases the subjectivity of the measurement as well as being error prone and time consuming.

Three dimensional (3D) imaging tools can potentially facilitate a solution for continuous, accurate, objective and non-disruptive measurements. These tools are capable of capturing points on surrounding surfaces. The technology employed to do so will determine the level of accuracy and required time to use the device. Currently, four main technologies for capturing the 3D information of surrounding surfaces exist: (1) laser scanning, (2) photogrammetry, (3) structured light sensing, and (4) 3D reconstruction using cameras with multiple focal length. While Laser scanning and photogrammetry have been employed for over a decade, structured light sensors and multiple focal length cameras have only been available since 2012. The main benefits of the recently developed technologies are their comparatively low cost and high speed of acquisition.

1.2 Problem statement

Of all the skilled trade work that affects an industrial construction's critical path, pipe fabrication is often the most complex and the most in need of rework (Goodrum et al. 2016). Design information is usually conveyed in the format of 2D isometric projections of the designed 3D BIM model, while a recent trend towards providing 3D drawings alongside the isometric projection is beginning to form. While improved information delivery reduces the probability of misinterpretation of a drawing, it does not address the need for a continuous quality control and measurement tool. Hence, engineers need a tool to keep track of the built status with respect to the design, accurately, objectively and in real time. Such a tool has the potential to be employed in industrial facilities to avoid errors in assemblies, which are costly rework scenarios.

Alternatively, recent advancements in 3D imaging, computer vision, computational geometry, augmented reality, information and workflow have enabled their users to access geometric information of the physical surrounding with an accuracy up to $\pm 1\ mm$. This improved control and awareness of 3D information can potentially reduce the risk of rework in tasks such as pipe fabrication and improve workers' productivity. However, lack of a real time framework has prevented these technologies from being further employed in this industry.

As discussed earlier, reducing rework and optimizing productivity in a fabrication and modularization environment could save industrial and commercial constructors up to 20% of the fabrication and construction labour costs. Furthermore, doing work right the first time and in the best way requires well trained workers, effective information delivery, feedback, and planning by developing a combination of innovative 3D imaging and analysis algorithms. These developments could be integrated with augmented reality tools to enhance effectiveness. This thesis is primarily focused on pipe fabrication within industrial construction. As a result of the envisioned solution, a pipe fitter will have a powerful tool that will overlay 3D scans of a work in progress with the 3D design of the work on his/her tablet computer in a way that will guide his/her next steps, help him/her avoid errors in fit ups and check tolerances. Implementation and integration of such technology raises important research questions.

In this thesis, three main questions towards the deployment of such technology in industrial construction and pipe spool fabrication in particular, are posed and investigated:

(1) How applicable are the new generation of portable scanners and what are their main benefits and limitations?

(2) Is utilization of a robust object finding algorithm feasible, given specific challenges existing in construction sites (i.e. occlusion, clutter and variations in point cloud density)?

(3) How to can the clutter points be removed without removing points belonging to the object of interest?

1.3 Thesis Structure

In Chapter 2, a thorough background study is presented on standard fabrication procedures in the piping industry. Then, different 3D imaging technologies and their application software are described. This thesis explores the applicability of recent portable 3D scanning sensors for real time assessments in Chapter 3. The next two chapters examine object finding and clutter removal algorithms, which are required post processing frameworks for these 3D scanners and devices to be employed in the industry. Chapter 6 is a summary of applications and limitations of the topics investigated in this thesis.

Chapter 2

Fabrication Processes and Technology Background

2.1 Pipe spool fabrication

Pipe spools are components of larger piping networks intended to carry water, steam, fluids, chemical gases, or fuel for industrial processes. Pipe spools are normally made in fabrication facilities, or fabrication shops, away from the construction site in a process that involves cutting, bending, forming, and fitting individual pipe components and finally welding them together. After the final quality check on the pipe spools they will then be shipped to the site.

Typically, 30% to 50% of the industrial construction work involves pipe spool fabrication. Each piping component is part of a larger assembly. A module constitutes from a number of assemblies which will be welded or bolted together at specific coordinates dictated by the design. Tight tolerances are usually stipulated to ensure that each pipe will fit within an assembly and assemblies meet each other at the designed location in modules. That is why within industrial construction, pipe fabrication is chosen as a primary focus of study in this thesis.

The next sections will explore the common practices in piping industry. (And how they will affect dimensional control frameworks). Figure 2-1 shows an overview of the next few sections.

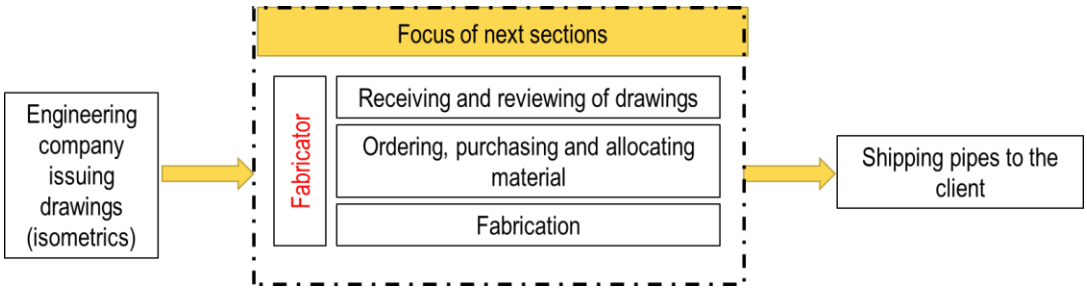

Figure 2-1. A general overview of the next sections

2.1.1 Receiving and reviewing drawings:

Piping scope is described and transmitted to contractors in the form of isometric drawings. In order to fabricate piping, contractors engage in a drafting process that manipulates the scope into manageable information pieces for pipe fabricators and welders and packages these pieces together with useful fabrication information on what are called cutsheets.

This process allows for:

- densely packaging fabrication-specific information onto a single drawing to facilitate the fabrication of a single unit of piping,
- fabrication of the largest possible pieces of piping that are able to be efficiently fabricated and transported,
- introduction of tracking elements (i.e. weld mapping) to enable progress and quality tracking,
- dictating (by choosing the endpoints / boundaries of spools) favorable locations for Yard Assembly Welds (YAW),
- removal of extraneous pipe assembly information from fabrication drawings that would otherwise clutter an already busy document, and
- a thorough review of piping scope for errors or discrepancies in the design.

2.1.2 Nomenclature

This section of the thesis will explore the common jargons used in the pipe fabrication industry.

ISO:

"ISO" is short for "isometrics," ISO's are not-to-scale symbolic line drawings that use isometric projection to represent the three-dimensional shape of the pipe on a two-dimensional drawing. Used in the context of pipe fabrication and assembly, isometric refers to the drawing itself, and not just the method of representation. ISOs are used in the module assembly yard or the project site to assemble spools into larger piping sections. As such, isometrics include information regarding the support of the piping sections. ISOs contain not only dimensions and orientations of the subject piping, but indicate the support and bolting materials required for the assembly as well (Figure 2-3). An example of a support component that is indicated only in the isometric (not in the cutsheets, described in the following section) is shown in Figure *2-2*. The shown component is referred to as "Shoe". An additional plate between the spool and the Shoe is welded. The purpose of the added plate is to avoid tearing of the spool in shear force.

Figure 2-2. Structural component, generally referred to as shoe.

Cutsheet:

The name "cutsheet" refers to cut lengths for individual pieces of straight pipes that are indicated on this drawing (the cut lengths required to fabricate the spool). Cutsheets are similar to isometrics in that they, too, are not-to-scale symbolic line drawings that use isometric projection to represent the three-dimensional shape of the pipe on a two-dimensional drawing. However, cutsheets are geared towards fabrication of pipe spools and not to assembly of pipe spools into larger pipe sections and their installation into a module or plant. As such, information required for assembly and installation, such as bolting and support material and location information are omitted. Instead, information that is useful to fabrication (typically in the shop), such as cut lengths of pipe required for fabrication, and labelling of welds (used for tracking and identification) are added. A single isometric may not necessarily correspond to a single cutsheet. Figure 2-3, Figure 2-4 and Figure 2-5 show examples of different combinations of isometric(s) and corresponding cutsheet(s).

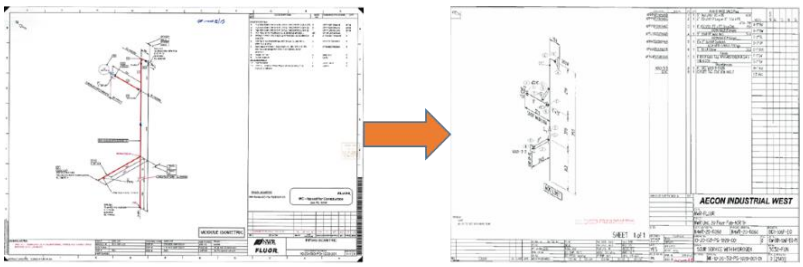

Figure 2-3. Single isometric translated to a single cutsheet. (a) Received isometric from engineering company. (b) Produced cutsheet for fabrication (refer to Appendix C for lager images)

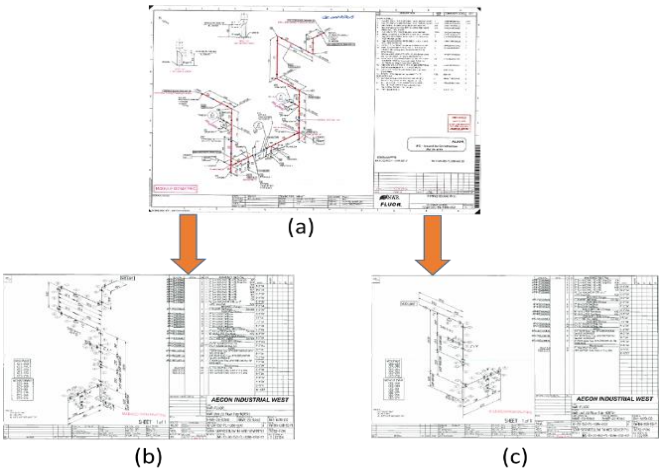

Figure 2-4. Single isometric translated to multiple cutsheets. (a) Isometric drawing. (b) and (c) cutsheets derived from a single isometric drawing (refer to Appendix C for lager images).

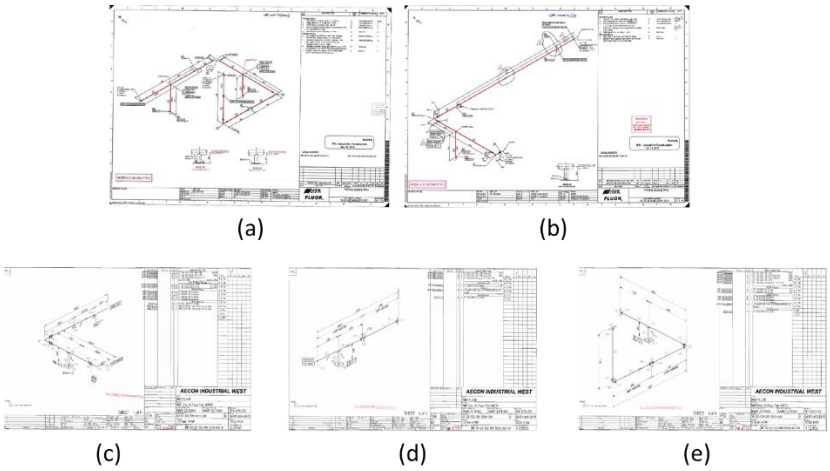

Figure 2-5. Multiple isometrics translated to multiple cutsheets. (a) and (b) isometric drawings of an assembly. (c), (d) and (e) cutsheets derived from the corresponding isometrics (refer to Appendix C for lager images).

Fab Weld:

Abbreviation for "fabrication weld," a fab weld is a weld performed in the pipe fabrication facility. Not to be confused with "field Weld," (abbreviated "FW") which is a weld performed at the construction site.

YAW:

Abbreviation for "Yard Assembly Weld," a yard assembly weld is a weld performed in the module assembly yard.

2.1.3 Workflow from design to fabrication and shipping:

Figure 2-6 shows an example a workflow starting from the design and finishing with the fabrication. The details of this workflow may vary depending on the nature of the project and client's request.

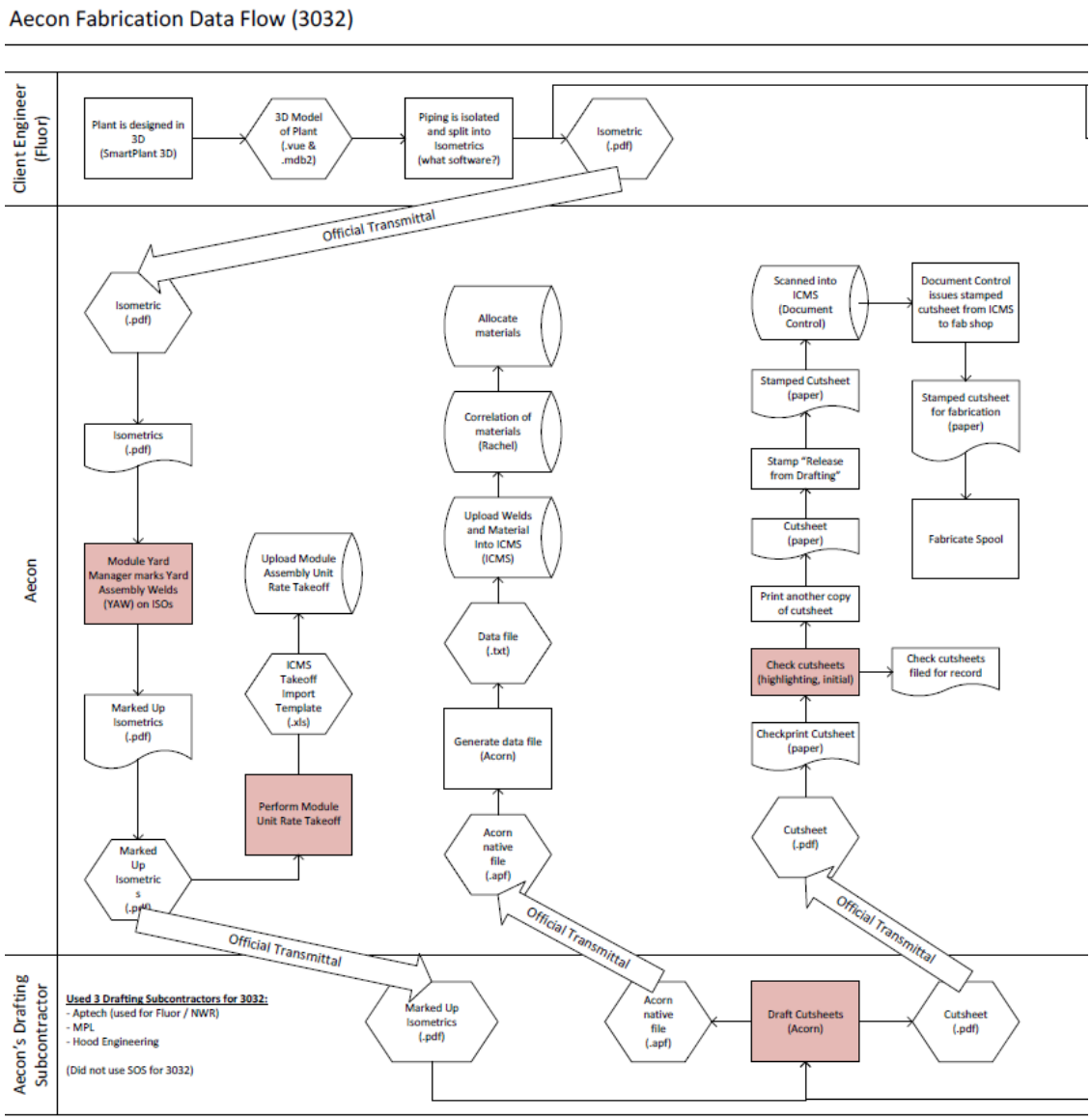

Figure 2-6. An example workflow from design to fabrication (larger image found in Appendix C).

Official transmittal is a package including design files that are transferred from the engineering company to the contractor (Figure 2-8). Once the design files (isometric drawings) are received from the engineering company (in this case, Fluor) the drafting group has to review the documents. The reviewing process includes number of tasks; such as: (1) making sure all of the dimensions are legible and correct, (2) making sure that the grading used for the pipe material is either available in inventory

or in the market (some materials may be out of stock for periods of time) and, (3) all of the site specific conditions have been taken into the account in the design drawings. A Request for Information will be issue if any of the above conditions are not met. (Figure 2-9). Figure 2-7 also shows an example for the plan view of a physical workflow in the fabrication facility.

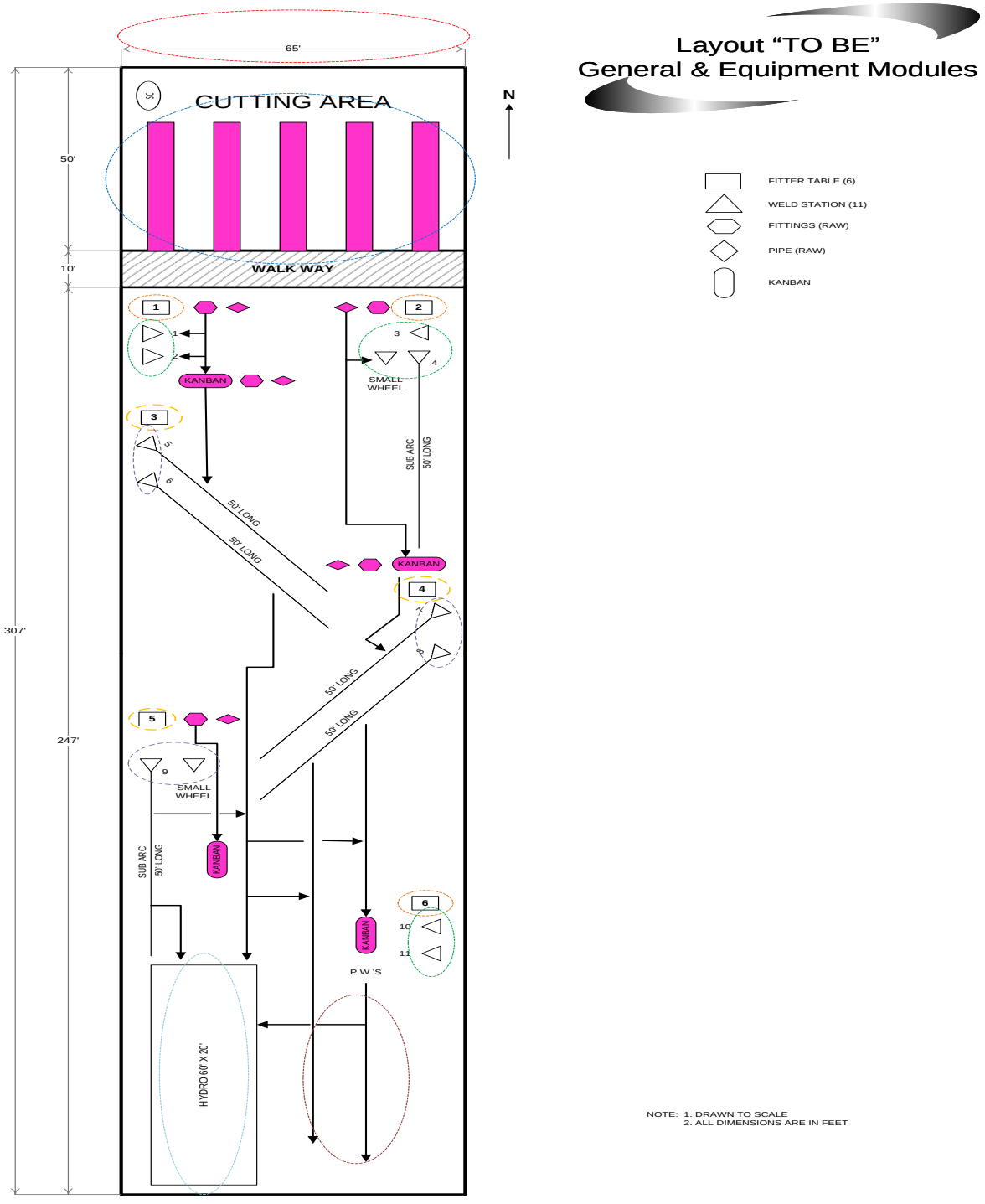

Figure 2-7. An example of a physical work flow inside of a fabrication facility.

FLUOR

Fluor Canada Ltd.
55 Sunpark Plaza SE
Canada, T2X 3R4

CONTRACTOR DOCUMENT TRANSMITTAL
Transmittal No: N4WR-K060-T-00309
Transmittal Date: 06-APR-2016

TO: N4WR-K060
AECON INDUSTRIAL WESTERN
7433 Harwin Houston TX 77036 7433 Harwin

Project Name: NWR PROJECT
Project No: 00NWR00
Authority: Thomas Rabb

ATTN: Houston
Description: **NRWR - K060 - AECON - FIELD REVISION - 1 PIPING ISOMENTRIC ISSUED FOR INFORMATION - FYI**

Issue Status: RE-IFC - Field Revision

Remarks:

Attached please find the following:

FLUOR DOC NO/REV	CLIENT DOC NO	STATUS	TITLE	SUPPLIER DOC NO/REV
10-20-ISO-PG-1013-001/F0-0		RE-IFC	PIPING ISOMETRIC - DRAWING LINE NUMBER 12-PG-1013-2 INCHES-ACA3-F	/

To:

Recipient	Company-Dept	POL	TRANS
AECON	N4WR-K060	1	

Fluor For Information:

Recipient	Company-Dept	POL	TRANS
Carlo Rebibis	FLUOR	1	
Dave Arthurs	FLUOR	1	
Jason Caines	FLUOR	1	
Micah Stewart	FLUOR	1	

Client For Information:

Recipient	Company-Dept	POL	TRANS

Transmittal issued by: Hermeen Kaur

Please acknowledge receipt of the above documents on behalf of the above listed Company by signing below and returning one copy of this transmittal form to Fluor PDDM.

Received By:_____ _____ Date: _____
(signature) (printed name)

Contractor signature on the Document Transmittal indicates acceptance of the work package and a commitment to work within the direct labor budget and the schedule contained therein. If Contractor believes that the budget or schedule is insufficient, Contractor will notify Company within 5 days with a proposed revision to same.

Contractor is responsible for previous CWP/documents revision disposal, maintenance and tracking of the latest revisions for the work and files.

06-Apr-2016 GT642_CONSOLIDATED_SUBCONT.REP Page 1

Figure 2-8. Official transmittal.

Stantec

APCDN

Engineering Work Directive (EWD)
EWD-CDH III-ME-0005

Client: Pembina Marketing Limited
Project #: 117202038
EWD #: EWD-CDH III-ME-0005
Originator: Burton Xu
# of Pages: 1
Date: 11/03/2016

Document(s) requiring change	Rev #	Title
EWP 4/5 Drawings	Rev. 0	Piping/Mechanical Package – Sept 1, 2016
EWP 4/5 Drawings	Rev. 1	Piping/Mechanical Package – Sept 29, 2016

Subject: Pipe Material Substitution

Description of required change

This EWD is being issued to formally capture substitution of pipe materials.

1. Due to the unavailability of the specified pipe material from pipe vendor, some API 5L pipe were purchased to substitute CSA Z245.1 pipe listed in the mentioned IFC packages.
2. These items have been addressed in the RFI-AIW-F0012 and RFI-AIW-F0013.

Supplier(s) or contractor(s) required to execute change

1. Below please find the summary of the pipe material substitution:

S/N	MTO in EWP package 4/5 to be substituted	Materials have been purchased
1	PIPE, NPS 20, 9.5 [illegible] WT, CSA Z245.1, GR. 359 CAT. II	PIPE, SEAM, NPS 20, 9.53mm WT, API 5L X52, PSL2, PE, DRL, BASE MATERIAL CVN @ -45C AS PER CSA Z662
2	PIPE, NPS 24, 12.7mm WT, CSA Z245.1, GR. 359 CAT. II	PIPE, ERW, NPS 24, 12.7mm WT, API 5L X52, PSL2, PE, DRL, BASE MATERIAL CVN @ -45C AS PER CSA Z662
3	PIPE, NPS 24, 9.5 [illegible] WT, CSA Z245.1, GR. 359 CAT. II	PIPE, ERW, NPS 24, 9.53mm WT, API 5L X52, PSL2, PE, DRL, BASE MATERIAL CVN @ -45C AS PER CSA Z662
4	PIPE, NPS 24, 12.7mm WT, CSA Z245.1, GR. 359 CAT. II (Yieldet)	PIPE, ERW, NPS 24, 12.7mm WT, API 5L X52, PSL2, PE, DRL, BASE MATERIAL CVN @ -45C AS PER CSA Z662 (Yieldet)
5	PIPE, NPS 30, 6.53mm WT, CSA Z245.1, GR. 359 CAT. II (Yieldet)	PIPE, SEAM, NPS 30, 6.5 [illegible] WT, API 5L X52, PSL2, PE, DRL, BASE MATERIAL CVN @ -45C AS PER CSA Z662 (Yieldet)
6	PIPE, NPS 20, 12.7mm WT, CSA Z245.1, GR. 359 CAT. II	PIPE, SEAM, NPS 20, 12.7 mm WT, API 5L X52, PSL2 / CSA GI 40E CDN @ -45C AS PER CSA Z662

Approval for EWD Issue

		Authentication
Responsible Engineer	Print name: Burton Xu Signature: [signature] Date: Nov 3, 2016	PROFESSIONAL ENGINEER ALBERTA BURTON XU Nov 3, 2016
Project Engineer	Print name: [illegible] Signature: [signature] Date: Nov 3, 2016	

Figure 2-9. An issued RFI.

After taking all the necessary measures to make sure the design drawings are correct, the drafting group will convert the isometric drawings to the cutsheets and cut-lengths. Two virtually parallel activities will begin once the cut-lengths and cutsheets are issued: (1) material allocation, and (2) fabrication.

Material allocation:

Once the cut-lengths are issued the material allocation will take place. The process starts with checking the inventory to see if the spool with the specified grading is available at the facility's inventory. If the spool with the specified grading does not exist, the company has to make a purchase order and purchase the specified pipe spool. Once the spool arrives at the site it will be picked by the yard's crane (Figure 2-10) and will be placed at the outside pipe racks. The pipes will be then pushed on the trollies entering the fabrication shop (Figure 2-11). The operator at the Vernon machine has access to the cut lengths and will cut each spool to the designed length and places them in the pipe racks inside the fabrication facility (Figure 2-12). Each pipe fitter will then pick up the pipe spool which he or she is assigned for the fitting and fabrication.

Figure 2-10. Delivered material will be picked by onsite crane and placed on the racks.

Figure 2-11. Pipes will be pushed on the trolley, entering the shop.

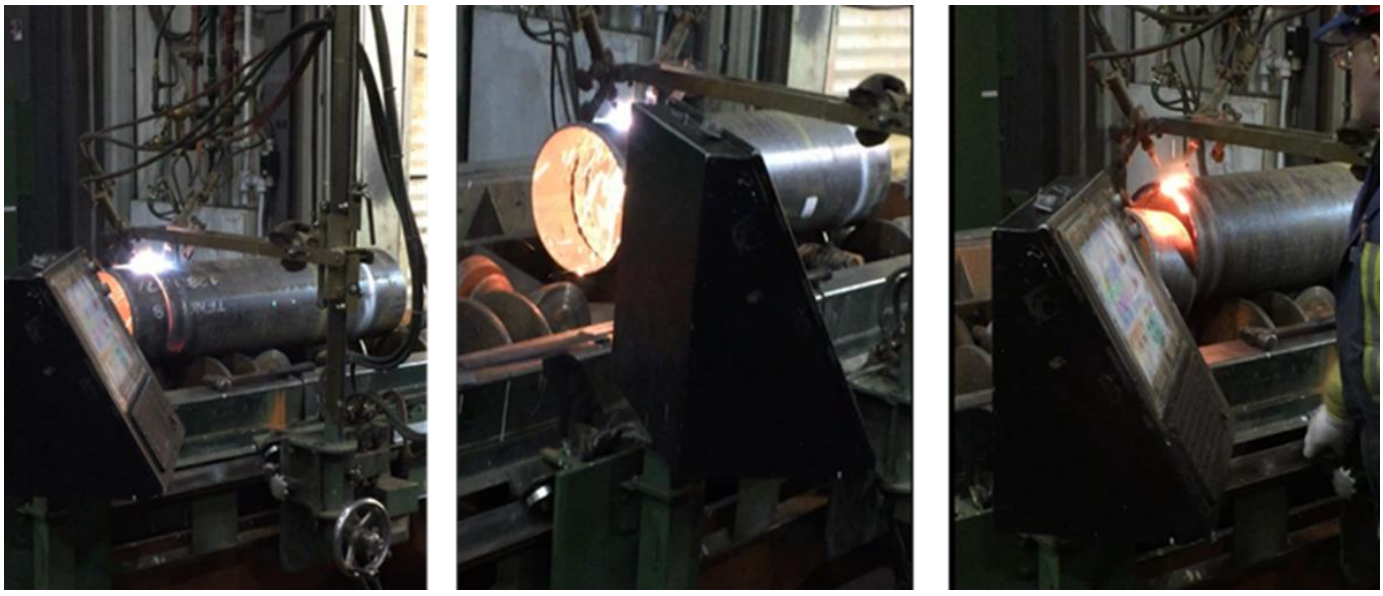

Figure 2-12. Pipe spools will be cut based on the issued cut-length and placed on the wrack for fabrication.

Fabrication:

Once the cutsheets are released from the drafting group the general foreman at the facility has to properly distribute the drawings amongst the fitters and welders. Each welder has a welding ticket which will specifically dictate what kind of weld he is allowed to perform. Also, each bay in the shop is designed for a specific pipe spool diameter. The proper distribution corresponds to accurately assigning jobs to welders and fitters. (Figure 2-13)

Figure 2-13. Distribution of drawings by the general foreman

Normally, fitters are responsible for interpreting the cutsheets and performing the tack welds according to the drawing(s). Once a tack weld is performed by the fitter, the spool will be shipped to the welding station for welding. One of the main tasks of fitters is to maximize the number of roll welds. Roll welds are welds in which the spool is rotating in a machine where the speed of the rotation is controlled by the welder. Roll welds have a better quality and take an order of magnitude less time to complete. (Figure 2-14)

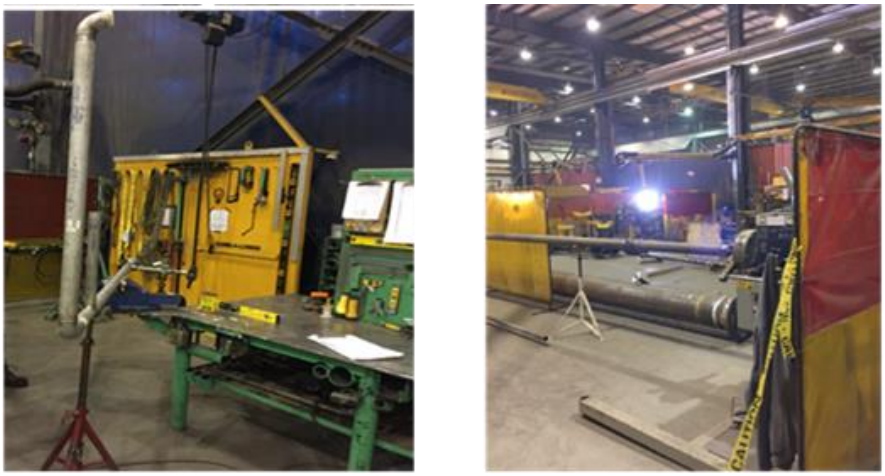

a b

Figure 2-14. (a) Fitting and (b) welding station.

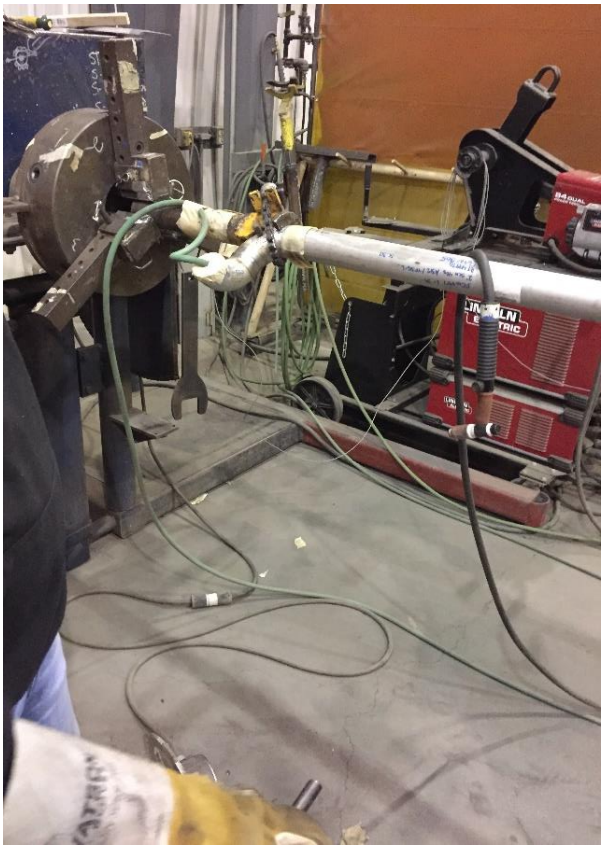

Figure 2-15. Roll welding.

a b

Figure 2-16. Tack weld vs. roll weld. (a) The fitter tack welds the flange to stabilize its location, orientation and angel. (b) A complete roll weld done by the welder.

Once the assembly is complete the quality control personnel will inspect the assembly. The person responsible for quality control will measure and compare all of the lengths and angles with respect to the drawings. He/She will also control the material and grading of the spool. Assemblies may or may not require hydro tests which will be the last test before the shipping. After confirmation of all the tests the spools will be picked up by the shop's crane and will be placed on the shipping truck to be transported to the site. (Figure 2-17). The quality control person responsible has to fill an NCR (Non Compliance Report) where a deviation from the design has occurred. (Figure 2-18 to 2-21). One of the main shortcomings of the current measures for detecting rework is the fact that the iteration a fitter takes to assemble a spool is not being taken into account. This means only mistakes that the fitter remains unaware of, will be recorded as rework in the format of NCR logs.

Figure 2-17. Spool ready to be shipped out.

AECON

EX015

NON-CONFORMANCE REPORT (NCR)

☒Shop ☐Field Comll:

ISSUED TO: Aecon FAB Shop	NCR No.: 3032-F01-NCR-021
DEPT / PLANT / LOCATION: SWP FAB SHOP	DATE: 28 OCT 15
TAG No / LINE No.: 10-20-ISO-PL-3259-002	JOB NO.: 3032-F01- Fluor/NWR Unit 20

DESCRIPTION OF NONCONFORMANCE:

Orifice flange on SCN 60085 installed incorrectly, tap installed North 45 deg down, and not South 45 deg down as required per Isometric

RECOMMENDED ACTION: ☐ SCRAP ☐ REWORK ☒ USE AS IS ☐ RETURN

ROOT CAUSE	INSPECTOR	SIGNATURE	DATE
Misinterpretation of detail	Tammy Murphy	TMurphy	28 OCT 15

PROPOSED DISPOSITION (Completed by addressee)
The spool containing the counterpart to this orifice flange has not yet been fabricated (SCN 60084). Aecon proposes, to avoid the risk of damage to the flange during rework, to leave spool 60085 as is, and revise the cut sheet for spool 60084 to show the tap at South 45 deg down, which would avoid interference with the tap on 60085.

NAME: Tammy Murphy SIGNATURE: TMurphy DATE: 28 OCT 15

ACCEPTANCE OF PROPOSAL

CLIENT APPROVAL: ☒ YES ☐ NO AUTHORIZED INSPECTOR: ☐ YES ☒ NO

	SIGNATURE	PRINT	DATE
Q.C REPRESENTATIVE:	TMurphy	Tammy Murphy	28 OCT 15
Fluor Representative:			23 Nov 2015
NWR Representative:		BRIAN McCARVEY	NOV 23/2015

COMPLETION OF DISPOSITION (ACTION COMPLETED):

Spool 60085 use as is

	INSPECTOR:	PRINT:	DATE:
COMPLETED:	TMurphy	Tammy Murphy	23-NOV-2015

FINAL SIGN OFF	SIGNATURE	PRINT	DATE
Q.C REPRESENTATIVE:	TMurphy	Tammy Murphy	23-NOV-2015
Fluor Representative:			NOV 23/2015
NWR Representative:		BRIAN McCARVEY	NOV 23/2015
DESIGN ENGINEER: (If applicable)	N/A	N/A	N/A

Revision 3
June 18, 2013

Page 1 of 1

Figure 2-18. NCR Log Page 1.

Re: 3032-F01-NCR-021
Dave Arthurs to: Dwayne Faulkner, Bernie Knierim 11/23/2015 01:26 PM

Dwayne / Bernie -

There is no impact on instrumentation functionality of the flange taps are on north or south side in orientation provided we have one tap on the upstream (high pressure) side of the orifice plate and one tap on the downstream (low pressure) side of the orifice plate. Additionally in this instance, the taps should be below horizontal per standard installation in liquid service.

I recommend moving forward with the proposed solution to the NCR to have the tap on spool 60084 located South at 45° down.

Cheers
Dave Arthurs, C.E.T., B.Mus | FLUOR CANADA LTD. | Senior Designer / Field Engineer – Control Systems |
dave.arthurs@fluor.com | IODC 40.4870 | Phone: +1.(780).640.2853 ext/ 5032 | www.fluor.com

Dwayne Faulkner Dave, As discussed prior, please see the attach... 11/23/2015 01:14:32 PM

From: Dwayne Faulkner/CA/Contr/FluorCorp
To: Dave Arthurs/CA/FD/FluorCorp@FluorCorp,
Date: 11/23/2015 01:14 PM
Subject: 3032-F01-NCR-021

Dave,
As discussed prior, please see the attached NCR for your review of the proposed disposition.

Regards
Dwayne Faulkner | FLUOR CANADA LTD. | QA, Mod Yard – NWR Project |

Dwayne.Faulkner@fluorconstructors.com | Cell Phone 780.446-4334 3032-F01-NCR-021.pdf

Figure 2-19. NCR Log Page 2.

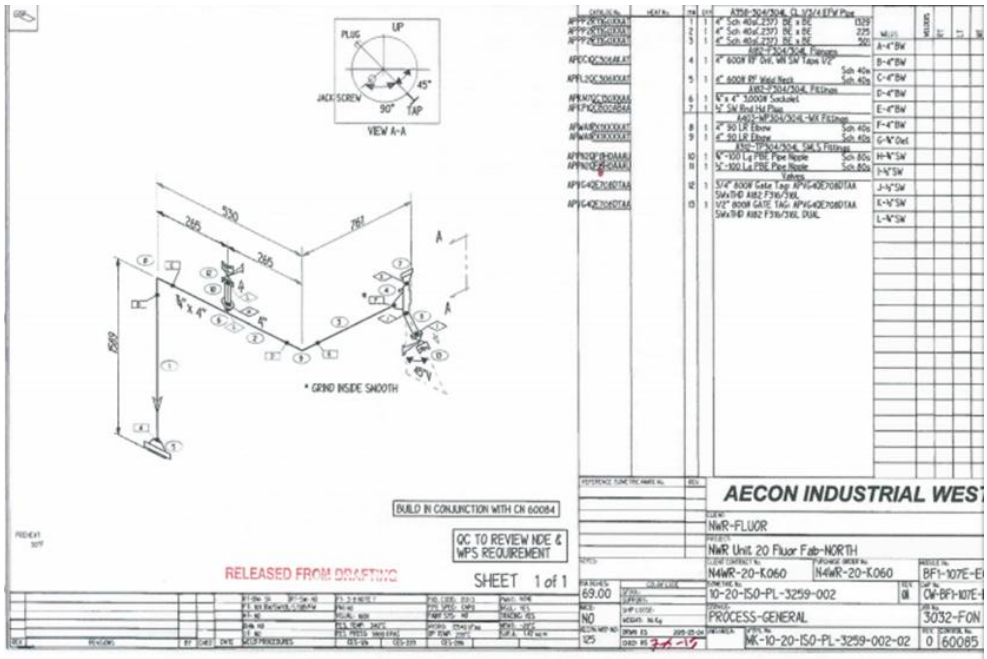

Figure 2-20. NCR Log Page 3.

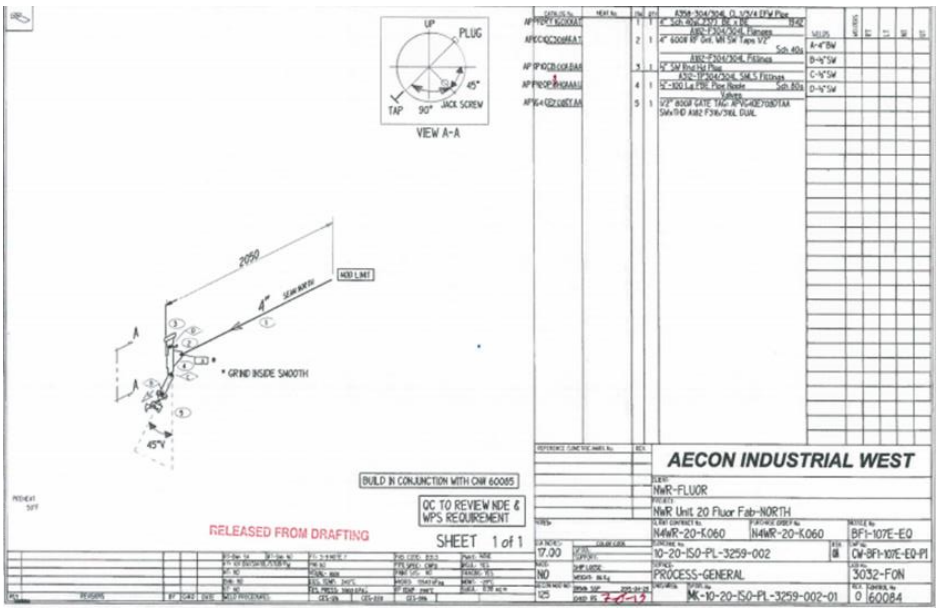

Figure 2-21. NCR Log Page 4.

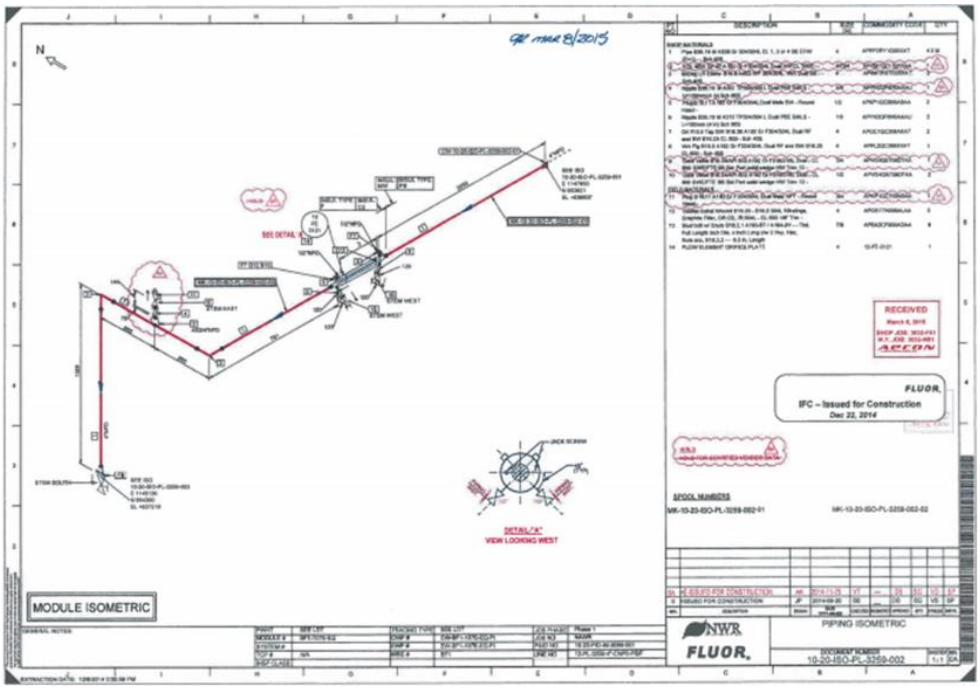

Figure 2-22. NCR Log Page 5.

2.2 Data acquisition tools and techniques

Various technologies are used in 3D scanning devices, and each technology has its own limitations, advantages and cost. This section will explore different methods of scanning and the technologies associated with each one. The four primary technologies are: (1) photogrammetry, (2) laser scanning,

(3) structured light, and (4) multiple focal length. The next 4 sub-sections are a detailed overview of each of these technologies.

2.2.1 Photogrammetry

To get measurements of surface points, the very first technique scientists came up with was photogrammetry (Burtch 2004), which emerged in the mid-nineteenth century. Photogrammetry is the science of measuring surface points and recovering coordination of points (ASPRS 2007). Based on the American Society for Photogrammetry and Remote Sensing (ASPRS) definition, photogrammetry and remote sensing are the art, science, and technology of obtaining reliable information about objects and the environment through processes of recording, measuring and interpreting photographic images and patterns of recorded radiant electromagnetic energy and other phenomena. Two main types of photogrammetry exists: (1) aerial photogrammetry and (2) close-range or stereo photogrammetry.

1. Aerial Photogrammetry: in this method the camera is vertically towards the ground mounted on an aircraft (drone) capturing multiple overlapping photos while the aircraft is flying on a certain path. Photos are then processed in a stereo-plotter where it lets an operator see two photos at once in a stereo view. Photos taken with this method are usually used in creation of digital elevation models and topographical maps.

2. Close-range or stereo photogrammetry: using this type of photogrammetry one is capable of acquiring point clouds using 2D images taken by a camera with known parameters. In machine vision and computer science literature, the word photogrammetry and stereo photogrammetry are used interchangeably. To get an accurate point cloud using this method usually one has to use a tripod and has to stay close enough to the object of interest. To reconstruct a point cloud of a certain object, at least two images has to be taken from the object. The common features between corresponding images are detected and using the relative position of the camera to the images a point cloud will be reconstructed. Researchers have worked on methods to more accurately and reliably detect points in the two corresponding frames (Balali et al. 2015).

One of the main advantages of photogrammetry is its lower cost compared to laser scanning. Another advantage of the photogrammetry is its integration with drones. Currently numerous research focus has been dedicated to the use of drones utilizing photogrammetry on construction sites. Drones are being used for quality inspection (Wang et al. 2015), safety inspection (Irizarry et al. 2012), field survey (Barry and 3D as built modeling (Fathi et al. 2015). Furthermore, in addition to the use of photogrammetry in drones, another important aspect of photogrammetry is their use in machine vision and robotic manipulation. Vision based control in robotics (Chaumette and Hutchinson 2006), intelligent surveillance (Guo et al. 2013) and object detection and mapping using SIFT (Scale Invariant

Feature Transform), SURF (Speeded-Up Robust Features) and LIFT (Learning Invariant Feature Transform) are only a few applications of photogrammetry in the machine vision's body of knowledge (Allaire et al. 2008, Knopp et al. 2010 and Huang et al. 2007). However, Photogrammetry can be time consuming and inaccurate in comparison with the data collected with laser scanners (Tang et al. 2010). For more accurate photogrammetry high resolution cameras should be utilized and multiple images of the inspected scene should be captured. Having to do so, the cost will rapidly increase and also the manipulation of massive data will become challenging. As such, photogrammetry will not be the primary source of acquiring 3D geometric data in this thesis.

2.2.2 Laser Scanning

The next subject to be discussed in this literature review is laser scanning. The recent developments of laser scanning technology has made the creation of as-built BIMs increasingly feasible (Tang et al. 2010). In order to have a reliable point cloud with less time than the processes employed within photogrammetry, the use of laser scanners is continuing to be further developed within construction. Laser scanners are already widely used, and function as a versatile tool for 3D geometric data acquisition. With the help of a sensor, a laser scanner measures the distances to points being scanned at speeds up to thousands of points per second and can achieve an accuracy at the millimeters to centimeter level (Staiger 2003). Phase shift and time of flight are the two main technologies being used in this industry.

1. Time of Flight: in this method the distance between an object to the laser scanner is obtained using the time that it takes for a laser beam from the moment that it has been shot out to the moment that it comes back. Having this time and the constant for the speed of the laser beam distances of points in the scene to the scanner will be calculated and recorded. Moreover, to compute [X,Y,Z] positions of a point, both horizontal and vertical angles have to continually change. This is accomplished by the scanner moving in a grid of 360 degrees in the horizontal plane and 330 degrees in the vertical plane. Needless to say, it takes time for the scanner's lens shoot all of this coordinates in space which is why the time of flight method has been known to be more time consuming than phased-base technology.

2. Phase shift: in this method the scanner has a constant beam of energy. By calculating the phase shift between the outgoing wave and the incoming wave it calculates the distance between a point and the sensor. In this method, it is possible to obtain points faster in comparison with the time of flight method, however its range is limited to 80 meters. Studies have also shown that time of flight scanners can achieve higher accuracies (San José Alonso et al. 2011).

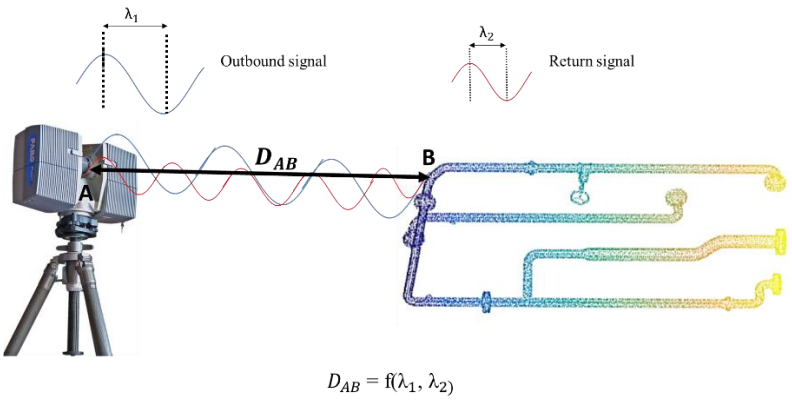

Figure 1: Comparison of Time of Flight and Phased Based Laser Scanning Technology

2.2.3 Structured-Light

A structured-light 3D scanner is a device for measuring the three-dimensional shape of an object using projected light patterns (infrared light in Microsoft Kinect and Structure IO) and a camera system (Furht, Ahson 2008). An infrared (IR) projector and one sensor within a certain distance of the projector. The projector projects speckle patterns on the objects and the sensor calculates the distance of a point to itself. In order to use triangulation, two separate images have to be captured (Figure 2-23).

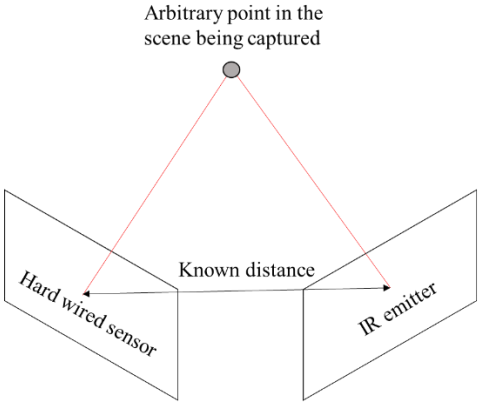

Figure 2-23. Triangulation used in structured light sensors

In terms of accuracy, the support group of Structure IO (one of the commercially available scanners, which uses structured light technology (Structure IO 2015) claims that the device can achieve an accuracy of 1% of distance measured. Since the accuracy of structured-light sensors (Figure 2-24) are significantly less than those of laser scanners (a FARO LS laser scanner can achieve an accuracy of 2

mm up to distances of 30 m (FARO 2014)), the error involved with 3D geometric data acquisition will be a focal point of study in the second chapter of this thesis.

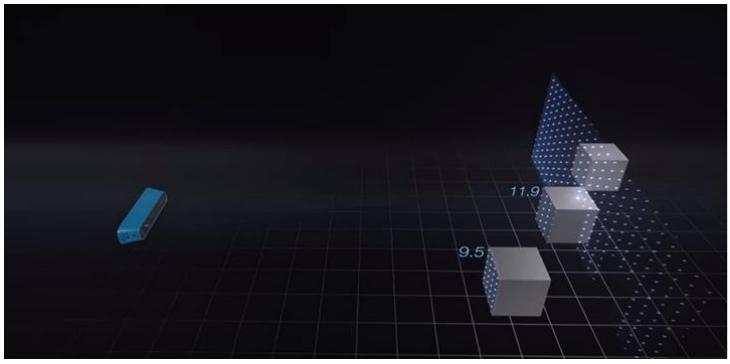

Figure 2-24. Speckle pattern used in structured light technology (Structure IO 2015)

2.2.4 Multiple focal length

As discussed earlier, Photogrammetry uses the mathematics of light rays to build up knowledge of the geometry of the scene. Regardless of the software used for reconstruction, the fundamental parameters of the camera would help to build up the correct geometric characteristics of the scene and the relative position of the camera to the scene. One of the key parameters is the focal length of the camera. The focal length of a lens will determine the magnitude and the angle of the light ray. A long focal length will have the light rays hit the image sensor at a shallower angles. In contrast to a long focal length, a short focal length will cover a larger field of view.

With advancements in photography technologies, cameras with multiple lenses and each lens with its own specific focal length are becoming available. This means instead of capturing one single image with a large lens, one can capture multiple images and then fuse those images to have one high quality image. This technology uses mirrors to adjust the camera modules to frame overlapping images over the field of view. This will allow to gather more light than a traditional camera. By assigning different exposures to different modules a very high dynamic range is achieved. Using multiple lenses will allow to capture images in 3D and would also allow to adjust the focal plane and the depth of focal length (Light 2016, Phtomodeler 2013).

2.3 Application Summary

In summary, as part of the research conducted in this thesis and also two other master students and a co-op student, an application software was developed. The application software aims to reduce risk of: (1) miscommunication of design information, (2) excessive fitting iterations, (3) assemblies being out

of tolerance, and (4) modules not fitting at the designed locations. The developed software takes advantage of 2-sided ISOs to improve communication of design information and using 3D imaging and augmented reality devices to provide frequent feedback on fabrication. The process starts with the worker scanning the as-built component. Once the scan is acquired, the scanned point cloud has to be superimposed on the 3D design (model) point cloud. The final step is to check if the assembly is compliant or not. Figure 2-25 summarizes the designed process and how it influences the research conducted in this thesis.

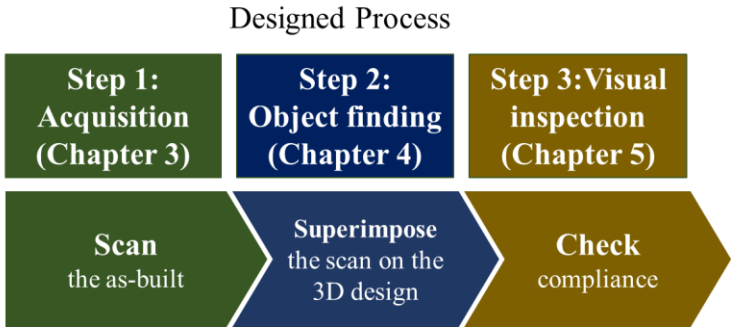

Figure 2-25. The designed process for the software and its correlation with the contents of this thesis

Chapter 3

A Preliminary Investigation of the Applicability of Portable Sensors for Fabrication and Installation Control of Industrial Assemblies

This chapter is based on the following published article in the proceedings of CSCE's Resilient Infrastructure 2016, London, Ontario, with the same title. Minor changes are made on some parts of the article to be more consistent with the body of the thesis. Thus, the content of this chapter is not exactly the same as the paper.

The contribution of the author in this publication is conducting the experiments, data analysis and drafting and partially editing the manuscript.

3.1 Introduction

Industrial construction comprises 10% to 20% of construction spending in Canada and U.S (U.S Census Bureau News October 2014). Typically, 30% to 50% of the industrial construction work involves pipe spool fabrication. Due to the complexity of pipe fitting, pipe fitters have a high impact on the critical path (Goodrum et al. 2016). In order to improve productivity and reduce additional cost in industrial construction, off-site fabrication is beneficial. Moreover, off-site fabrication is normally less expensive, safer, and more sustainable, and results in higher quality fabrication in comparison to on-site construction. These advantages result from the controlled conditions, more accurate quality control, and reduced construction waste possible when working offsite (Haas, Fagerlund 2002). For these reasons, modularization and industrial fabrication has become a part of growing trend towards off-site fabrication (Han et al. 2012).

Generally, 54% of total construction defects are due to human factors such as craft worker insufficient skill, or supervisor error (Opfer 1999). The improved quality control and productivity of modularization is a potential solution to reduce such defects. However, inevitable defects experienced during modular construction are costly and time consuming to repair (Akinci et al. 2006a). Additionally, 10% to 20% extra structural material is typically used to stiffen and strengthen modules for transportation and handling and loading, nevertheless damage and geometric defects may still occur which leads to rework. The aforementioned statistics emphasizes the importance of proper and time efficient defect detection in modular construction. Furthermore, it has been reported that 6% to 12% of construction cost is because of rework caused by defects detected late (Burati Jr et al. 1992). In addition to the previous statistics, approximately 15% of construction waste is caused by late detection of defective components in either the construction or maintenance phase (Yue et al. 2006). In conclusion, these

statistics indicate the importance of proper, timely and reliable defect detection and the importance of integrated frameworks that can detect such defects efficiently and timely.

In order to overcome the challenges involved with the detection and prevention of fabrication defects, various approaches have been taken. 3D imaging has been found an effective tool for capturing the as-built status of construction components. However, continuous, accurate and cost efficient data acquisition in off-site fabrication facilities and on construction sites is required to effectively use this information as part of a quality control process. Additional practical applications of laser-scanning technology have been introduced, such as automated progress tracking, safety planning, and realignment planning (Nahangi et al. 2014). Real time processing of the acquired laser scans is a challenge that still needs to be addressed for all of these applications. This challenge is due to the preprocessing steps that need to be performed in order to generate reliable 3D point clouds.

Although various frameworks have been developed in order to reduce rework, an improved method for real-time data acquisition integration is still necessary. This study is conducted to examine the applicability of recently commercialized sensors in order to address the challenges of real-time data acquisition. The challenges and opportunities of using such sensors in the off-site fabrication of pipe spools was investigated. The key objective of this chapter is to use structured-light-based sensors to identify the challenge and developing an integrated framework for defect detection, in a time-effective framework.

3.2 Background

A range of diverse applications of 3D imaging in construction have been proposed. Some key applications in construction using 3D imaging include: progress tracking (Turkan et al. 2012a), automated inspection and material tracking (Bosché 2010, Memarzadeh et al. 2013, Yang et al. 2010), safety (Chi and Caldas 2011), motion tracking (Brostow et al. 2008), and structural health monitoring, such as concrete crack depth assessment (Liu, Cho et al. 2014).

Various methods have been investigated to assess the as-built status of construction projects. Abourizk (AbouRizk 2010) introduced visualization and simulation for reducing rework and optimizing project costs. In an effort to reduce cost and improving the required time for accurate data acquisition, researchers have also investigated using unmanned aerial vehicles (UAV's) for monitoring the built environment (Ham et al. 2016). Other researchers have focused on the potential of using static overlaying between the as-built and as-designed states for project control. This approach requires point cloud registration between the as-built and as-designed states. For instance, Yue et al. overlaid a design model of a facility with the as-built point cloud to identify which data points belong to a specific object

and to detect the deviations between the as-built and as-designed conditions (Yue et al. 2006). Moreover, 3D imaging has been used to automate continuous quality assessment of fabricated assemblies with different approaches such as ICP (iterative closest point) for robust point cloud registration, or skeleton-based registration for discrepancy detection (Nahangi and Haas et al. 2016, Nahangi and Haas et al. 2014). 3D imaging using laser scanning technology has also been used for the creation of as-built building information models (BIM) (Tang et al. 2010).

In summary, for reducing the cost and avoiding delays on construction projects, especially in industrial construction, it is crucial to detect defects in a timely and costly efficient manner. To address this challenge, different approaches have been studied, such as visualization and 3D imaging. The research described in this chapter investigates the use of recently commercialized sensors for real-time geometric data acquisition, and analysis to allow reliable detection and quantification of misalignments. In this chapter of this thesis, as-built 3D point clouds were obtained using a structured-light-based sensor (Structure IO).

3.3 Methodology

In this section, the key steps of the proposed method for real-time defect detection are explained. Figure 2-1 shows the sequence of steps and the flow of information for the proposed method. The method compares the real-time scanned data for a pipe assembly and registers the 3D point cloud with the as-designed state integrated in the BIM.

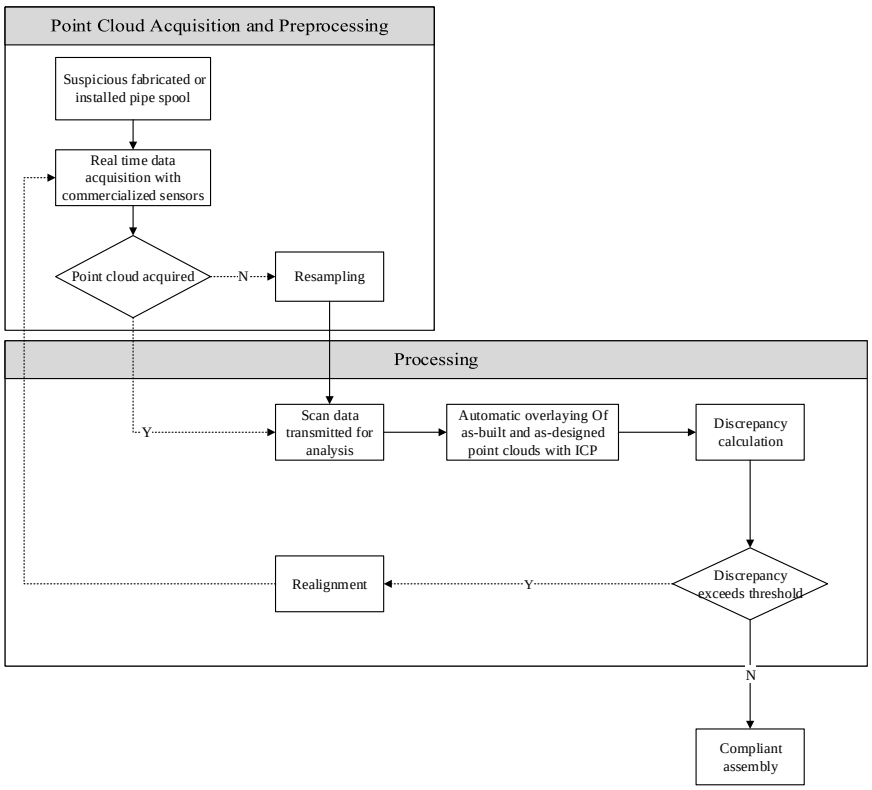

Figure 3-1. Proposed framework for real-time defect detection in modular assemblies.

The process of real-time defect detection consists of two main steps: (1) scanning the object-of-interest, and (2) registration of the point cloud acquired with the model for discrepancy detection. The first step requires scanning the object of interest, transferring the acquired point cloud to a processing machine and manually finding the object of interest in the acquired scene. Once the appropriate data has been acquired, automatic registration of the as-built (scanned) point cloud with the as-designed point cloud begins using a PCA (Principal Component Analysis) algorithm followed by ICP for fine registration. These registration steps can be performed in real time. Once the two point clouds have been registered, a discrepancy calculation is performed to visualize whether the component is compliant or not. Each step is described in the following sections.

3.3.1 Point Cloud Acquisition and Preprocessing

A recently commercialized 3D scanning device was used to obtain the as-built point cloud. As shown in Figure 2-2, this sensor scans the object of interest within the manually defined boundary box. The output of the scan is in .obj format which contains coordination of scanned points. After acquiring the initial scan, the object of interest (pipe spool) has to be manually located in the scene and only then can be registered to the design point cloud for further processing.

Due to the presence of materials and construction equipment in the scenes being captured, it is almost impossible to take a scan without clutter. That is why the next two chapters focus on automation of finding the object of interest and then removing the clutter points. However for this study, both of these steps were performed manually. After manually removing the clutter, the point cloud may need to be resampled for better representation. The process of converting a sparse point cloud to a dense point cloud is called resampling. Resampling makes it easier to represent the scan point cloud and to visually compare it with the model. Figure 0-2 illustrates the necessity of resampling in the scanned point cloud of relatively large objects, whereas the point cloud acquired in smaller pipe spool did not need resampling. For this purpose, a triangle and the vertices representation of mesh in the STL (stereo lithography) format are uniformly resampled. This will improve the registration and deviation quantification.

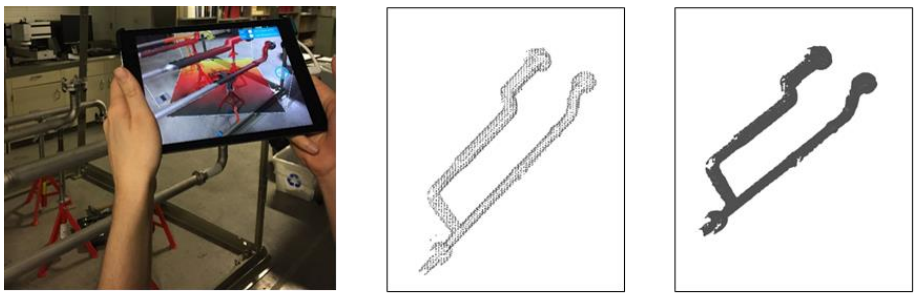

Figure 0-2. Preprocessing required for the proposed method. (a) Data acquisition using Structure IO. (b) as-built point cloud before resampling (sparse point cloud acquired by sensor), and (c) dense point cloud after resampling.

3.3.2 Point Cloud Registration and Discrepancy Analysis

Once the scan data is acquired and the required preprocessing steps are performed, the point cloud is imported to the processing section of the framework. The portion of the 3D CAD model (which may be integrated within the building information model) that corresponds to the scanned object is then isolated and processed to generate the as-designed point cloud.

The next step is to automatically superimpose the point clouds representing the built and designed states. Automatic registration allows easier and more reliable quantification and localization of defects. As mentioned earlier, the registration step presented here consists of two steps:

(1) Coarse registration using PCA (Principal Component Analysis) to roughly align the two point clouds. Registration involves with an optimization of error between the two point clouds representing the built and designed states. The initial state for finding the optimal solution is critical in the optimization process. Improper initial values may cause getting stuck in local minima (Nahangi and 2014). The alignment of principal axes is ambiguous in PCA. In order to address this inadequacy and finding an appropriate initial state that will result in finding the correct global optimum, a loop was designed to check any possible combination of principal axes. The algorithm will then extract the orientation with the minimum error of corresponding points in the coarse registration step. Using this loop, will improve the robustness of the registration step. Figure 0-3 illustrates the problem of PCA if all the combinations of the axes are not checked.

(2) Fine registration using ICP (Iterative Closest Point) (Besl et al. 1992). In this step, the algorithm finds the best match between the two states being compared. Based on (Salvi et al. 2007), ICP is sufficiently quick and robust to be used for real-time fabrication.

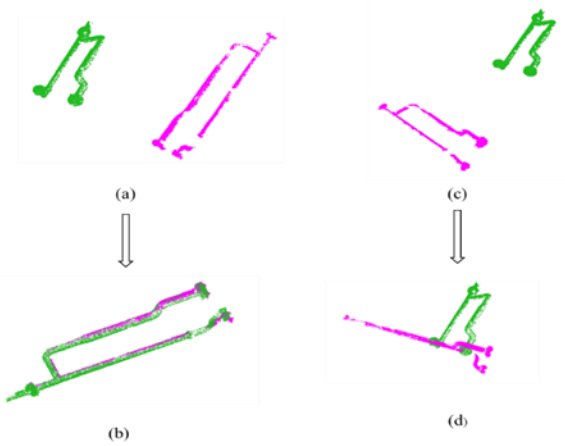

Figure 0-3. Illustration of dependency of PCA to the initial position without using the described loop. (a) Oriented Initial state. (b) Resulted registration. (c) Not oriented initial state. (d) Wrong results using PCA without the described loop.

Once the point cloud registration has been performed, discrepancies can be detected with 3 methods:

(1) Using the method presented in (Nahangi and Haas2014), makes it possible to calculate translational and rotational errors between corresponding points in the model and scanned data. This method makes the use of a robotics analogy and quantifies the incurred deviations using a kinematics chain and geometric relationship between branches of a pipe spool. However, the accuracy of the sensor used was insufficient for reliable analysis using this method.

(2) Point to point distance calculation. Each point in the scan will be compared with its closest point in the model and the distance will be reported.

(3) Approximating the error by the Root Mean Square (RMS) value. In order to measure the performance of assembly the RMS was used. RMS value is calculated as:

$$RMS = \left[\frac{1}{n}\sum_{i=1}^{n} {d_i}^2\right]^{0.5} \qquad (3.1)$$

where, n is the number of corresponding points between the scan and model point cloud, and d is the Euclidean distance between each pair of points.

In terms of pipe fabrication and tolerances for prefabricated pipe assemblies there are specified codes identifying general guidelines for pipe fabrication (Pipe Fabrication Institute 2000).

Table 0-1. Linear tolerance along the pipe length [Pipe Fabrication Institution Standard ES-03]

Pipe Size	Under 10"	12" to 24"	24" to 36"	Over 36"
Acceptable Tolerance	±1/8"	±3/6"	±1/4"	Increasing by plus or minus 1/16" for each 12" in diameter over 36"

Table 0-2. Angularity and Rotation Tolerances [Pipe Fabrication Institution Standard ES-03]

Type	Acceptable Tolerance
End preparation for weld	Shall not deviate from indicated position by more than 1/32" across the land for inert gas weld joints or 3/32" for other joints
For Bending Tolerances	Tolerance minimum radius and minimum tangent see PFI standard ES-24
Rotation of flanges	From the indicated position measured, 1/16" max
Alignment of Flanges and Ends	Shall not deviate from indicated position measured across any diameter more than 3/64" per foot or 1/32" whichever is greater

Once basic compliance checking is performed, decision regarding the shipment of the pipe spool will be made. After such basic compliance checking, the pipe spool is ready to be shipped to the construction site. Nevertheless,

if inspections on a pipe spool reveals a non-compliancy, the pipe spool will be sent back to the shop instantly. This framework has the potential to improve the time wasted for repairing and realigning defective assemblies on construction sites.

3.4 Results

The methodology described in the preceding sections was tested using a structured-light sensor to capture the as-built geometry of two small pipe spools. The Spool I is approximately 40×40×40 cm in overall orthogonal dimensions, and the Spool II is 200×50×30 cm. The dissimilarity in the size and proportions of these two spools was found to affect the results which will be discussed below. (Figure 3-4)

(a) (b)

Figure 3-4. The pipe spools used for experimental studies. (a) Spool I, and (b) Spool II.

In order to identify defective assemblies, a threshold in RMS value is identified. Defective assemblies are expected to have larger errors in the registration step. A set of experiments on the smaller pipe spool was performed to calibrate the RMS value based on the compliancy status of a typical assembly. In these experiments three compliant assemblies, one non-compliant with small rotational deviation, and three non-compliant were tested. Table 0-3 shows the results for calibrating the RMS value for identification of compliancy vs. non-compliancy. The RMS in Figure 0-5-(e), equals 0.0088 m, whereas the RMS in the intentionally defected assembly is 0.015 m. This value should be calibrated for each assembly.

Table 0-3. RMS value for different assemblies and the classification associated for each one in Pipe Spool II.

Experiment number	Intentional Status	RMS (m)	Classification
1	Compliant	0.0092	OK
2	Compliant	0.0088	OK
3	Compliant	0.0098	Suspicious
4	Non-Compliant	0.0105	Not-OK
6	Non-Compliant (Slightly)	0.0096	Suspicious
7	Non-Compliant	0.0129	Not-OK
8	Non-Compliant (immense error)	0.0242	Not-OK
9	Non-Compliant (immense error)	0.0150	Not-OK

For Spool II in the experiment, a threshold value is set for identifying the compliancy of the spool. This value is to 0.009 *m*. The configurations that have an average error more than 0.01 *m* were then deemed to be defective, and those below 0.009 *m* were considered to be compliant. However, the values between 0.01 *m* and 0.009 *m* are the ones that the device is not accurate enough to identify. Such configuration are therefore classified as suspicious.

In *Figure* 0-5-(d), a non-compliant configuration was tested. The results signify that the assembly is non-compliant with the model. Using such a framework by craft workers will allow them to detect the defective assemblies before causing delay to the project schedule. The defective assemblies can then be realigned or repaired before it leaves the work station, thereby reducing rework and improving productivity on construction sites. On the other hand, in Figure 0-5-(e), where the assembly is compliant with the 3D model, the two point clouds are superimposed perfectly.

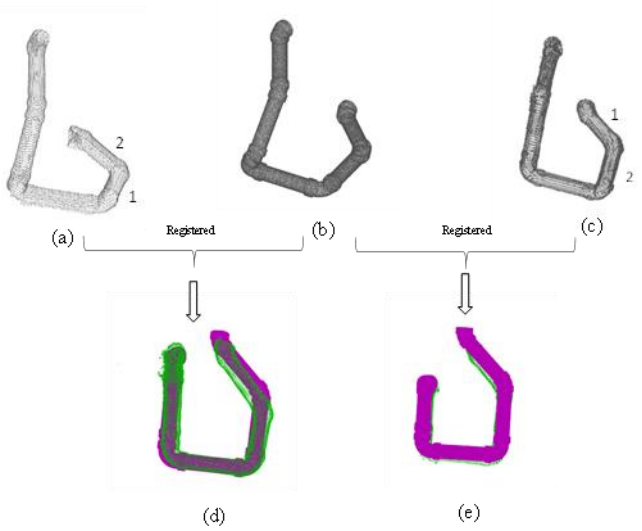

Figure 0-5. Registration results for Spool II. (a) Defected as-built model where faces 1 and 2 should be replaced with each other; (b) 3D CAD model converted to point cloud; (c) compliant as-built model; (d) Results for registration of models (a) and (b)); (e) Results for registration of models (a) and (c)

The as-built scans obtained using the commercial structured light sensor were found to be adequate for compliance checking of the small pipe spools using the process developed in this research. However, inaccuracies in the scan data were observed when used with the relatively longer pipe spool. The result for the longer pipe spool is shown in Figure 0-6, where a significant deviation between the apparent lengths of the spool was evident in the point cloud registration even though no real error existed. The maximum length of the pipe spool in Figure 0-5 was 40 *cm*, and maximum length of the spool in Figure 0-6 was 200 *cm*. There are various reasons why the error manifested in Figure 0-6 occurs: (1) since the employed sensor uses the same technology as Microsoft Kinect (Khoshelham et al. 2012), the random error of depth measurement increases when the distance to the sensor increases. Consequently, in a 2 *m* pipe spool if the 3D data is captured in one frame, there would be substantial error in the point cloud captured. (2) Trying to capture points from closer distance requires moving while capturing. This action by itself causes numbers of errors:

- Since pipe spools are relatively featureless objects, the accuracy of data collection may be compromised.
- Various scanning devices use different sensors such as an accelerometer and/or a gyroscope to detect relative movements of the scanning device to aid in the reconstruction of the scanned point cloud. Moving the scanning device along the object length may cause positional errors due to limitations of these sensors to result in cumulative error in the scanned data.

- Other factors such as interference of sunlight to the scene has significant impact on the quality of captured data as it is empowering the sensor's IR (infrared) emitter.

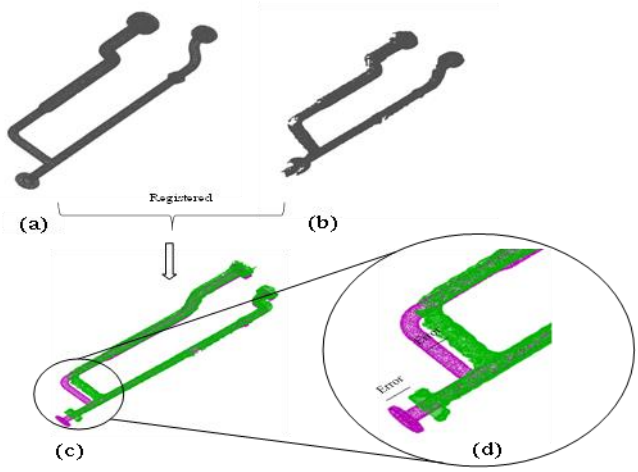

Figure 0-6. (a) 3D CAD model transferred to point cloud, (b) Resampled scanned data, (c) Registration results (d) Error occurred using sensor on a relatively large object (2 m)

3.6 Conclusions and recommendations based on Chapter 3 research

A method was proposed to address the essential need for continuous monitoring of industrial assemblies. A preliminary investigation was performed to assess the applicability of commercialized sensors for real-time fabrication control of industrial pipe spools. This study aimed to find a solution to minimize the time for data acquisition. A framework was developed to reduce the rework caused by misalignments induced in the fabrication shops. For validating and verifying the performance of the proposed method, a case study was conducted on two objects altered in size and shape. Promising results were obtained when applied to a smaller pipe spool, whereas results obtained for a larger pipe spool contained errors in the scanned point cloud that compromised the compliance analysis. This error might be due to the loss of key frames in the 3D reconstruction of the scanned object.

The structured light technologies are experiencing advancements every day. This means that even though the current state of the particular scanner is facing a challenge dealing with large objects, the future generation of these scanners will be more robust to the size of objects being scanned. This study is a proof of concept for using these technologies for real time fabrication quality control in pipe spool fabrication facilities. The current state may not be able to detect small deviations, but they can still be useful for early detection of incurred gross misalignment.

Chapter 4

Automated BIM-Based Finding of 3D Objects in Cluttered Construction Point Cloud Models

This chapter is based on the following submitted article with the same title in the Computer-Aided Civil and Infrastructure Engineering journal. Minor changes are made on some parts of the article to be more consistent with the body of the thesis. Thus, the content of this chapter is not exactly the same as the paper. The contribution of the author in this publication is conducting all experiments, data analysis and partially drafting and editing the manuscript. This study has been submitted on March 28th, 2017.

4.1 Introduction

Automated modeling of fabricated construction components is the bottleneck in automatic and continuous monitoring of civil infrastructure (Dimitrov and Golparvar-Fard 2015). In particular, preprocessing the massive data collected on construction sites is key for effective and electronically-integrated modeling of the built environment. Automated modeling is necessary for various key applications such as progress monitoring, status assessment, and quality control. For example, imperfections and fabrication errors may cause huge rework costs to the projects if they are not effectively monitored and corrected. In 2010, Canada's construction industries (i.e. residential, non-residential engineering, repair, and other construction sectors) accounted for 6
% of Canada's gross domestic product (GDP), contributing $73.8 billion (Statistics Canada 2010). In a typical construction project, rework costs between 2% and 20% of a project's contract amount (CII 2011). According to (Dissanayake et al. 2003), rework is defined as: "Activities in the field that have to be done more than once, or activities, which remove work previously installed as part of the project regardless of the source, where no change order has been issued and no change of scope has been identified by the owner". Geometric non-compliance is one of the main factors causing rework in a project, in general, and in the fabrication processes, in particular.

To reduce rework, rigorous and continuous inspections throughout the fabrication process are required. Conventional methods for quality control and rework mitigation utilize humans with manual direct contact measuring devices such as tapes and calipers. Manual execution of such tasks increases the subjectivity of information as well as other errors and limitations incorporated with intervention. This includes measuring locations with difficult access or spots having hazardous materials. Furthermore, the conventional methods are not only limited by human capabilities, but also, they are time consuming and may cause interruption in the production process. This results in depriving the managers of continuous monitoring and quality control on the fabrication process. Consequently, utilization of

conventional methods will fail to acquire accurate, rapid, and continuous geometric compliance monitoring systems.

Advancements in 3D imaging technology have allowed its users to collect spatial data from their surroundings in a short time period, and with an acceptable accuracy level. Laser scanners measure the distances to points being scanned at speeds up to thousands of points per second (Park et al. 2007). Most of the applications of laser scanning in construction, including automated compliance control (Nahangi and Haas 2014), and schedule and progress tracking (Turkan et al. 2012b) rely on either manual or partially automated identification, location, orientation, and extraction of the object-of-interest. Other methods rely on techniques, such as (Bosche et al. 2008a), that were premised on a priori knowledge of scanner location and orientation with respect to site coordinates. This is due to the indiscriminate data acquisition by the capturing devices. The point clouds acquired with a laser scanner will include clutter (unwanted objects in the background or surroundings of the object-of-interest), and uncaptured surfaces when the objects are occluded. The variation in the density of a point cloud and the existence of noise, which usually occurs on the edge surfaces, are also among the challenges in the automation of the object extraction process. Other contributing factors such as lighting conditions and site specific circumstances can also influence the quality of the captured point cloud (Sharif et al. 2016), which will exacerbate the complexity of the 3D object recognition process. An incomplete point cloud of a fabricated component is another common challenge. The aforementioned challenges reveal the complexity of formalizing an automated framework for object-of-interest isolation from a cluttered 3D point cloud.

The manual extraction of an object-of-interest in a cluttered point cloud is inadequate, inaccurate, and inefficient in terms of the required time and the level of skill required (Figure 0-1). An automated and rapid object finding framework has the potential to be employed in automated object locating, robotic manipulation, and quality control processes in construction. A rapid framework will avoid late detection of possible defects, and therefore the cumulative error arising from infrequent fabrication monitoring (Golparvar-Fard et al. 2009a).This study aims to develop a robust framework for efficient and automated finding of an object-of-interest in cluttered point clouds. This framework is capable of addressing some of the major challenges in this area including:

- **Density variation**: various types of sensors offer different levels of density in the point cloud acquired. The desired framework for object isolation must be insensitive to the density of the point cloud used.
- **Clutter presence**: presence of unwanted objects in the background and surrounding the object-of-interest is the key motivation for automated recognition and isolation of the objects-of-interest.

- **Occlusion and incompleteness occurrence**: in visual sensing and vision-based data acquisition sensors, line of sight is a substantial parameter for capturing complete and reliable data. In the case that the objects are not visually tracked by sensors, some parts or components might be missing. The subsequent analyses and models are therefore influenced by such incomplete data (Nahangi and Haas 2016). The desired framework should also be relatively robust to incomplete point clouds.

A robust framework for automated finding of objects-of-interest from cluttered and unprocessed 3D point cloud models is presented in this chapter. The framework is based on the mathematical model first presented by (Papazov and Burschka 2010). Comparatively, this framework has three primary steps: (1) creating and storing a library of features from point pairs of 3D models using an invariant local feature, (2) finding the potential matching pairs from the point cloud with the code library generated using a RANSAC-based hypothesis testing, and (3) match refinement and isolation using an ICP-based (Iterative Closest Point) registration step. The key contribution of this study is the adaptation and application of a robust framework for automated finding of 3D objects in cluttered point cloud models from a construction environment. The framework is tested under various circumstances in order to investigate its performance for addressing the major challenges discussed previously, including density variation, clutter presence, and incompleteness of the captured data. First, the related background is thoroughly investigated in the following section to clearly identify the knowledge gap and the key contribution of this work. Next, the proposed methodology and its components are described. Finally, experimental results and analyses are provided to quantify the performance of the proposed method.

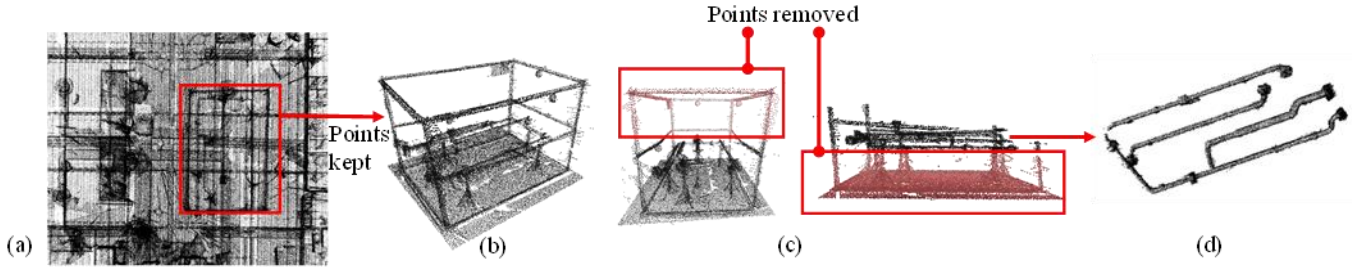

Figure 0-1. Clutter removal example. (a) A facility is scanned; (b) surrounding objects are removed; (c) secondary attachments in the proximity of the object-of-interest (i.e. stands and supporting objects) are removed. (d) The object is finely retrieved by manually removing noise and other points remained. The isolation point cloud is then ready for further processing (e.g. automated registration for discrepancy quantification and quality control)

4.2 Background

4.2.1 Terminology definition

For the purpose of consistency and rigorousness throughout this manuscript, the following terms are defined and described as follows:

Detection: refers to the process in which the presence of an object is identified in an acquired point cloud.

Finding: refers to the process in which the presence of the object is not only sensed but also its geometric characteristics such as dimensions, location, and orientation are identified. The term "*recognition*" however, corresponds to identification and characterization of all the objects that meet the recognition criteria in the scene.

Segmentation: refers to the process of classifying points from the surface of an object in one set and from a cluttered and noisy point cloud.

Isolation: refers to the process of extracting a segmented object from the 3D point cloud and representing it as a single dataset.

This section focuses on a comprehensive review of the existing methods for finding 3D objects from various perspectives with respect to some applications in construction automation. A general overview is first provided from the computer science perspective. Existing challenges and various categories of 3D object recognition are also briefly discussed. Major applications in the construction literature and the existing research challenges are then discussed. Although there have been numerous research studies in automated object recognition from 2D images (Balali et al. 2015), video frames (Park et al.2012, Zhu and Brilakis 2010), and depth images (Ray and Teizer 2012) for a wide range of applications in construction, this paper only focuses on finding 3D objects in cluttered point clouds and the research challenges involved.

4.2.2 3D object recognition: general categories and existing challenges from the computer science perspective

The problem of finding an object-of-interest has been widely investigated in the computer science literature. Vision-based control in robotics (Chaumette and Hutchinson 2006), intelligent surveillance (Guo et al. 2013) and mobile manipulation (Quigley et al. 2009) are only a few applications, which are well developed and widely used in the related body of knowledge.

However, finding objects in the aforementioned applications is relatively limited to 2D scene capturing approaches such as 2D images or 2D snapshots from video frames. Unprecedented opportunities have

recently become feasible with the significant improvements in 3D data acquisition, and there has been extensive work on 3D object recognition from 3D scenes (i.e. 3D point clouds). However, most of the existing frameworks are computationally very intensive, and therefore insufficiently effective and applicable. The required processing time is the major drawback for automated 3D object recognition and modeling in construction automation.

According to (Guo et al. 2014), object recognition methods can be grouped into two main approaches: (1) global features or 3D keypoint detection and localization, and (2) local features characterization and localization. The former approach includes 3D SIFT (scale invariant feature transform) (Allaire et al. 2008), 3D LIFT (learning invariant feature transform) (Huang et al. 2007) and 3D SURF (speeded-up robust features) (Knopp et al. 2010), which are performed on either depth images (2.5D) or 3D meshes. Such methods are incapable of finding 3D objects from 3D point clouds. The local features approach is thus more widely used for 3D object recognition from 3D point clouds. This approach includes signature-based and histogram-based methods such as spin images (Johnson and Hebert 1999), point signature (Chua and Javis 1997), and point pair features (Papazov and Burschka 2010). Based on the extensive survey by (Guo et al. 2014), local features have been found to be more efficient for 3D object recognition from 3D point clouds.

4.2.3 3D object recognition: application in construction

In built environments, it is imperative to find objects-of-interest automatically and effectively to assess their as-built status and map critical construction performance metrics. Such metrics include as-built progress compared to the as-planned schedule (Golparvar-Fard et al. 2012, Kim et al. 2013), or as-built shape or geometry compared to the as-designed geometry (Chen et al. 2016, Nahangi and Haas 2014) In this section, object recognition in the construction literature is investigated from three perspectives: (1) automated as-built modeling, (2) quality control and automated modeling, and (3) progress tracking.

4.2.3.1 Object recognition for automated as-built modeling

As discussed by (Pătrăucean et al. 2015), as-built BIM creation is challenging due to the complexity of construction components. However, some components represented by explicit geometric shapes can be detected, recognized, and modeled given a 3D point cloud representing the built environment. Some examples include MEP (mechanical, electrical, plumbing) components, in general, and cylindrical objects (e.g. pipes and elbows), in particular. This research area is also known as scan-to-BIM in the related literature (Bosché et al. 2015).

(Rabbani et al. 2007) presented a generalized Hough-based method for detecting and recognizing industrial and piping elements with some basic explicit shapes. The processing time for recognizing objects from point clouds was substantial and therefore ineffective, because they were using the Hough transform in 3D. This method was also incapable of recognizing and modeling elbows and T-sections. (Ahmed et al. 2014) presented a method for detecting and reconstructing cylindrical objects such as 3D pipes using a modified Hough Transform-based method. Their method overcomes the computationally intensive 3D Hough Transform by projecting points into orthogonal slices (planes) and then applying a 2D Hough-based circle detection. Their approach was also reported to be incapable of finding T-sections and elbows and it was only applicable on cylindrical objects laid out in orthogonal directions.

(Son et al. 2014) presented a curvature-based cylindrical object recognition which was found to be capable of finding elbows and intersections. However, their method relied on an accurate and complete 3D point cloud as an input, and it is therefore inadequate for finding complicated cylindrical branches. (Lee et al. 2013) presented a skeleton-based method for 3D reconstruction of industrial elements. The skeleton- based method was also inadequate and inaccurate in the case that an incomplete 3D point cloud is imported to their framework. According to (Nahangi and Haas 2016), incomplete point clouds will change the skeletons representing the centerlines, and will therefore create errors in the radius detection and recognition.

A curvature-based segmentation method with applications to MEP components was then presented by (Dimitrov et al. 2015). Although their method is sufficiently accurate in recognizing various components from a cluttered scene, it is still computationally expensive. Their method requires curvature calculation on a resampled point cloud, which is then used for checking connectivity of components. Assuming that time-effective process controllers are desirable, in practice, their curvature-based method is incapable of addressing the time related aspects and challenges. (Dimitrov et al. 2016) then extended the curvature-based segmentation to model arbitrary shapes given a noisy and cluttered 3D point cloud model. Their recent work takes the advantage of the previously segmented components. It then employs non-uniform rational B-splines (NURBS) for modeling arbitrary shapes in the form of explicit and closed form mathematical functions. This is directed toward the ultimate goal of scan-to-BIM creation. (Zhang et al. 2015) presented a framework for planar patch detection from cluttered point clouds. The segmentation of planar patches is based on normal vector calculation and spectral clustering which was found to be robust.

4.3.2.2 Object recognition for quality control and as-built status assessment

One other key application for automated object recognition is to assess the as-built status or geometric quality of the components compared to the as-designed drawings integrated in the BIM. This area is also known as scan-vs-BIM in the related literature.

A framework for automated discrepancy quantification of fabricated serial components was presented based on the as-built point clouds of components automatically registered and compared with their 3D models. The isolation step was performed manually, which was disconnected from the fully automated framework. Automated isolation of the components is therefore the key to expedite the entire process. The method was then extended to parallel assemblies with a strategy for realigning the defective assemblies (Nahangi et al. 2015); however, lack of an automated step to automatically extract an object-of-interest given a point cloud was still a drawback for integration with automated fabrication process controllers.

A skeleton-based method for discrepancy quantification was then presented, in which the object isolation step was still performed manually (Nahangi and Haas 2016). Recently, (Czerniawski et al. 2016b) presented a 3D model-based object-of-interest recognition and isolation method, where curvature was a signature or descriptor of the model. A bag-of-features with two-way curvature descriptors was created in order to represent the 3D model of an object-of-interest. The feature was then searched in a 3D point cloud transformed to the feature space. The hypothesis testing and matching was then performed using a bi-variate histogram-based voting scheme. This method was limited to the objects where curvature is a meaningful representative (e.g. industrial object, in general, and cylindrical pipes, in particular). Although, the method was capable of extracting arbitrary 3D objects from cluttered point clouds automatically and with a high recognition rate (90% in average), its computational time is still a drawback for the applications desired.

4.2.4 Object recognition for progress tracking

Object detection and recognition has been widely used to track the progress of components compared to the as-planned schedule integrated with the BIM. Generally, for the purpose of progress tracking, detecting an object will be sufficient to measure the as-built schedule and compare with the as-planned schedule.

An image-based framework for automated progress tracking using statistical correspondence for object detection was presented (Golparvar-Fard et al. 2012). (Turkan et al. 2012b) presented a framework based on the object detection method previously developed by (Bosche and Haas 2008b). The object detection and progress tracking is based on the level of overlap between the as-planned and as-built 3D point clouds that are finely aligned. (Kim, et al. 2013) presented a training-based framework for

automated progress tracking that used an SVM-based classifier for major objects in a building (i.e. columns, beams and slabs).

Other than the aforementioned major application in construction, 3D object segmentation and recognition are also used for some secondary applications. For example, (Czerniawski et al. 2016a) used a similar approach to (Zhang et al. 2015) for automated removal of planar regions for facilitating and expediting the recognition of cylindrical objects. A density-based clustering step was used to cluster and segment various planar regions represented by their normal vectors. Recently, (Chen et al. 2016) presented a framework for equipment localization using a principal axes descriptor and a training-based approach used for detection.

In summary, the problem of robust and efficient finding of a 3D object in 3D point cloud models as well as its major research challenges has remained an elusive goal. The following section frames the knowledge gap from the conducted literature review, and identifies the major contribution of the work in the current study. A summary of the investigated studies along with a general categorization from different perspectives is also provided in Table 0-1.

4.2.5 Knowledge gap and research contribution

As discussed, for finding 3D objects in cluttered point cloud models of construction environments, the previously developed frameworks are either relatively ineffective in terms of processing time or are not fully automated. As well, the existing methods are limited to explicit shapes and geometries such as MEP components (cylindrical objects) or some simple structural components (concrete beams and columns with rectangular cross section). They are therefore not robust for construction components with complex and arbitrary geometries. This chapter presents an automated and robust framework for finding 3D object-of-interest within cluttered and noisy point clouds. A simple and abstract representation of the framework is illustrated in Figure 0-2. The framework developed is capable of addressing some of the major research challenges discussed previously (e.g. density, noise, and incompleteness). The method takes advantage of existing 3D models integrated with the BIM. The model-based 3D object-of-interest finding framework is described in the following section.

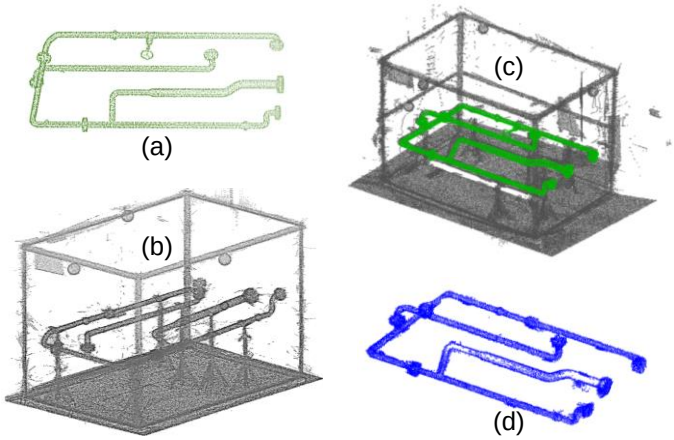

Figure 0-2. Graphical abstract of the presented framework: (a) 3D model converted to a point cloud, (b) cluttered 3D scene, (c) localized model on the scene, and (d) found and isolated object from the scene.

Table 0-1. Summary of 3D object recognition methods existing in the construction.

Reference	Identification status	Method	Research stream in construction	Specific application in construction
(Papazov et al. 2012)	Recognition	3D Hough transform	3D modeling	Industrial elements
(Ahmed et al. 2014)	Recognition	2D Hough transform	As-built BIM	Cylindrical pipes
(Son et al. 2014)	Recognition	Curvature	As-built BIM	Cylindrical pipes
(Lee et al. 2013)	Recognition	Skeleton	As-built BIM	Cylindrical pipes
(Dimitrov and Golparvar-Fard 2015; Dimitrov et al. 2016)	Segmentation	Curvature, NURBS	As-built BIM	MEP components
(Zhang et al. 2015)	Detection	Normal vector	As-built BIM	Planar components
(Nahangi et al. 2015)	Recognition	NA (manual isolation)	As-built status assessment	Serial and parallel
(Czerniawski et al. 2016b)	Recognition	Curvature	As-built status assessment	Serial and parallel
(Golparvar-Fard et al. 2012)	Detection	Statistical	Progress tracking	Any type
(Bosche and Haas 2008; Turkan et al. 2012)	Detection	Closest points	Progress tracking	Any type
(Kim et al. 2013)	Detection	SVM based classifier	Progress tracking	Column, beam, slab
(Czerniawski et al. 2016a)	Recognition	Normal vector	Object isolation	Planar regions
(Chen et al. 2016)	Detection	PCA	Automated monitoring	Construction equipment

4.3 Methodology

An overview of the implemented methodology for finding arbitrary shapes within cluttered point clouds is illustrated in Figure 0-3. It is derived primarily from (Papazov and Burschka 2010) basic algorithm and adopted to the class of construction object recognition problems addressed here. The result is then extensively examined for performance. The method has three primary steps: (1) model library generation, (2) scene representation, and (3) matching. The first step can be performed in the offline

phase, meaning that the library can be generated and stored for further calculation. The second step is to calculate features for hypotheses tested in the matching step (Step 3). The primary steps for finding arbitrary objects are described in the following sections.

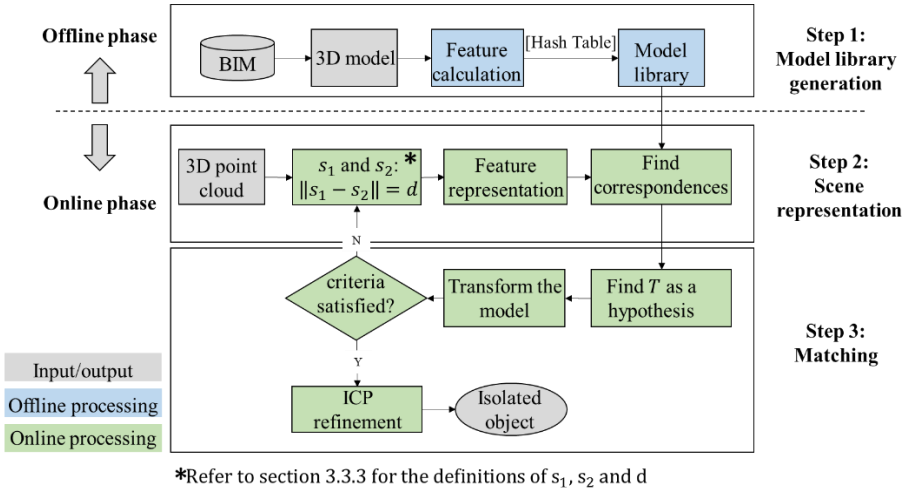

Figure 0-3. Proposed methodology for BIM-based object finding of construction assemblies has three major steps: (1) Model library generation, (2) Scene representation, and (3) Matching.

4.3.1 Inputs and preprocessing

The required inputs for the proposed algorithm are the following:

(1) 3D *Model* denoted by M: in order to generate the model library the 3D model should be available in the point cloud format. The solid objects existing as the CAD drawings integrated with the BIM are converted to 3D point clouds using one of the methods well discussed by (Corsini et al. 2012). Poisson disk sampling is used in this work for converting 3D solid objects into point

(2) 3D point cloud or the *Scene* denoted by S: that represents the as-built state or the scene being investigated. Both M and S are preprocessed by constructing their weighted octree structures. Bin subdivision in weighed octree is calculated based on the mean of all points that each bin contains wherears in the normal octree subdivisions spilts bins at their central coordinate (i.e. one bin subdivides into 8 equally sized bins). This step is required to normalize the density of the input point clouds. Moreover, octree represents a uniformly resampled point cloud resulting from the original input point cloud. Such a process is similar to voxelization for down sampling or resampling a 3D point cloud. A hypothetical example of weighed octree construction of a typical point cloud (*Model* and *Scene*) is illustrated in Figure 0-4.

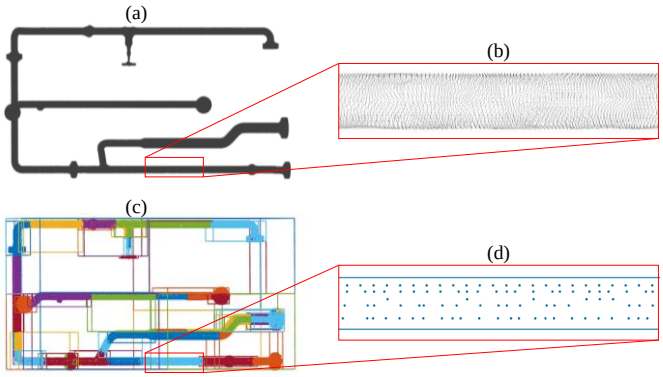

Figure 0-4. Density normalization using weighed octree: (a) a model after density normalization using octree (c), a zoomed-in window is shown for illustrating density before (b), and (d) density after normalization using octree structuring.

4.3.2 Model library generation

Model library generation is performed for creating the feature space of the objects and shapes existing in the scene captured. This step can be performed beforehand, because it remains unchanged for a given shape or geometry. In other words, a library of objects can be created and stored in a database for further processing. The feature space used in this chapter is similar to the feature defined in (Papazov and Burschka 2010). The only difference between the feature set used here with the previously defined feature set in (Drost et al. 2010) is the distance element between the point pair. The local feature set used in this work is illustrated in Figure 0-5.

As illustrated in Figure 0-5, a three-dimensional local feature descriptor is used to represent the model. The feature set for a point pair (p_1, p_2) is denoted by $F(p_1, p_2)$ and is calculated as follows:

$$F(p_1, p_2) = (f_1, f_2, f_3) \qquad (1)$$

in which, $f_1 = \angle(n_1, d)$, $f_2 = \angle(n_2, d)$, $f_3 = \angle(n_1, n_2)$. The operator $\angle$ returns the angle between the two input vectors. This feature set is similar to the feature set used previously (Czerniawski et al. 2016a); However, the assumption of reducing one dimension from the local feature set, makes it computationally less intensive and therefore more time effective. Moreover, removal of the *distance* element from the feature set, results in similar dimensionality for the remaining elements, and therefore it reduces the complexity of the feature space. This distinctive feature is useful in storing the feature descriptors more efficiently. All points in the model are uniformly resampled and the feature set is then created.

The key for calculating the feature descriptor is the normal vector at a resampled point cloud. The normal vector is calculated using a four-step algorithm as follows:

1- Calculate k-nearest neighbours (KNN) given a point in a point cloud ($p \in P$).

2- Assign the calculated neighborhood to the point p.

3- Fit a plane to the neighborhood.

4- Assign the plane's normal vector to the point p ($n.p_i$).

The k value for identifying the size of the neighborhood around a point will affect the accuracy of normal vector calculation and therefore the isolation retrieval. The framework has been found very robust to the size of the neighborhood for normal vector calculation. The procedure for normal vector calculation is similar to the principal component analysis (PCA) for normal vector extraction. More detail about normal vector calculation can be found in (Czerniawski et al. 2016b).

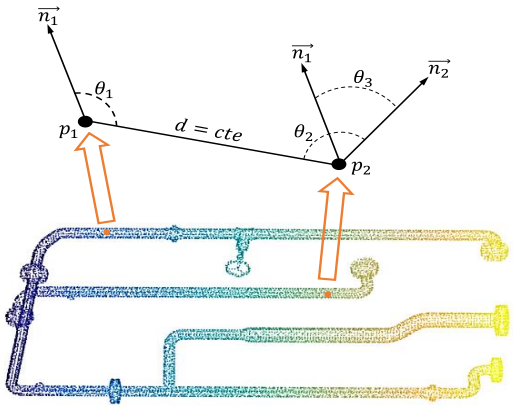

Figure 0-5. Local feature descriptor used for object extraction. The distance between the point pair is set constant. This assumption reduces the level of complexity and therefore reduces the processing time for feature space creation.

A 3D hash table is used to store the library of features. The feature elements $F = (f_1, f_2, f_3)$ are used to hash the entries in the table. The hash table is divided with an arbitrary cell size, which is found to have a negligible impact on the robustness of the framework. The calculated feature sets are then assigned to the corresponding cell in the table. This method has been found very efficient for the search phase, and therefore improves the time related aspects of the framework. Figure 4-6 shows the creation of a hash table for a hypothetical 3D shape.

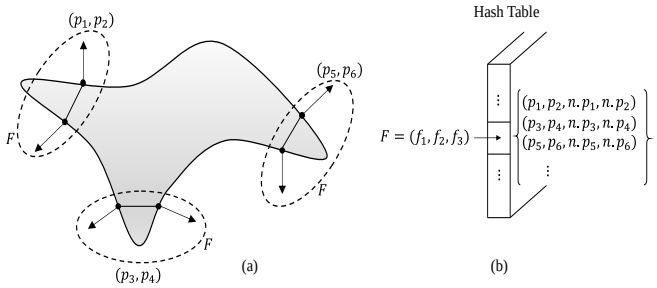

Figure 4-6. A hypothetical 3D shape is illustrated to show the procedure for generating the model library and storing the feature descriptor. (a) Arbitrary point pairs are resampled from the model point cloud and the feature set is calculated. (b) The feature sets is calculated. (b) The feature sets are then used to hash the table for representing the model (i.e. points with similar feature sets with a threshold value $\Delta\theta$ are hashed in a similar cell).

To find various models, the hash table and the model library can be extended; that means the features for various models can be accumulated in an original hash table. This method for storing the model feature sets in the same library avoids recalculating features for previously generated shapes. Model library generation with the required steps is summarized in Algorithm 1.

Algorithm 1: Model library generation

Input: 3D model point cloud $\{M\}$

Output: Model library $\{\mathbb{M}\}$

Null $\{\mathbb{M}\} : \emptyset \rightarrow \{\mathbb{M}\}$

For all points (m_1) in 3D model: $m_1 \in M$

Find all points $\{m_2\} \subseteq M$ such that $\|m_1 - m_2\| = d$

For all points in $\{m_2\} \subseteq M$

- Create the point pair (m_1, m_2)
- Calculate the feature descriptor: $F = (f_1, f_2, f_3)$
- Populate $\mathbb{M}$: store (m_1, m_2) and normal vectors $(n.m_1, n.m_2)$ in the corresponding cell (f_1, f_2, f_3), in the hash table $\mathbb{M}$

End for

End For

Report $\mathbb{M}$

4.3.3 Scene representation

Once the models are described using the feature set explained, and the library of the objects are created, the online mode is performed. The online mode starts with a RANSAC (Random Sample Consensus)-based search. The regular RANSAC search for 3D objects is inefficient and almost impossible for realistic or practical sized point clouds. In contrast, the feature library is used for making the search more efficient and robust for real-sized point clouds. The sampling process for the RANSAC-based matching is illustrated in Figure 0-7.

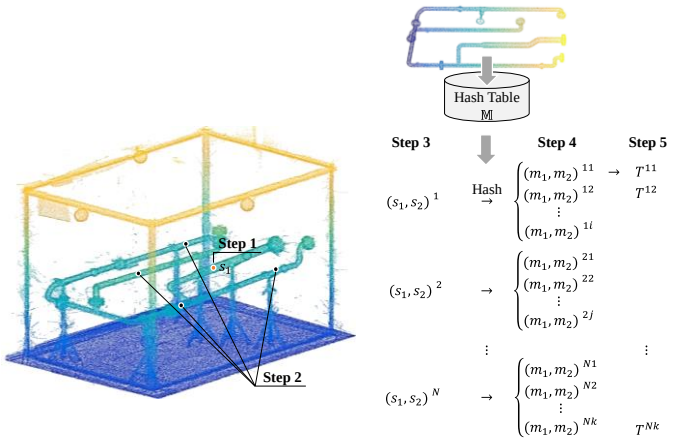

Figure 0-7. Scene representation for one typical iteration in the RANSAC-based matching algorithm. Step 1: an arbitrary point s_1 is selected. Step 2: all possible s_2's are calculated. Step 3: all possible pairs (s_1, s_2) are created, and the features are calculated. Step 4: potential matching pairs are extracted from the hash table using the features calculated. Step 5: The transformation T is then calculated.

To start searching for potentially matching pairs, the *Scene* (S) is uniformly resampled (s_1). For each point resampled, all points $\{s_2\}$ that are distanced at d are stored to create a potential pair (s_1, s_2). The feature elements are then calculated to identify the matching pairs from the *Model* (M) stored in the hash table. The point set (s_1, s_2) and the corresponding normal vectors $(n.s_1, n.s_2)$ are then matched with the existing pairs and normal vectors in the hash table. In other words, the potential matching pairs from the *Model* and *Scene* create a hypothesis to be tested in a RANSAC-based matching step. The matching step is described in the following section.

4.3.4 Matching

The matching step is combined with the *Scene* representation. The matching step is an iterative process based on the criteria defined for testing the hypotheses created from S. For all potential matching pairs identified from the hash table, the transformation (T) that aligns the features (i.e. points and their normal

vectors) from the *Model* and *Scene* is calculated. For calculating the transformation$T$, PCA (principal component analysis) is used for aligning two sets of four points in the *Model* and the *Scene*. The set of four points include the two points of the pair being investigated, and two arbitrary points located on the normal vectors starting from the points. In this chapter, the two points are located at the end of the unit normal vector starting from the point. Figure 0-8 illustrates the calculation of the point sets of four to be matched from the two datasets.

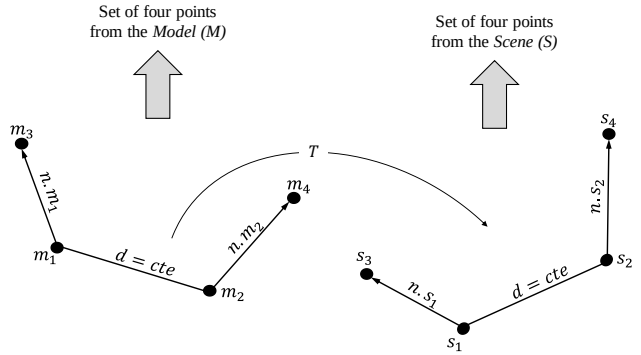

Figure 0-8. Calculation of the point sets to be matched using principal component analysis. The four points include the pairs as two points: $(\mathrm{m}_1, \mathrm{m}_2)$ or $(\mathrm{s}_1, \mathrm{s}_2)$, and two points, $(\mathrm{m}_3, \mathrm{m}_4)$ or $(\mathrm{s}_3, \mathrm{s}_4)$, located at the end of a unit normal vector starting from each point. $\|\mathrm{m}_1 - \mathrm{m}_3\| = \|\mathrm{m}_2 - \mathrm{m}_4\| = 1$, and $\|\mathrm{s}_1 - \mathrm{s}_3\| = \|\mathrm{s}_2 - \mathrm{s}_4\| = 1$. The rigid transformation T can then be calculated using PCA.

The method described for transformation calculation (hypothesis generation) is found to be robust and quick. Therefore, the online phase remains very time effective to be implemented in real-time applications. The entire *Model* is then transformed using the previously calculated transformation: $M^* = T \times M$.

M^* and S are then compared to test the hypothesis generated. For this purpose and to test the goodness of the transformation calculated (hypothesis), the number of inliers is computed. A support term (λ_s) is therefore defined to investigate the appropriateness of the hypothesis. In other words, λ_s identifies an additional criterion for the RANSAC-based matching algorithm used here.

For each hypothesis (T) generated, the support term is calculated as: $\lambda_s(M, T) = m_s/m$, where, m_s is the number of points that support a matching criterion. Such a matching criterion is defined as the number of points from the transformed *Model* (M^*) in close proximity to the *Scene* (S).

The matching step is performed until either a maximum number of iterations is reached or a pre-defined portion of the points in the *Model* are retrieved from the scan. These two criteria are identified to stop the RANSAC-based hypothesis testing framework.

Once the best hypothesis is found using the previously explained framework, the match is refined using a post iterative closest point (ICP) alignment. The initial coarse alignment will be improved using a post ICP alignment with a few number of iterations to find the best match between the two data sets. This step augments the accuracy of the method for correct finding, because the datasets were resampled to improve the time effectiveness of the framework. Some information is missing during resampling because of the reduction in the density of the point cloud; however, this issue is compensated using this post ICP refinement. Algorithm 2 summarizes the processing tasks explained in Step 2 and Step 3. Figure 0-9 shows an example of the post-ICP refinement of the match found using the feature space and the RANSAC-based search.

Algorithm 2: Scene representation (Step 2) and matching (Step 3)

Input: Model library $\{\mathbb{M}\}$ and Scene (S)

Output: Isolated object-of-interest $\{S_i\}$ from S: $S_i \subseteq S$

Repeat N times

- Randomly select s_1
- Calculate all points $\{s_2\}$ such that: $\|s_2 - s_1\| = d$
- Create all pairs (s_1, s_2)

  For all pairs (s_1, s_2)

  - Calculate $F(s_1, s_2) = (f_1, f_2, f_3)$
  - Find potential matching pairs in the model (m_1, m_2) by (f_1, f_2, f_3) as the key to the hash table $\mathbb{M}$.
  - Create the set of four points from S and M: $S^4 = (s_1, s_2, s_3, s_4)$ and $M^4 = (m_1, m_2, m_3, m_4)$.
  - Find transformation T that matches M^4 to S^4 using PCA
  - Transform the entire model with T: $M^* = T \times M$
  - Calculate $\lambda_s(M, T) = m_s/m$
  - Find T and M^* associated with the highest λ_s

End For

End Repeat

- Refine the match as: $M^* \leftarrow M^* \times ICP(M^*, S)$
- Find correspondences $S_i \subseteq S$ of M^* in S

Report S_i

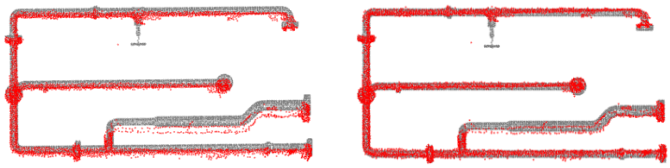

(a) (b)

Figure 0-9. Refinement of the match using a post-ICP registration. Aligned point clouds (a) Before, (b) after ICP registration.

As illustrated in Figure 0-9, the 3D model slightly deviates from the scene after calculating the initial transformation using the RANSAC-based hypothesis testing. Such deficiency is resolved by performing the post-ICP refinement step. The ICP registration requires only a few iterations to refine the alignment. The effective parameters are summarized in Table 0-2 and were established using experiments in this study. The effectiveness of the parameters is reported in section 3.4.3.

Table 0-2 Values of the effective parameters for the set of experiments performed

Parameter	Description	Value
d	Distance between the point pairs	$0.75\rho^*$
$\Delta\theta$	Cell size for the hash table	12^o
λ_s	Overlap ratio for the RANSAC	0.15
t	Time criteria for RANSAC	20 *sec*
iterations	ICP iterations for post refinement	5

$^*\rho = diam(M)$, where $diam$ returns the largest distance between a pair in a point set.

4.4 Verification and Validation

In this section, the described framework is implemented and its performance is measured by designing a set of experiments. The method is validated on two cases to evaluate its capability on various geometries and shapes. The framework is implemented and programmed in a MATLAB-based platform

integrated with C++ and a function library distributed by (Papazov and Burschka 2010). The processing times reported in the following sections are benchmarked on a processing machine with a 3.7×12 GHz processing unit and a 32 GB RAM.

4.4.1 Design of experiments

For verifying and validating the proposed methodology, a set of experiments are designed and performed. The experiments are carried out on a small-scale pipe spool (as a curvilinear object) and a structural frame (as a rectilinear object). The object-of-interest is in a laboratory environment, where other unwanted objects are scanned in the background or in the close proximity of the object-of-interest. For 3D point cloud acquisition, laser scanning is employed in this study. A FARO LS 840-HE is used for scanning the lab facilities. Physical properties of the laser scanner used in this study can be found in Table 4-3.

Table 4-3. Summary of physical properties of the 3D scanning device (FARO LS 840-HE)

Factor	Value
Accuracy	± 3*mm* at 25*m*
Scanning range	0.6*m* – 40*m*
Acquisition speed	120,000 *points/sec*
Angular resolution	0.009º

For comparing the results in the cases investigated, and measuring the performance of the framework, two critical metrics are reported:

1- Processing time: is the required time for both model library generation (offline phase), and matching (online phase). Tracking the processing time enables the applicability of such a method for developing real-time frameworks for process control.

2- Retrieval accuracy: is the average error between the transformed *Model* and the *Scene*. This is represented by a root mean square (RMS) of the Euclidean distance between the corresponding points. As mentioned earlier, two construction components are used in the experiments: (1) a small- scale pipe spool, and (2) a small-scale structural frame. The latter is chosen to verify the robustness of the proposed algorithm for finding structural elements from cluttered laser scans. Previous studies (Czerniawski et al. 2016a) were directed toward recognizing cylindrical objects (e.g. pipe spools). However, the method presented in this chapter can find

any shape and geometry robustly and effectively. More information about the components used in the experiments is provided in Table 0-4.

Table 0-4. Construction components used in the experiments

Point cloud	Bounding dimensions	Element type	ID used for results
Pipe Spool	$3m \times 2m \times 0.5m$	Curvilinear	PS
Box Frame	$3.5m \times 2m \times 2m$	Rectilinear	BF

4.4.2 Effective variants

To investigate the capability of the framework for addressing the existing challenges for efficient finding of objects (discussed earlier), the experimental setup is tested under various circumstances. Three major variants are investigated: (1) density of the 3D point cloud used in the isolation framework, (2) clutter existing in the *Scene*, and (3) completeness of the object-of-interest in the 3D point cloud acquired. A wide range of such variants is considered and their impact on the verification metrics (processing time and retrieval accuracy) is analyzed in the following sections.

4.4.2.1 Density

For investigating the effect of density on the results, a dimensionless metric is defined. The metric is called density ratio, which is the proportion of the number of points in the *Scene* to the constant number of points in the *Model*. Various density ratios are investigated by down sampling the originally acquired point cloud as the *Scene*. Down sampling is performed incrementally to evaluate how the recognition rate is affected. Another metric is also defined to monitor the recognition rate. Recognition rate (*RR*) is defined as follows:

$$RR = \frac{TP}{\|s\|} \tag{4.2}$$

in which, the nominator TP (True Positive) is the number of truly found points, and the denominator $\|s\|$ is the size of the object-of-interest (s) in the Scene ($s \subseteq S$). Table 0-5 and Table 0-6 show the summary of the analyses for the effect of density on the recognition rate. Figure 0-10 shows typical results using various density ratios for the isolation of PS from cluttered point clouds.

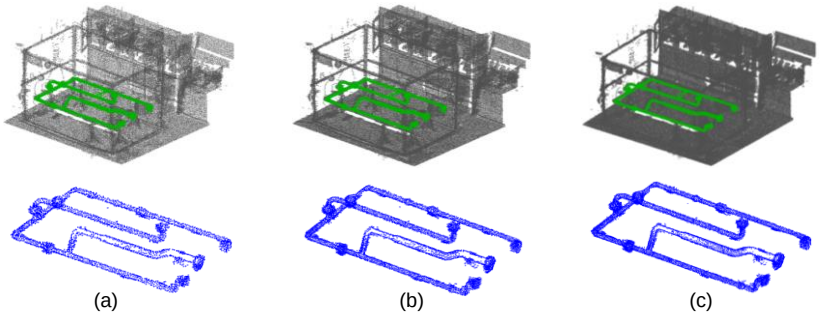

Figure 0-10 Effect of density on the accuracy of the object-of-interest isolation. Three density ratios are illustrated. Density ratios is 5 for (a), 10 for (b), and 20 for (c). The top figures are cluttered point clouds with the model aligned with the object-of-interest, and the bottom figures show the isolated object from the point clouds.

Table 0-5 Summary of the analyses on the effect of density on the critical metrics for Pipe Spool

Density ratio	Number of points	RR	RMS (*cm*)	Time (*sec*)
0.3	3000	0	Failed	Failed
1	10000	0	Failed	Failed
2	20000	0	Failed	Failed
5	50000	0.956	1.34	27.5
8	80000	0.930	1.28	26.8
10	100000	0.929	1.31	25.1
20	200000	0.924	1.25	19.2

Table 0-6. Summary of the analyses on the effect of density on the critical metrics for Box Frame

Density ratio	Number of points	RR	RMS (*cm*)	Time (*sec*)
0.3	3000	0	Failed	Failed
1	10000	0	Failed	Failed
2	20000	1	2.92	15.8
5	50000	0.995	2.86	22.9
10	100000	0.979	2.82	22.9
16	160000	0.983	2.81	22.9

For the PS case, the average RMS value for successfully isolated objects is 1.28 *cm* with a standard deviation of 0.03 *cm*. For the BF case, the average RMS value is 2.85 *cm* with a standard deviation of 0.04 *cm*. This shows that the RMS value remains unchanged for the successful cases. In other words,

the negligible change in the RMS value implies that the object-of-interest isolated from the laser scan is robustly identified using various density ratios. Another observation is that the recognition rate (*RR*) increases as the density ratio passes a minimum threshold value and it then remains relatively unchanged. Figure 0-11 shows the relationship between the density ratio and the recognition rate for the PS and BF cases investigated.

As shown in Table 0-5, Table 0-6, and Figure 0-11, for lower density ratios, the isolation of the object-of-interest is unsuccessful. Unsuccessful isolation means that the final transformation found by the algorithm is incorrect and the isolated point set does not correctly correspond to the object-of-interest. This might be due to the over simplification of the scan occurring during the down sampling phase. Down sampling may also cause inaccuracies in the calculation of normal vectors. As explained previously, the accuracy of the normal vector calculation step is a key in the recognition and isolation process. Therefore, for lower density ratios, the object may not be represented sufficiently densely, which fails accurate normal vector calculation, and consequently, the object isolation given a cluttered point cloud.

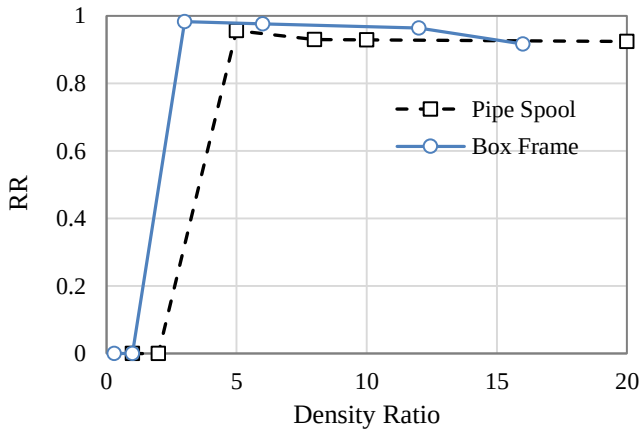

Figure 0-11. Effect of density on the recognition rate

The processing time reported in Table 0-5 and Table 0-6, is the time required for the alignment of the 3D model within the point cloud. The isolation time, which requires nearest neighbor calculation, and a post ICP refinement is excluded from the processing time reported in the results. The post-processing time for calculating the closest points and refining the match is expected to be exponentially increasing as the density of the point cloud increases (Rusinkiewicz and Levoy 2001).

4.4.2.2 Clutter

For investigating the effect of clutter on the object recognition and isolation framework, the experimental objects are tested under various circumstances with varying clutter. The 3D point cloud

used as the *Scene* is tested with an incrementally increased clutter around the object-of-interest. For quantifying the amount of clutter in the *S*, *clutter ratio* is defined as:

$$Clutter\ ratio = \frac{\|S - (S \cap s)\|}{\|s\|} \qquad (4.3)$$

in which, *S* is the 3D point cloud (*Scene*), and *s* is the object-of-interest. In other words, clutter ratio is the proportion of the amount of clutter to the size of the object-of-interest. The clutter ratio is dimensionless. The recognition rate (*RR*), as defined previously, is then calculated for each clutter ratio. Experimental results for the PS and BF objects are summarized and reported in Table 4-7 and Table 0-8.

Table 4-7. Summary of the analyses on the effect of clutter on the critical metrics for Pipe Spool

Clutter ratio	Number of points	RR	RMS (*cm*)	Time (*sec*)
51.295	322191	0.764	1.30	20.9
12.191	81272	0.929	1.28	13.2
7.466	52156	0.974	1.28	15.3
1.473	15236	0.985	1.28	8.1
0.707	10514	0.984	1.28	0.8

Table 0-8. Summary of the analyses on the effect of clutter on the critical metrics for Box Frame

Clutter ratio	Number of points	RR	RMS (*cm*)	Time (*sec*)
20.794	322191	0.764	2.81	17.4
17.604	279072	0.929	2.81	15.8
9.579	158692	0.974	2.81	13.2
5.087	91302	0.985	2.83	12.1
3.053	60796	0.984	3.69	10.9

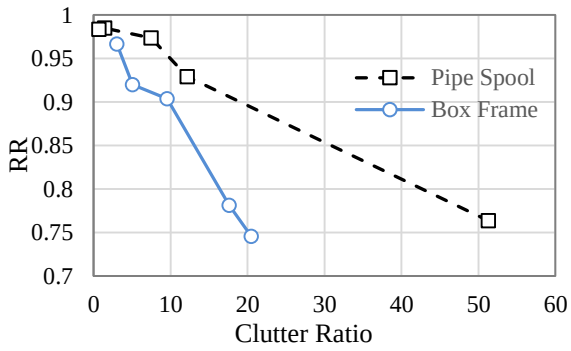

Figure 0-12. Effect of clutter on the recognition rate

As seen in Table 4-7 and Table 0-8, the recognition rate decreases as the clutter ratio increases. It signifies that clutter presence affects the accuracy of the isolated object from a point cloud; however, the object is still successfully and robustly found. The RMS value of the isolated object is calculated for various clutter ratios. For the PS object, the average RMS (root mean square) value is 1.28 *cm* with a standard deviation of 0.01 *cm*. For the BF, average RMS value is 2.99 *cm* with a standard deviation of 0.35 *cm*. Low standard deviation signifies that the isolated object remains unchanged for the various clutter ratios. Figure 0-12 shows how the recognition rate changes with the clutter ratios for the PS case.

As seen in Figure 0-12, recognition rate decreases as the clutter ratio increases for both cases. This might be due to the existing noise in the scene. However, the object (3D model) is successfully aligned within the point cloud, and it is therefore successfully isolated from the scene. The level of recognition rate achieved even in the most cluttered case in the experiments is sufficiently reliable for enhancing further assessments on the isolated object. Such further assessments include quality control, deviation analysis and discrepancy quantification (Nahangi et al. 2015, Nahangi and Haas 2014). Figure 0-13 shows a typical example of the effect of existing clutter on the isolation of the PS object. In this case, clutter is gradually removed manually, and the framework is applied. Figure 0-13-(a) shows the fully cluttered point cloud (original scan), and Figure 0-13-(e) shows the least amount of clutter existing around the object-of-interest (PS object). Figure 0-13-(f) and Figure 0-13-(g) show the final results after the recognition and isolation framework is applied.

4.4.2.3 Completeness

In order to investigate the effect of completeness on the isolation framework, various combinations of the comprising branches and elements of the investigated objects are tested. The desired pipe spool to be isolated from the point cloud is comprised of multiple branches. Branches are manually removed from the input point cloud to test the capability of the framework for recognizing and isolating the object, in the case of incomplete and missing data. Incomplete data might be due to occlusion or the

line-of-sight during data acquisition. Completeness ratio is defined as the metric to quantify completeness vs. incompleteness of the data. Completeness ratio is the proportion of the size of the object in the imported point cloud, to the size of the completely scanned point cloud of the object-of-interest. It should be noted that density and clutter ratios are kept unchanged while incompleteness is being investigated.

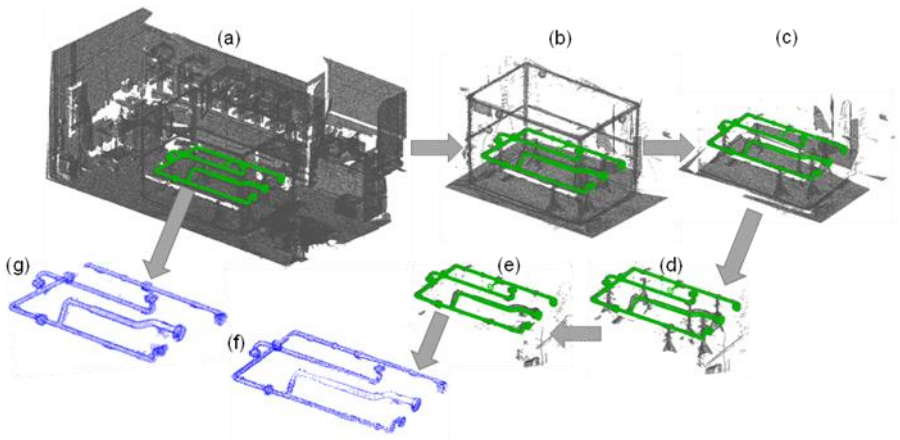

Figure 0-13 Typical results for the effect of clutter on the accuracy of the object extracted from 3D point clouds. A cluttered scene is investigated in five stages: (a) the scene is fully cluttered, (b) background is removed, (c) some obviously unwanted objects are removed (structural components), (d) planar clutter (ground, walls and ceilings if any) is removed, (e) secondary and support attachments (holder jacks and stands) are removed. (f) The isolated object from manually cleaned point cloud. (g) The isolated object from fully cluttered point cloud.

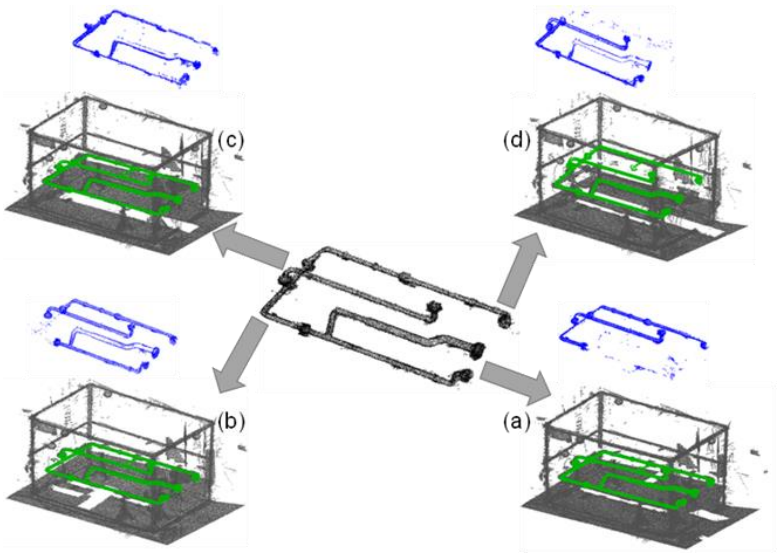

Figure 0-14. Object recognition and isolation with incomplete and missing data. The point cloud in the middle shows a completely scanned object. Each branch is manually removed in four different steps and the capability of the algorithm developed is tested under missing and incomplete data. The object recognition only fails in (d) because the removed branch contains critical features in finding the correct transformation. In cases (a), (b), and (c), object recognition and isolation is successful.

Rather than the recognition rate, success rate is calculated for measuring the effect of incompleteness. Success rate (SR) is a binary metric (1 if successfully isolated and 0 if isolation is failed).

Table 0-9 and

Table 0-10 show the effect of incompleteness on the success rate for recognizing and isolating the investigated objects.

Table 0-9. Effect of completeness on isolating Pipe Spool from a cluttered laser scan

Completeness ratio	Number of points	SR	Time (sec)
0.958	74177	1	22.8
0.923	77842	1	22.9
0.913	74979	1	23.1
0.903	73363	0	Failed

Table 0-10. Effect of completeness on isolating Box Frame from a cluttered laser scan

Completeness ratio	Number of points	SR	Time (sec)
0.993	157631	1	20.2
0.985	156449	1	20.1
0.980	157631	1	19.7

As reported in Table 0-9 and

Table 0-10, a threshold in the completeness ratio must be met in order to ensure recognizing and isolating the objects successfully. Figure 0-14 illustrates how various branches are manually removed from the imported point cloud into the recognition framework. Various branch removal results in different completeness ratios that affects the success rate in the recognition framework.

4.4.3 Parameters effectiveness

The effective parameters reported in Table 0-2 were established using experiments in this study. However, two scenarios were identified that caused the finding algorithm to fail using the proposed parameters. The two scenarios are, (1) multiple objects being recognized and (2) failure to detect object of interest. In order to resolve the first issue λ_s was increased so that only the object with the maximum overlay percentage would remain as the isolated object. In the second case, the required time for RANSAC algorithm was increased up to 40 seconds and in cases λ_s was also reduced. To measure the effectiveness of the proposed parameters, an effectiveness ratio (ER) was defined. Effectiveness ratio was defined as the proportion of the times that the object of interest was isolated using the proposed set of parameters to the total number of times the object of interest was successfully isolated from the point cloud. Table 0-11 and Table 4-12 illustrate the results of using the proposed parameters.

Table 0-11. Effectiveness ratio for the proposed parameters on isolating Pipe Spool from a cluttered *laser scan*

Parameter	Value	ER

λ_s	0.15	0.92
t	20 *sec*	0.92

Table 4-12. Effectiveness ratio for the proposed parameters on isolating Box Frame from a cluttered laser scan

Parameter	Value	ER
λ_s	0.15	0.91
t	20 *sec*	0.91

Results show that the proposed parameters are sufficiently robust to be integrated with the automated finding algorithm.

4.5 Conclusion and Future Work

A model-based 3D object recognition and isolation framework was adapted and examined to extract the construction elements of interest from cluttered laser scans. The framework was desired to be sufficiently robust and therefore reliable to be integrated with the automated and integrated construction process controllers. In summary, this method employs a local feature of point pairs as a descriptor or a local signature. The methodology for 3D object recognition and isolation has three primary steps:

1- Model library generation for the elements existing in the building information model. The library of objects and their describing features calculated are stored in a hash table that enhances an efficient and quick search.

2- Scene representation by calculating the features for potential point pairs and testing hypotheses in a RANSAC-based hypothesis testing engine.

3- Matching and refining by transforming the 3D model on the acquired point cloud and refining the match by a post-ICP registration step.

An experimental study is performed for two different construction objects: a pipe spool (PS) as an MEP component, and a box frame (BF) as a structural element. Density, clutter, and completeness are thoroughly investigated to test the robustness of the framework. Processing time and recognition rate are recorded as the verification metrics in the various cases are tested and investigated. Some interesting observations and insights of the experimental study are listed as follows:

- It was shown in the experiments that if a threshold value is met as the required level of density, the object-of-interest is robustly isolated from the point cloud.

- It was demonstrated that even with a massively cluttered point cloud, the algorithm is capable of extracting the object from the clutter surrounding it; however, the level of noise increases inevitably, as the clutter increases. It therefore requires a finer post refinement for noise removal.
- The algorithm also works in cases that an incomplete point cloud is imported to find and isolate the object-of-interest. This capability addresses the unavoidable occlusion challenge on the data acquisition phase.

The framework in this chapter can be used to find a wide range of curvilinear and rectilinear construction components and elements, in contrast with the previous methods that were focused on some specific and explicit geometries. Since the feature set used to represent an object is not limited to an explicit geometry, it can even extract very complicated geometries including sophisticated connections and surfaces. This was verified and validated by testing two relatively sophisticated geometries within various construction sectors (i.e. MEP and structural elements).

As the framework is robust to the density and completeness of the point cloud acquired to represent the scene, there is an emerging potential for integrating the framework with image-based 3D point cloud techniques. Currently, inadequate number of images or insufficient level of overlap between the images are the sources of inaccuracies in the image-based and structured-light-based techniques for 3D point cloud generation. However, because the developed framework is robust to incompleteness and density of the point clouds used, such inadequacy might be bypassed. Moreover, considering that the utilization of image-based frameworks for data acquisition is less expensive comparing to the laser-based techniques, it is important to explore the integration of the framework with image-based or structured-light-based sensors in future research.

Although the recognition and localization of the 3D model is performed in a significantly faster timeframe, the isolation module takes the dominant part of the time required for processing. Faster and more effective search strategies such as kd-tree and graph theory may improve the processing time for the isolation, and this inadequacy may be appropriately addressed. This could be a potential research direction for future work. In the case that the isolation module is effectively utilized and the processing time is reasonably quick, the entire framework may be integrated with structured-light based data acquisition sensors for the development of (near) real-time process controllers. Such integrated platforms are currently being developed by the authors.

The features and descriptors of construction objects can be calculated and stored as a new dimension to the BIM, considering the fact that the model library generation phase is performed in the offline phase. It can consequently save the processing time for model library generation, if the shape

descriptors are integrated with the BIM. This new addition is currently under investigation by the authors.

While the investigated framework proved to be somewhat effective, it was not used as part of the developed software. The developed software was aimed to be highly practical for the use of pipe fitters on the fabrication floor. The investigated algorithm suffers from two drawbacks which will make its use impractical in industry: (1) The software requires two input variables: (a) overlap percentage, and (b) termination time. In order for the software to operate properly the user has to have priory knowledge on how to choose the two variables. (2) Purchasing the license key for the used software package could be highly costly. A semi-manual algorithm was used instead. The utilized algorithms is more intuitive from the user's perspective, less costly and takes less time. A three pair point matching method is used were the workers have to only select three corresponding points between the acquired scan and model point cloud to superimpose the point clouds.

Chapter 5

Optimal Nearest Neighbour Calculation for Automated Retrieval of Construction Elements from Cluttered Point Clouds

This chapter is based on the following published article in the proceedings of Resilient Infrastructure 2017, Vancouver, with the same title. Minor changes are made on some parts of the article to be more consistent with the body of the thesis. Thus, the content of this chapter is not exactly the same as the paper.

The contribution of the author in this publication was conducting the experiments, data analysis and partially drafting and editing the manuscript.

5.1 Introduction

3D image acquisition tools are becoming more prevalent in the construction industry as they have become more affordable and as design information shifts from traditional 2D drawings to 3D BIM models. 3D scanners enable their users rapid access to accurate information regarding the geometric conditions on a job site or in a construction facility. Traditionally, laser scanners have been the most reliable and accurate source of 3D data (Bosche and Haas 2008b) .Photogrammetry and structured light scanners offer lower cost solutions but with compromised accuracy (Golparvar-Fard et al. 2009b). Increased competition, demand and innovation is pushing the development of all areas of 3D data acquisition and is resulting in higher quality technology being available at increasingly lower prices.

One area of substantial use of these tools is the development and implementation of scan vs. BIM frameworks for early detection of construction defects. Typically, 15% of construction rework is due to late detection of defective components (Burati Jr et al. 1992). Late detection of defects can result in project schedule delays, cost overruns and cost propagation in projects with sensitive schedules. Consequently, early detection of defects in construction projects has become a prime concern for stakeholders. Geometric non-compliance is a major source of defects in construction. Advancements in 3D image acquisition tools have enabled users to have access to geometric data in real-time and make early detection of such deficiencies feasible (Brilakis et al. 2011). Comparing the design information to the as-built data provides an assessment of the fabrication quality and can be done by superimposing the 2 point clouds (3 by n matrices of geometric coordinates) to inspect the geometric compliance of the completed assembly (Chapter 2).

One of the challenges with comparing a scan point cloud with a model point cloud is that the scan contains clutter points, which are points from the object's environment that get captured when acquiring the scan (Chapter 3). To compare the two point clouds the object of interest must be isolated in the scan by removing the clutter points. To isolate the object of interest, the object must first be found within the point cloud before the clutter can be removed. Chapter 3 thoroughly investigated and examined a robust framework for automated object finding. Once the object of interest is found, scene point cloud will be superimposed onto the design point cloud, post-processing algorithms have to be employed to properly isolate the object of interest by removing the clutter. Automating the accurate extraction of objects of interest from spatial data is the fundamental enabler for further developments in automated spatial analysis. The goal when decluttering a point cloud is to isolate the points that correspond to the object of interest from a complete point cloud without removing points belonging to the object of interest Figure 5-1 shows the process for isolating an object of interest from a scene point cloud.

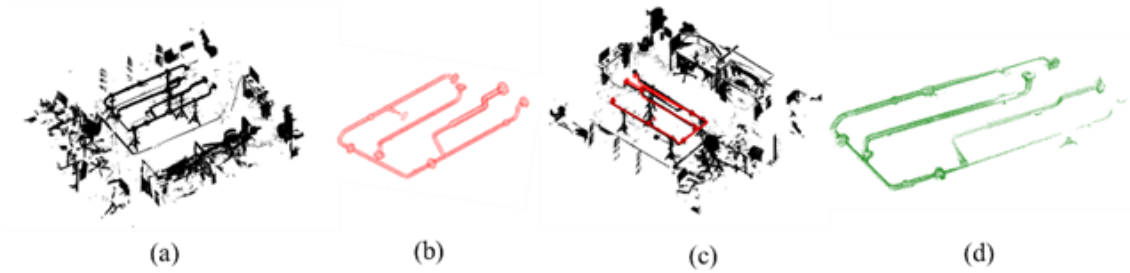

Figure 5-1. Abstract of the process from scan acquisition to object isolation. (a) Acquired scan of the scene including clutter points. (b) BIM model of the object of interest in point cloud format. (c) Model superimposed on the scan. (d) Resulting point cloud

Classification methods have been investigated in literature and multiple algorithms have been developed by researchers. One such application of the algorithms is clutter removal, where classification methods facilitate the retrieval of points on the object of interest from the point cloud. These methods include graph-cut based method (Pan et al. 2016) and structure less nearest-neighbor techniques composed of K-nearest neighbours methods (Bhatia 2010). Nearest neighbor search algorithms have been found to be the most effective (Bajramovic et al. 2006) for removing clutter. A variety of KNN searching algorithms are used in point cloud modeling (Zhao and Meng 2009) to calculate surface curvature in addition to noise and clutter removal.

KNN is acknowledged as a simple, robust and effective method for classification of points as belonging to either the object of interest or to the clutter. Nonetheless, KNN still faces two main shortcomings as a post-processing technique (Jiang et al. 2007): (1) the distance function used to measure the differences and similarities between the 2 point clouds is the standard Euclidean distance, and (2) the neighborhood

size is artificially assigned as an input parameter K, biasing the algorithm by the arbitrary nature of the K value chosen. Since the accuracy of the algorithm is highly dependent on the K value, researchers have proposed several models for selecting this value. For example, Xie proposed a model named Selective Neighborhood Naive Bayes, also known as SNNB (HWLZLM, SNNB). The basic idea is that multiple K values are tested and the one with the highest estimated accuracy to classify the data is selected. As stated in (Guo et al. 2003), the simplest approach to selecting the K value in this model is to run the algorithm multiple times with different K values and to identify the K associated with the best trial.

To evaluate the success of the exclusion of clutter from the point cloud, the method presented in this chapter uses two measures: (1) number of points erroneously remaining in the point cloud,(2) number of points erroneously removed from the point cloud. The main contribution of this chapter is the selection of an optimal K value depending on the number of points in the as-design point cloud and in the as-built point cloud. The method was administered on cylindrical objects (pipe spools). The accuracy of the model was tested and found to have an R square value equal to 0.75.

The following sections of this chapter is organized as follows. In Section 5.2, a survey of 3D imaging methods in construction and post-processing techniques for finding the object of interest in a point cloud is provided. In Section 5.3, the methodology for the experiment conducted is described. In Section 5.4, includes details of applying the proposed methodology. Discussion and future works has been discussed in Section 5.5.

5.2 Background

Two main areas have been investigated: (1) the use of 3D-imaging in construction, and (2) post-processing algorithms for removing clutter in point clouds. A focus was placed on K-Nearest Neighbor post-processing algorithms as this study utilized a KNN technique as the primary method for the clutter removal algorithm.

5.2.1 3D-imaging in construction

Currently, ground-based laser scanners are the superior acquisition technology used as they can provide the highest accuracy and density point clouds. Bosche and Haas used laser scanners to develop a framework for construction object recognition using the projection of the BIM model onto the relative position of the scanner (Bosche and Haas 2008b). Turkan presented a framework for automatic project schedule updating based on the object recognition method previously developed by Bosche (Turkan et al. 2012b). Nahangi developed a method for progress tracking using robotics analogy and forward kinematics with a focus on mechanical, electrical and piping components (Nahangi et al. 2015).

Coupling 3D design models with the acquisition of high quality 3D spatial data has made it possible to directly compare a completed industrial component with its design model. Akinci presented a method for comparing as-planned 3D design information (CAD model) with periodic imaging of critical construction components (Akinci et al. 2006b). A great deal of research has gone into using 3D designs with 3D spatial data to evaluate pipe spool assemblies as they are critical for industrial construction projects including refineries and power plants. Pipe spool assemblies are typically prefabricated in shop and then sent to the site to be assembled which requires accurate fabrication and an incident-free transportation to the site. This has prompted researchers to investigate methods to better regulate the prefabrication to ensure that spools are being fabricated within tolerance. Nahangi developed an automated approach for monitoring and assessing fabricated pipe spools and structural systems using automated scan-to-BIM registration (Nahangi, and Haas 2014, Nahangi et al. 2015). The method reliably detects the presence of dimensional non-compliance. Lee introduced a new method to extract critical points and centerlines in pipelines to reconstruct the model and compare it with BIM for progress tracking (Lee et al. 2012). These methods still leave room for improvement and further development to better assess the as-built conditions of pipe spools.

5.2.2 Post-processing algorithm: retrieval of object-of-interest

Manually removing clutter is a tedious task that requires automation to allow it to be part of a practical 3D imaging application in construction. Researchers have investigated and developed multiple frameworks using Nearest Neighbor (NN) methods for finding and recognizing objects of interest in point clouds (Czerniawski et al. 2016b). NN methods can be classified into two categories: 1) Structure Less NN techniques, which overcome the memory limitation issue, where the whole data sets are classified into training data and sample data points and distance is then calculated to find the nearest neighbor, and 2) Structure Based NN algorithms which reduce the computational complexity by structuring the data into different organisations such as Ball Tree (Liu et al. 2006), KD-Tree (Friedman et al. 1977) and NB-Tree (Kohavi 1996). In this study, a KD-Tree was used to structure the points of the point cloud in a 3D space. An Approximate Nearest Neighbor Search algorithm was then performed on the sorted data to extract the desired points from the point cloud. Jiang surveyed improved KNN search algorithms that either improve the distance function, the neighborhood size or the class probability estimation (Jiang et al. 2007).

The main contribution of this chapter is to develop and evaluate an effective process that facilitates the retrieval of an object from a point cloud scene. The method was applied to cylindrical objects, pipe spools, and presents a mathematical solution to determine the optimal K-value to retrieve an object of interest from a cluttered point cloud.

5.3 Methodology

The methodology for optimal object retrieval of cylindrical objects from point clouds and the flow of information between various components is illustrated in Figure 5-2. The objective of the proposed method is to determine a mathematical solution to find the optimal threshold value in the decluttering process utilizing a KNN (K Nearest Neighbour) algorithm. KNN is performed to remove points in the scan point cloud that do not correspond to the model point cloud. For each point in the model, K points in the scan point cloud that are closest to that point will be selected and stored in a new point cloud or matrix. The goal is to store all points from the scan that correspond to the model and remove all points that are considered clutter. Increasing the threshold value (K) in the algorithm will increase the number of clutter points that are accepted as corresponding to the model (False Positive) and decreasing the K value will increase the number of points corresponding to model that are incorrectly deemed to be clutter (False Negative) Figure 5-5.

Two criteria have been defined to determine how successfully desired points are extracted from the scan for each K value. The criteria are defined as follows:

$$\text{Void Rate (VR)} = \frac{\text{Number of points corresponding to the model and removed erroneously}}{\text{Number of points in the point cloud after applying KNN}} \quad (5.1)$$

$$\text{Noise Rate (NR)} = \frac{\text{Number of clutter points that are incorrectly accepted}}{\text{Number of points in the point cloud after applying KNN}} \quad (5.2)$$

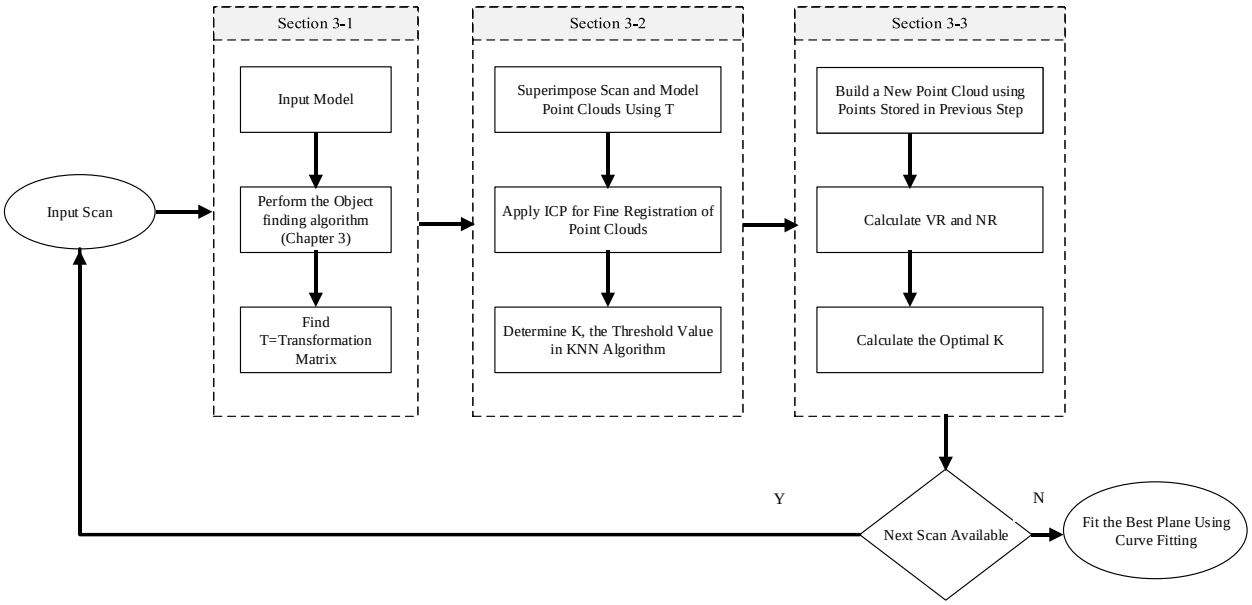

Figure 5-2. Research methodology and the flow of information between different components.

The optimal K value is one where both VR and NR are minimized. Assuming that minimizing both criteria is of equal importance, the optimal value will be determined by intersecting VR (Void Rate) and NR (Noise Rate) trend lines (Figure 5-6 and Figure 5-7). Experiments were carried out on a pipe spool assembly in Ralph Haas Infrastructure and Sensing Analysis laboratory at the University of Waterloo. The assembly measures approximately 2m× 1.5m consisting of four individual pipe spools. (Figure 5-3)

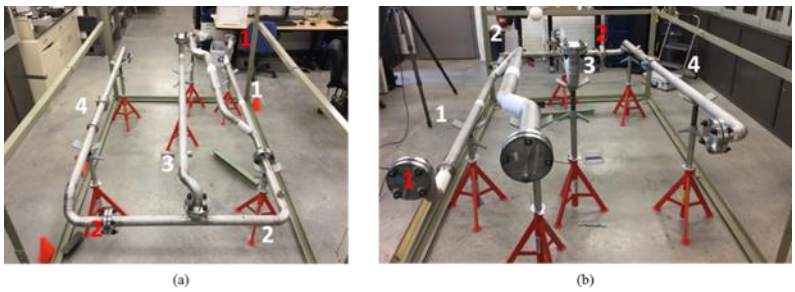

Figure 5-3. The test pipe spool assembly. Angular distortions to the assembly were induced at the flange numbers one and two, numbered in red. Branches are numbered in white for further reference in the article.

5.3.1 Finding the object of interest

A set of experiments was carried out on an industrial pipe spool to verify the proposed methodology for optimal clutter removal using a KNN algorithm on cluttered 3D point clouds. The object-of-interest,

the pipe spool, is located in a laboratory environment and is surrounded by other unwanted objects that get scanned resulting in noisy point clouds.

Five different scenarios were generated using the pipe spools. Four scans were taken from different locations for each scenario. The four scans were taken to ensure that a complete representation of the assembly in each scenario was captured. The first scenario is the case were the assembly complies with the design. In second scenario a rotational error has been imposed on flange number 1. The third scenario has a rotational error imposed at flange number 1. In the final two scenarios, the assembly was disassembled into its component spools (Figure 5-4) and the component spools were each individually tested for optimal extraction. In the fourth scenario all the individual spools comply with their designs and in the fifth scenario deviations have been imposed on branches one and four. A total of 11 scene point clouds were acquired.

(a) (b)

Figure 5-4. Disassembled spools for scenarios four and five. (a) All spools are compliant to the design. (b) Branch numbers one and four have been distorted.

Once scanning is completed the object must be found in the scans. This study utilized the algorithm provided in Chapter 3 (Papazov and Burschka 2010) to find the object of interest. This algorithm requires two inputs. The first input is the BIM (as-designed) model in Stereo Lithography (STL) format. The second input is the scene or the as-built point cloud. Once the two inputs are loaded into the object finding algorithm, a transformation matrix is computed and outputted. The transformation matrix is a 4×4 matrix which consists of a 3×3 matrix describing a 3D rotation of the point cloud and a 3×1 vector describing the translation. From the eleven acquired scenes, seven had the object of interest detected by the object finding algorithm.

5.3.2 Point cloud isolation

In order to ensure that all the surfaces of the object of interest (pipe spools) were captured, scans were taken from four perspectives. These four scans were then merged into a single point cloud. The operation of merging point clouds of the same scene, taken from different angles, is referred to as registration. To register a point cloud, three corresponding points must be identified and selected in each scan. White spheres (shown in (Figure 5-3) were placed in the scene to be used as the corresponding points between scans for registration. "Faro Scene," a commercially available software was used to merge the point clouds together. Once the scans were registered, the resulting point cloud was down sampled from its initial two million points to approximately two hundred thousand points. The initial point cloud was too dense for the purpose of this study and down sampling allowed the computation time to be reduced for the algorithm. Down sampling populates a new point cloud by sampling points from the original point cloud and was done according to Poisson-disk distribution which resulted in the point cloud where the points were equally distributed across all surfaces. In other words, an equal number of points would be found for any two arbitrarily chosen surfaces of equal area. For more information on the down sampling algorithm please refer to (Corsini et al. 2012).

Given the two point clouds and the transformation matrix the extraction of the object of interest was calculated (see Algorithm 1). A third point cloud was calculated using stored points from the scene point cloud that have been determined to correspond to the model point cloud. The filtering process was performed using a KNN algorithm. This study includes an iterative step where the K value changes to examine its effect on the success of object extraction. The processes in this section are summarized below in Algorithm 1.

Algorithm 1: Scene representation, matching and Isolation

Input: Model point cloud ($\mathbb{M}$), Scene point cloud (S) and Transformation matrix (T)

Output: Isolated object-of-interest point cloud (S_i) from S: $S_i \subseteq S$

Superimpose M on S using T

Perform ICP for fine registration

Select a K value

Create a new K $\times$ M matrix (N)

Repeat M times

For $M_i \in M$

- Find K nearest point from (S) to (M)
- Store points in matrix (N)

End For

End Repeat

Report N

5.3.3 Calculation of Void Rate and Noise Rate

After down sampling and performing Algorithm 1, the success of Algorithm 1 was measured by performing Algorithm 2, described below. The success of object extraction was measured with two defined criteria. As explained in Section 5.3.1, Void Rate and Noise Rate are the two parameters for measuring the accuracy of the extraction. The accuracy was changed by changing the K value. Figure 5-5 shows an example of a false positive and a false negative.

Figure 5-5. Challenges of removing clutter points without removing points on the object of interest. (a) Example of remaining clutter points after clutter removal for K equal to 8. (b) Example of removed points from the object of interest for the same K value.

Algorithm 2: Void Rate and Noise Rate at a Certain K value

Input: Model point cloud ($\mathbb{M}$), Scene point cloud (S) ,Transformation matrix (T) and Isolated point cloud (N)

Output: Noise Rate (NR) and Void Rate (VR)

$K = \{1, 10, 50, \sqrt{M}, \sqrt{S}, \frac{\mathrm{M}}{\mathrm{S}}\}$

Repeat for all $K_i \in \{K\}$

- Manually remove remained clutter points in (N) and store the trimmed point cloud as (N_2)
- Manually remove clutter points from (S) and store the trimmed point cloud as (N_3)
- n = number of points in N_2

- m = number of points in N_3

- q = number of points in N

Remained noise after decluttering = q-n

Mistakenly removed points after decluttering = m-n

- Calculate VR and NR

  - VR = $\frac{m-n}{q}$

  - NR = $\frac{q-n}{q}$

End Repeat

Report *VR, NR* and K_i

5.3.4 Best Fit and Optimization

After performing Algorithm 2, a set of VR and NR values was calculated where each member of the set was calculated based on a distinct K value. To find the optimal K value for each scan, NR and VR values were graphed with respect to their corresponding K value as shown in Figure 5-6 . Once tabulated, trend lines were fitted to each data set. The optimal K value for each scan was then calculated based on the intersection of the trend lines. The intersection point was found by solving the system of equations created by the two trend lines. This process was repeated for all of the scans acquired. MATLAB's curve fitting tool was used to fit the data set of optimal K values and the size of the corresponding model and scan point clouds to a mathematical model. The results of this section are discussed in Section 5.4. Algorithm 3, used to fit the mathematical model, is described below.

Algorithm 3: Finding the Best Fit with Varying K value

Input: Model point cloud ($\mathbb{M}$), Scene point cloud (S) , Set of Optimal K values of testing sample {K'}

Output: equation of best fit plane

- Normalize M and S values

- Import M, S and K' value into the optimization tool

- Use linear regression to find the best fit plane

- Calculate $R^2$to evaluate goodness of the plane

Report parameters of the fitted plane *and* R^2

5.4 Results

Applying Algorithms 1 and 2, as defined in Section 5.3, will generate VR and NR values for each K value used for each scene considered. Table 5-1 provides a summary of the results obtained by applying the algorithms on scene one (compliant spool assembly).

The headings used in the table are defined as follows:

M: number of points in model point cloud

S: number of points in scan point cloud

K: threshold value used in KNN search algorithm

N: number of points in isolated point cloud

m: number of points after manually removing points that are considered as noise in the initial scan point cloud

n: number of points in the isolated point cloud (after applying the clutter removal algorithm) that correspond to the object of interest

q: number of points in the isolated point cloud

Table 5-1. VR and NR values computed using different K values for scene 1

M	S	K	N	m-q	n-q	q	VR	NR
12061	81272	1	3546	33	2648	6161	0.42	0.005
12061	81272	7	5447	437	1151	6161	0.18	0.07
12061	81272	10	5668	481	974	6161	0.158	0.078
12061	81272	50	6882	776	55	6161	0.009	0.125
12061	81272	110	7464	1307	4	6161	0.006	0.2121
12061	81272	285	7935	1798	24	6161	0.003	0.29

Figure 5-6 shows the curves that were fit to the data summarized in Table 5-2. VR and NR must be minimized to find the optimal K value for each scan. To do so, a trend line was fitted to both VR and NR data sets. The optimal K value was calculated as the solution to the system of equations created by the VR and NR trend lines. Figure 5-6 graphically depicts the calculation of the optimal K value for scene number one.

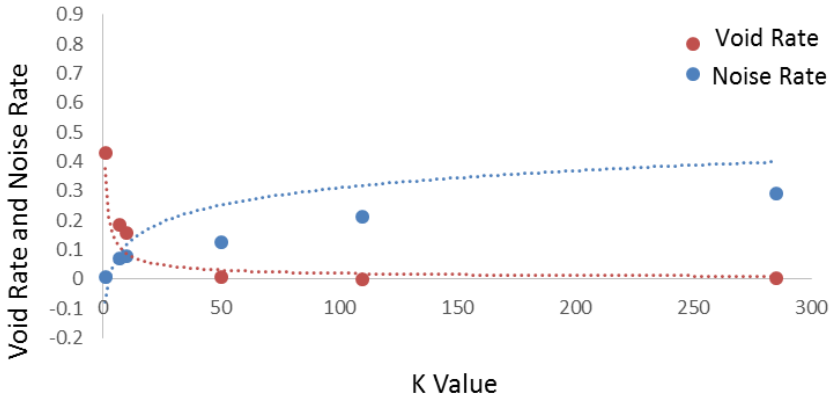

Figure 5-6. Calculation of optimal K at the intersection of VR and NR trend lines.

For each scan, a logarithmic equation was used to fit a line to the void rate (VR) data points while a power equation was used to fit a line to the noise rate (NR) data points. Equations (5.3) and (5.4) below illustrate the general formats of equations that were used to calculate the trend lines that best fit the data points.

$$Y = a \ln x + b \text{ and } {R_1}^2 \qquad (5.3)$$

$$Y = \acute{a}x^{\acute{b}} \text{ and } {R_2}^2 \qquad (5.4)$$

In equation (5.3), ${R_1}^2$ denotes the root mean square values between the observed data points and the corresponding VR values predicted by the trend line. Similarly, ${R_2}^2$ denotes the root mean square values between the observed data points and the corresponding NR values predicted by the trend lines. Solving the system of equations defined by equations (5.3) and (5.4) provides the optimal K value for each scan.

Table 5-2. Parameter values for fitted lines and subsequent optimal K calculation.

Scene No.	a	b	$\acute{a}$	$\acute{b}$	${R_1}^2$	${R_2}^2$	$K_{optimal}$
1	0.0487	-0.0195	0.832	-1.12	0.92	0.81	11
2	0.036	-0.035	0.2478	-0.495	0.87	0.83	17
3	0.052	-0.0417	0.0458	-0.273	0.96	0.46	6
4	0.196	-0.2294	0.0965	-0.122	0.66	0.45	7
5	0.2938	-0.2586	-0.021	0.13	0.81	0.47	5
6	0.1371	-0.1559	0.4918	-0.68	0.73	0.80	8
7	0.0982	-0.0573	1.0744	-0.65	0.88	0.66	9

A 3D plot was generated with the size of the scan point cloud on the x axis, the size of the model point cloud on the y axis and the optimal K value computed on the z axis. A best fit plane was then fitted to this plot. The equation of this best fit plane provides a mathematical solution to find the optimal K value based on the size of both the scan and model point clouds. Equation (5.5) shows the parametric form of the equation used to fit the plane. Table 5-4 shows the inputs and predictions that the model used to generate the variables.

$$K_{optimal} = a_1 M + a_2 S + a_0 \qquad (5.5)$$

M and S denote to the number of points in the scene and model point clouds, respectively. a_1, a_2 and a_3 are the coefficients that were determined. MATLAB's curve fitting tool was used to best fit the plane. Table 5-3 and Table 5-4 summarize the parameters calculated within their 95% confidence interval. Table 5-4 shows both the observed and predicted optimal K values, along with the R^2 for plane that was fit.

Table 5-3. Coefficients calculated for the best fit plane.

	a_0	a_1	a_2
Most Probable Value	9.14	2.706	2.05
Lower Bound Value Within %95 Level of Confidence	5.26	-1.52	-2.18
Upper Bound Value Within %95 Level of Confidence	13.02	6.93	6.27

To calculate the coefficients the input data had to be normalized. The mean and standard deviation for the number of points in the scan were calculated to be 9.3+e4 and 3.67+e4 respectively. The number of points in the model point clouds was also standardized with a mean value of 1.05+e4 and a standard deviation of 1.533+e3.

Figure 5-7 show a graphical representation of the plane fitted to the data and the residual values between the data sets and the predictive model.

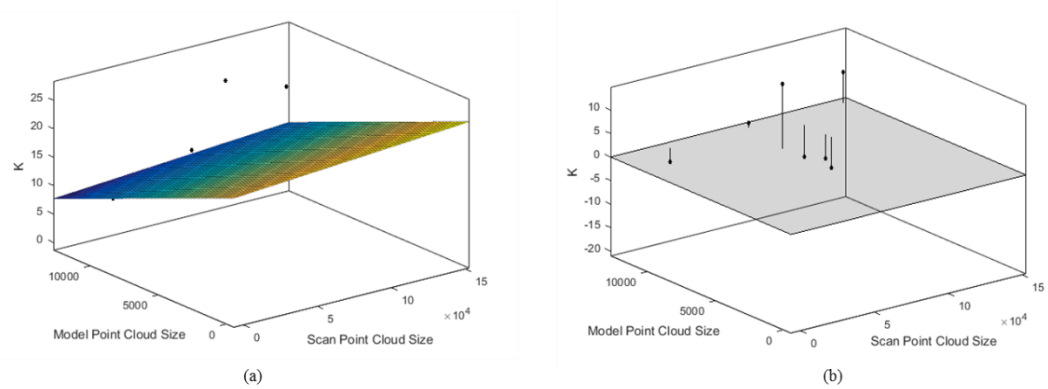

Figure 5-7. Graphical representation of the fitted plane to predict optimal K value. (a) 3D representation of the predictive model. (b) Residual values from the predictive plane.

To determine the goodness of fit, R^2 was calculated. R^2 was calculated by dividing the sum of squares due to regression (SSR) over total some of squares (SST).

Table 5-4. Comparison of the calculated K values and the predicted values using the fitted plane along with a measure of the goodness of fit.

	Observation		Predicted	SSE	SST	SSR	R^2
Scene Size	Model Size	Optimal K	Optimal K				0.75
81272	12061	11	10	1	3.45	0.73	
145265	12061	14	11	49	78.45	3.45	
28009	12061	6	9	9	9.87	0.02	
108007	8864	7	14	49	4.5	23.59	
108007	10841	5	12	49	17.16	8.16	
108007	9327	8	13	25	1.306	14.87	
74569	8864	9	15	36	0.02	34.30	
	Mean	8.6	Sum	218	114.85	1 880	

5.5 Conclusion and recommendations based on Chapter 5 research

This chapter of the thesis presented a case study in which clutter points were optimally removed from a scan point cloud. A mathematical closed form solution was provided for calculating the optimal K value for removing clutter points in a point cloud based on number of points in scan and model point clouds using a KNN algorithm. Experimental data was gathered by scanning a pipe spool assembly under different configurations with respect to the compliance of the assembly. The individual spools from the assembly were also experimented on individually to provide additional data points to develop a more accurate model. A plane was ultimately fitted to the data providing an R square value of 0.75.

To develop a more widely adaptable model, objects with different geometric shapes have to be tested using the developed algorithm.

While KNN is a simple, robust and effective method for classification of points as being either part of the object of interest or as clutter, it is ineffective when it is assessing a scan of an object that has a gross misalignment compared to its model. With respect to pipe spools, two examples of gross misalignment that make KNN ineffective are: when a pipe that is substantially longer than the design is used and when an elbow is installed with a 90^{o} rotation from the design. In both of these instances, KNN will not recognize the points in the scan that do not correspond to the model are part of the erroneous assembly and will remove these points as if they are clutter.

The authors will pursue more accurate prediction models such as, neural networks, Bayesian network and other machine learning algorithms to develop a more robust solution for clutter removal. However, depending on the application, mathematical closed form models may not be accurate enough and are vulnerable to errors.

Chapter 6

Thesis Summary, Conclusions and Future Work

6.1 Summary

3D imaging technologies have the potential to be employed for checking the work in progress against the design information and acceptance specification industrial construction processes. However, a number of challenges exists for these technologies to be applied in industrial pipe spool fabrication facilities. One of the challenges is the necessity for real time 3D point cloud acquisition. Any acquisition technology/tool that disrupts the fabrication process is not appreciated by the industry. That is why Chapter 3 focuses on the use of low cost range cameras for real time data acquisition. A number of challenges were identified for the current state of these technologies for large objects. These challenges include: (1) being vulnerable to movement due to utilization of inaccurate sensors for localization and mapping, and (2) being sensitive to the lighting condition, object colour (reflectivity), short scanning range (up to 5 m), and non-linear increase in error while moving away from objects. However, the rate to which computational processing power is increasing coupled with more accurate sensors becoming available at lower costs, has led the author to believe that these challenges will be addressed in near future and the application of these sensors will increase substantially.

Once a reliable and accurate point cloud is captured, two challenges are identified. Chapter 4 focuses on experimenting and adapting an object finding method to address the major object finding challenges in construction. Occlusion, clutter and incomplete scans are unavoidable parts of scanning in construction sites. Manually selecting an object of interest in a point cloud is a time consuming process, which has to be semi- or fully automated. The examined method works in cases where an incomplete point cloud is imported to find and isolate the object-of-interest. This capability addresses the unavoidable occlusion challenge in the data acquisition phase. It was also shown that if a threshold value is met as the required level of density, the object-of-interest is robustly isolated from the point cloud. And finally, it was demonstrated that even with a massively cluttered point cloud, the algorithm is capable of extracting the object from the clutter surrounding it; however, the level of noise increases inevitably, as the clutter increases.

To improve the clutter removal process, Chapter 5 focuses on a mathematical solution to optimally choose the threshold value in the KNN algorithm. The optimization is set to minimize number of outliers while minimizing the number of removed points on the object of interest.

6.2 Research contributions and conclusions

The contributions of the work are as follows: (1) a number of challenges and advantages of applying low cost range cameras using structured light technology for quality control in pipe spool fabrication facilities were identified and discussed, (2) a robust object finding method was adapted and studied experimentally to address major challenges in construction, (these challenges include: occlusion, clutter, and density variation,) and (3) a mathematical closed form solution was provided to optimize the threshold value used in KNN algorithm to optimally remove clutter points.

Following from these contributions are three conclusions:

(1) While a number of challenges were identified when using these low cost range cameras, their resulting point clouds were sufficiently accurate on smaller scans. This means that these sensors, if applied correctly, can be valuable for real time applications.

(2) With increased computational power, a one-to-one comparison of point sets utilizing RANSAC could be applied to find MEP components automatically and robustly, even in highly occluded and cluttered point clouds. For more practical purposes, a semi-automated method where users have to choose three corresponding points between the scan and model point clouds could be utilized. Using these three points, a PCA (principal component analysis) will be applied to roughly align the two point clouds followed by an ICP (iterative closest point) to locally optimize the overlay between the scan and model.

(3) The success of the clutter removal algorithm is highly dependent on the used threshold value of K. The optimization provided will minimize the number of outliers and removed points from object of interest. For more accurate categorization of data points more sophisticated algorithms and data training methods should be utilized such as deep neural networks.

6.3 Limitations

The evaluation of the applicability of real time sensors is conducted on two cases. More cases with variations in size, lighting, object colour, speed of scan and etc. should be conducted to better evaluate the limitations of these devices.

While the RANSAC based object finding algorithm proved to be somewhat effective for automatic finding, it relies on an overlap parameter. Although this parameter is calibrated for the two case studies and proved to be effective, its performance could decline when it is applied to other objects and construction elements. Also, it was implemented using commercial software, which is not completely defined.

Mathematical closed form solutions are vulnerable to the extreme data points and may yield wrong answers. In order to use a more sophisticated data classification algorithm more data points should be acquired.

6.4 Future work

In Chapter 4, the recognition and localization of the 3D model is performed in a significantly faster timeframe, the isolation module takes the dominant part of the time required for processing. Faster and more effective search strategies such as kd-tree and graph theory may improve the processing time for the isolation, and this inadequacy may be appropriately addressed. This could be a potential research direction for future work. Also, to extend the study conducted in Chapter 5, a more widely adaptable model has to be developed. The model has to consider the impact of objects with different geometric shapes.

The author will study the impact of an integrated framework utilizing portable scanners and real time visual feedback on pipe fitters productivity to quantitatively measure the effectiveness of a framework integrating all three contributions of this work.

References:

AACE INTERNATIONAL, 2016-last update, Cost Estimate Classification System- As Applied in Engineering, Procurement, And Construction For The Process Industries. Available: http://www.aacei.org/toc/toc_18R-97.pdf.

ABOURIZK, S., 2010. Role of simulation in construction engineering and management. Journal of Construction Engineering and Management, 136(10), pp. 1140-1153.

AHMED, M.F., HAAS, C.T. and HAAS, R., 2014. Automatic detection of cylindrical objects in built facilities. Journal of Computing in Civil Engineering, 28(3), pp. 04014009.

AKINCI, B., BOUKAMP, F., GORDON, C., HUBER, D., LYONS, C. and PARK, K., 2006a. A formalism for utilization of sensor systems and integrated project models for active construction quality control. Automation in Construction, 15(2), pp. 124-138.

AKINCI, B., BOUKAMP, F., GORDON, C., HUBER, D., LYONS, C. and PARK, K., 2006b. A formalism for utilization of sensor systems and integrated project models for active construction quality control. Automation in Construction, 15(2), pp. 124-138.

ALLAIRE, S., KIM, J.J., BREEN, S.L., JAFFRAY, D.A. and PEKAR, V., 2008. Full orientation invariance and improved feature selectivity of 3D SIFT with application to medical image analysis, Computer Vision and Pattern Recognition Workshops, 2008. CVPRW'08. IEEE Computer Society Conference on 2008, IEEE, pp. 1-8.

ASPRS, 2007-last update, American Society of Photogrammetry and Remote Sensing: Photogrammetry. Available: http://www.photogrammetry.com/.

BAJRAMOVIC, F., MATTERN, F., BUTKO, N. and DENZLER, J., 2006. A comparison of nearest neighbor search algorithms for generic object recognition, Advanced Concepts for Intelligent Vision Systems 2006, Springer, pp. 1186-1197.

BALALI, V., SADEGHI, M.A. and GOLPARVAR-FARD, M., 2015. Image-based retro-reflectivity measurement of traffic signs in day time. Advanced Engineering Informatics, 29(4), pp. 1028-1040.

BARRY, P. and COAKLEY, R., 2013. Field accuracy test of RPAS photogrammetry. International Archives of the Photogrammetry, Remote Sensing and Spatial Information Sciences, 40, pp. 1.

BESL, P. and MCKAY, H., 1992. A method for alignment of 3-D shapes. IEEE Trans Pattern Anal Mach Intell, 14(2), pp. 239-256.

BHATIA, N., 2010. Survey of nearest neighbor techniques. arXiv preprint arXiv:1007.0085, .

BOSCHE, F. and HAAS, C., 2008a. Automated retrieval of 3D CAD model objects in construction range images. Automation in Construction, 17(4), pp. 499-512.

BOSCHE, F. and HAAS, C., 2008b. Automated retrieval of 3D CAD model objects in construction range images. Automation in Construction, 17(4), pp. 499-512.

BOSCHÉ, F., 2010. Automated recognition of 3D CAD model objects in laser scans and calculation of as-built dimensions for dimensional compliance control in construction. Advanced engineering informatics, 24(1), pp. 107-118.

BOSCHÉ, F., AHMED, M., TURKAN, Y., HAAS, C.T. and HAAS, R., 2015. The value of integrating Scan-to-BIM and Scan-vs-BIM techniques for construction monitoring using laser scanning and BIM: The case of cylindrical MEP components. Automation in Construction, 49, pp. 201-213.

BRILAKIS, I., DAI, F. and RADOPOULOU, S., 2011. Achievements and challenges in recognizing and reconstructing civil infrastructure, Proceedings of the 15th international conference on Theoretical Foundations of Computer Vision: outdoor and large-scale real-world scene analysis 2011, Springer-Verlag, pp. 151-176.

BROSTOW, G.J., SHOTTON, J., FAUQUEUR, J. and CIPOLLA, R., 2008. Segmentation and recognition using structure from motion point clouds. Computer Vision–ECCV 2008. Springer, pp. 44-57.

BURATI JR, J.L., FARRINGTON, J.J. and LEDBETTER, W.B., 1992. Causes of quality deviations in design and construction. Journal of Construction Engineering and Management, 118(1), pp. 34-49.

BURTCH, R., 2004. History of photogrammetry. Notes of the Center for Photogrammetric Training, .

CHAUMETTE, F. and HUTCHINSON, S., 2006. Visual servo control. I. Basic approaches. IEEE Robotics & Automation Magazine, 13(4), pp. 82-90.

CHEN, J., FANG, Y., CHO, Y.K. and KIM, C., 2016. Principal Axes Descriptor for Automated Construction-Equipment Classification from Point Clouds. Journal of Computing in Civil Engineering, , pp. 04016058.

CHI, S. and CALDAS, C.H., 2011. Image-based safety assessment: automated spatial safety risk identification of earthmoving and surface mining activities. Journal of Construction Engineering and Management, 138(3), pp. 341-351.

CHUA, C.S. and JARVIS, R., 1997. Point signatures: A new representation for 3d object recognition. International Journal of Computer Vision, 25(1), pp. 63-85.

CII, 2011. A Guide to Construction Rework Reduction. Construction Industry Institute (CII) Implementation Research Team 252.

CORSINI, M., CIGNONI, P. and SCOPIGNO, R., 2012. Efficient and flexible sampling with blue noise properties of triangular meshes. IEEE Transactions on Visualization and Computer Graphics, 18(6), pp. 914-924.

CZERNIAWSKI, T., NAHANGI, M., WALBRIDGE, S. and HAAS, C., 2016a. Automated Removal of Planar Clutter from 3D Point Clouds for Improving Industrial Object Recognition, ISARC. Proceedings of the International Symposium on Automation and Robotics in Construction 2016a, Vilnius Gediminas Technical University, Department of Construction Economics & Property, pp. 1.

CZERNIAWSKI, T., NAHANGI, M., HAAS, C. and WALBRIDGE, S., 2016b. Pipe spool recognition in cluttered point clouds using a curvature-based shape descriptor. Automation in Construction, 71, pp. 346-358.

DIMITROV, A. and GOLPARVAR-FARD, M., 2015. Segmentation of building point cloud models including detailed architectural/structural features and MEP systems. Automation in Construction, 51, pp. 32-45.

DIMITROV, A., GU, R. and GOLPARVAR-FARD, M., 2016. Non-Uniform B-Spline Surface Fitting from Unordered 3D Point Clouds for As-Built Modeling. Computer-Aided Civil and Infrastructure Engineering, .

DISSANAYAKE, M., FAYEK, A.R., WOLF, H. and TOL, A.V., 2003. Developing a Standard Approach for Construction Field Rework Assessment, Construction Research Congress@ sWind of Change: Integration and Innovation 2003, pp. 1-8.

DROST, B., ULRICH, M., NAVAB, N. and ILIC, S., 2010. Model globally, match locally: Efficient and robust 3D object recognition. CVPR 2010, pp. 5.

EUROSTAT, 2017-last update, Construction Production (volume) Index Overview. Available: http://ec.europa.eu/eurostat/statistics-explained/index.php/Construction_production_(volume)_index_overview.

FARO, 2014-last update, FARO Laser Scanner LS 840/880. Available: http://www2.faro.com/FaroIP/Files/File/Techsheets%20Download/IN_LS880.pdf.

FATHI, H., DAI, F. and LOURAKIS, M., 2015. Automated as-built 3D reconstruction of civil infrastructure using computer vision: Achievements, opportunities, and challenges. Advanced Engineering Informatics, 29(2), pp. 149-161.

FRIEDMAN, J.H., BENTLEY, J.L. and FINKEL, R.A., 1977. An algorithm for finding best matches in logarithmic expected time. ACM Transactions on Mathematical Software (TOMS), 3(3), pp. 209-226.

FURHT, B. and AHSON, S.A., 2008. Handbook of mobile broadcasting: DVB-H, DMB, ISDB-T, and mediaflo. CRC Press.

FURUKAWA, Y., CURLESS, B., SEITZ, S.M. and SZELISKI, R., 2009. Reconstructing building interiors from images, Computer Vision, 2009 IEEE 12th International Conference on 2009, IEEE, pp. 80-87.

GOLPARVAR-FARD, M., PEÑA-MORA, F. and SAVARESE, S., 2009a. D4AR–a 4-dimensional augmented reality model for automating construction progress monitoring data collection, processing and communication. Journal of information technology in construction, 14(13), pp. 129-153.

GOLPARVAR-FARD, M., PEÑA-MORA, F., ARBOLEDA, C.A. and LEE, S., 2009b. Visualization of construction progress monitoring with 4D simulation model overlaid on time-lapsed photographs. Journal of Computing in Civil Engineering, 23(6), pp. 391-404.

GOLPARVAR-FARD, M., PEÑA-MORA, F. and SAVARESE, S., 2012. Automated progress monitoring using unordered daily construction photographs and IFC-based building information models. Journal of Computing in Civil Engineering, 29(1), pp. 04014025.

GOODRUM, P.M., MILLER, J., SWEANY, J. and ALRUWAYTHI, O., 2016. Influence of the Format of Engineering Information and Spatial Cognition on Craft-Worker Performance. Journal of Construction Engineering and Management, 142(9), pp. 04016043.

GUO, G., WANG, H., BELL, D., BI, Y. and GREER, K., 2003. KNN model-based approach in classification, OTM Confederated International Conferences" On the Move to Meaningful Internet Systems" 2003, Springer, pp. 986-996.

GUO, Y., BENNAMOUN, M., SOHEL, F.A., WAN, J. and LU, M., 2013. 3D free form object recognition using rotational projection statistics, Applications of Computer Vision (WACV), 2013 IEEE Workshop on 2013, IEEE, pp. 1-8.

GUO, Y., BENNAMOUN, M., SOHEL, F., LU, M. and WAN, J., 2014. 3D object recognition in cluttered scenes with local surface features: a survey. IEEE Transactions on Pattern Analysis and Machine Intelligence, 36(11), pp. 2270-2287.

HAAS, C.T. and FAGERLUND, W.R., 2002. Preliminary research on prefabrication, pre-assembly, modularization and off-site fabrication in construction.

HAM, Y., HAN, K.K., LIN, J.J. and GOLPARVAR-FARD, M., 2016. Visual monitoring of civil infrastructure systems via camera-equipped Unmanned Aerial Vehicles (UAVs): a review of related works. Visualization in Engineering, 4(1), pp. 1-8.

HAN, S.H., AL-HUSSEIN, M., AL-JIBOURI, S. and YU, H., 2012. Automated post-simulation visualization of modular building production assembly line. Automation in Construction, 21, pp. 229-236.

HUANG, F.J., BOUREAU, Y. and LECUN, Y., 2007. Unsupervised learning of invariant feature hierarchies with applications to object recognition, Computer Vision and Pattern Recognition, 2007. CVPR'07. IEEE Conference on 2007, IEEE, pp. 1-8.

HWLZLM, X. and SNNB, Z., A selective neighborhood based naive bayes for lazy learning, Proceedings of the Sixth Pacific-Asia Conference on KDD, pp. 104-114.

IRIZARRY, J., GHEISARI, M. and WALKER, B.N., 2012. Usability assessment of drone technology as safety inspection tools. Journal of Information Technology in Construction (ITcon), 17(12), pp. 194-212.

JIANG, L., CAI, Z., WANG, D. and JIANG, S., 2007. Survey of improving k-nearest-neighbor for classification, Fuzzy Systems and Knowledge Discovery, 2007. FSKD 2007. Fourth International Conference on 2007, IEEE, pp. 679-683.

JOHNSON, A.E. and HEBERT, M., 1999. Using spin images for efficient object recognition in cluttered 3D scenes. IEEE Transactions on Pattern Analysis and Machine Intelligence, 21(5), pp. 433-449.

KHOSHELHAM, K. and ELBERINK, S.O., 2012. Accuracy and resolution of kinect depth data for indoor mapping applications. Sensors, 12(2), pp. 1437-1454.

KIM, C., SON, H. and KIM, C., 2013. Automated construction progress measurement using a 4D building information model and 3D data. Automation in Construction, 31, pp. 75-82.

KNOPP, J., PRASAD, M., WILLEMS, G., TIMOFTE, R. and VAN GOOL, L., 2010. Hough transform and 3D SURF for robust three dimensional classification. Computer vision–ECCV 2010, , pp. 589-602.

KOHAVI, R., 1996. Scaling Up the Accuracy of Naive-Bayes Classifiers: A Decision-Tree Hybrid. KDD 1996, Citeseer, pp. 202-207.

LARS MIERITZ, 2012-last update, Gartner Survey Shows Why Projects Fail. Available: https://thisiswhatgoodlookslike.com/2012/06/10/gartner-survey-shows-why-projects-fail/.

LEE, J., KIM, C., SON, H. and KIM, C., 2012. Automated pipeline extraction for modeling from laser scanned data, International Symposium on Automation and Robotics in Construction (ISARC) 2012.

LEE, J., SON, H., KIM, C. and KIM, C., 2013. Skeleton-based 3D reconstruction of as-built pipelines from laser-scan data. Automation in Construction, 35, pp. 199-207.

LIGHT, 2016-last update, L16 a New Generation in Cameras. Available: https://light.co/.

LIU, T., MOORE, A.W. and GRAY, A., 2006. New algorithms for efficient high-dimensional nonparametric classification. Journal of Machine Learning Research, 7(Jun), pp. 1135-1158.

LIU, Y., CHO, S., SPENCER JR, B. and FAN, J., 2014. Concrete crack assessment using digital image processing and 3D scene reconstruction. Journal of Computing in Civil Engineering, 30(1), pp. 04014124.

MEMARZADEH, M., GOLPARVAR-FARD, M. and NIEBLES, J.C., 2013. Automated 2D detection of construction equipment and workers from site video streams using histograms of oriented gradients and colors. Automation in Construction, 32, pp. 24-37.

NAHANGI, M., CZERNIAWSKI, T., HAAS, C.T., WALBRIDGE, S. and WEST, J., 2015. Parallel systems and structural frames realignment planning and actuation strategy. Journal of Computing in Civil Engineering, 30(4), pp. 04015067.

NAHANGI, M. and HAAS, C.T., 2016. Skeleton-based discrepancy feedback for automated realignment of industrial assemblies. Automation in Construction, 61, pp. 147-161.

NAHANGI, M. and HAAS, C.T., 2014. Automated 3D compliance checking in pipe spool fabrication. Advanced Engineering Informatics, 28(4), pp. 360-369.

NAP.EDU, 2002-last update, Completing the Big Dig: Managing the Final Stages of Boston's Central Artery/Tunnel Project. Available: https://www.nap.edu/read/10629/chapter/4.

OPFER, N., 1999. Construction defect education in construction management, ASC proceedings of the 35th Annual Conference, California Polytechnic University, ASC 1999.

PAN, R. and TAUBIN, G., 2016. Automatic segmentation of point clouds from multi-view reconstruction using graph-cut. The Visual Computer, 32(5), pp. 601-609.

PAPAZOV, C. and BURSCHKA, D., 2010. An efficient ransac for 3d object recognition in noisy and occluded scenes, Asian Conference on Computer Vision 2010, Springer, pp. 135-148.

PAPAZOV, C., HADDADIN, S., PARUSEL, S., KRIEGER, K. and BURSCHKA, D., 2012. Rigid 3D geometry matching for grasping of known objects in cluttered scenes. The International Journal of Robotics Research, , pp. 0278364911436019.

PARK, H., LEE, H., ADELI, H. and LEE, I., 2007. A new approach for health monitoring of structures: terrestrial laser scanning. Computer-Aided Civil and Infrastructure Engineering, 22(1), pp. 19-30.

PARK, M. and BRILAKIS, I., 2012. Construction worker detection in video frames for initializing vision trackers. Automation in Construction, 28, pp. 15-25.

PĂTRĂUCEAN, V., ARMENI, I., NAHANGI, M., YEUNG, J., BRILAKIS, I. and HAAS, C., 2015. State of research in automatic as-built modelling. Advanced Engineering Informatics, 29(2), pp. 162-171.

PHTOMODELER, 2013-last update, Camera Fundamentals and Prameters in Photogrammetry. Available: https://info.photomodeler.com/blog/camera-fundamentals-and-parameters-in-photogrammetry/.

PIPE FABRICATION INSTITUTE, 2000.

QUIGLEY, M., BATRA, S., GOULD, S., KLINGBEIL, E., LE, Q., WELLMAN, A. and NG, A.Y., 2009. High-accuracy 3d sensing for mobile manipulation: Improving object detection and door opening, Robotics and Automation, 2009. ICRA'09. IEEE International Conference on 2009, IEEE, pp. 2816-2822.

RABBANI, T., DIJKMAN, S., VAN DEN HEUVEL, F. and VOSSELMAN, G., 2007. An integrated approach for modelling and global registration of point clouds. ISPRS journal of Photogrammetry and Remote Sensing, 61(6), pp. 355-370.

RAY, S.J. and TEIZER, J., 2012. Real-time construction worker posture analysis for ergonomics training. Advanced Engineering Informatics, 26(2), pp. 439-455.

RUSINKIEWICZ, S. and LEVOY, M., 2001. Efficient variants of the ICP algorithm, 3-D Digital Imaging and Modeling, 2001. Proceedings. Third International Conference on 2001, IEEE, pp. 145-152.

SALVI, J., MATABOSCH, C., FOFI, D. and FOREST, J., 2007. A review of recent range image registration methods with accuracy evaluation. Image and Vision Computing, 25(5), pp. 578-596.

SAN JOSÉ ALONSO, J., MARTÍNEZ RUBIO, J., FERNÁNDEZ MARTÍN, J. and GARCÍA FERNÁNDEZ, J., 2011. Comparing time-of-flight and phase-shift. The survey of the Royal Pantheon in the Basilica of San Isidoro (León), ISPRS Workshop "3D-ARCH 2011.

SHARIF, M., NAHANGI, M., HAAS, C., WEST, J. and IBRAHIM, M., 2016. Resilient Infrastructure.

SIEBERT, S. and TEIZER, J., 2014. Mobile 3D mapping for surveying earthwork projects using an Unmanned Aerial Vehicle (UAV) system. Automation in Construction, 41, pp. 1-14.

SON, H., KIM, C. and KIM, C., 2014. Fully automated as-built 3D pipeline extraction method from laser-scanned data based on curvature computation. Journal of Computing in Civil Engineering, 29(4), pp. B4014003.

STAIGER, R., 2003. Terrestrial laser scanning technology, systems and applications, 2nd FIG Regional Conference Marrakech, Morocco 2003.

STATISTA, 2015-last update, Value added of U.S. Construction industy as a percentage of Gross Domestic Product between 2007 and 2015. Available: https://www.statista.com/statistics/192049/value-added-by-us-construction-as-a-percentage-of-gdp-since-2007/.

STATISTICS CANADA, 2010.

STEVE LEBLANC, 2007. It's Official: Boston's Big Dig Will Be Done. The Washington Post.

STRUCTURE IO, 2015-last update. Available: http://structure.io/.

TANG, P., HUBER, D., AKINCI, B., LIPMAN, R. and LYTLE, A., 2010. Automatic reconstruction of as-built building information models from laser-scanned point clouds: A review of related techniques. Automation in Construction, 19(7), pp. 829-843.

TURKAN, Y., BOSCHE, F., HAAS, C.T. and HAAS, R., 2012a. Automated progress tracking using 4D schedule and 3D sensing technologies. Automation in Construction, 22, pp. 414-421.

TURKAN, Y., BOSCHE, F., HAAS, C.T. and HAAS, R., 2012b. Automated progress tracking using 4D schedule and 3D sensing technologies. Automation in Construction, 22, pp. 414-421.

U.S CENSUS BUREAU NEWS, October 2014.

WANG, J., SUN, W., SHOU, W., WANG, X., WU, C., CHONG, H., LIU, Y. and SUN, C., 2015. Integrating BIM and LiDAR for real-time construction quality control. Journal of Intelligent & Robotic Systems, 79(3-4), pp. 417.

YANG, J., ARIF, O., VELA, P.A., TEIZER, J. and SHI, Z., 2010. Tracking multiple workers on construction sites using video cameras. Advanced Engineering Informatics, 24(4), pp. 428-434.

YUE, K., HUBER, D., AKINCI, B. and KRISHNAMURTI, R., 2006. The ASDMCon project: The challenge of detecting defects on construction sites, 3D Data Processing, Visualization, and Transmission, Third International Symposium on 2006, IEEE, pp. 1048-1055.

ZHANG, G., VELA, P.A., KARASEV, P. and BRILAKIS, I., 2015. A Sparsity-Inducing Optimization-Based Algorithm for Planar Patches Extraction from Noisy Point-Cloud Data. Computer-Aided Civil and Infrastructure Engineering, 30(2), pp. 85-102.

ZHAO, C. and MENG, X., 2009. An improved algorithm for k-nearest-neighbor finding and surface normals estimation. Tsinghua Science & Technology, 14, pp. 77-81.

ZHU, Z. and BRILAKIS, I., 2010. Concrete column recognition in images and videos. Journal of Computing in Civil Engineering, 24(6), pp. 478-487.

Appendix A

MATLAB code: finding the optimal K value for clutter removal

```
clear all;
clc;

s=textread('lab_scan.txt');
scan=pointCloud(s);

m=textread('model.txt');
model = pointCloud(m);

m(:,4)=1;
mt=m';
A = [-0.828077197   -0.000714839    -0.560613871    288.2137451;
-0.560241342    0.037523892 0.827479005 -387.1165771;
0.020445079 0.999295533 -0.031473041    -101.2927094;
0   0   0   1];

c=A*mt;
ct=c';
ct=ct(:,1:3);
t_model=pointCloud(ct); %Transformed model


n=round(scan.Count/t_model.Count); %number of nearest neighbors (k)
n=8
filter_scene=zeros(n*t_model.Count,3);

for i=1 : t_model.Count
   point = t_model.Location(i,:);
   [indices,dists] = findNearestNeighbors(scan,point,n);

   for j=1:n
      filter_scene((i-1)*n+j,:) = scan.Location(indices(j),:); % here we are reading all the coordinates of nearest
neighbors and puting them in a matrix of closest points
   end


end

f_scene=pointCloud(filter_scene);

[tform ,ft_model, rmse]=pcregrigid(t_model,f_scene,'Extrapolate',true,'MaxIterations',50);

figure('units','normalized','outerposition',[0 0 1 1])
subplot(1,2,1)
pcshowpair(f_scene,ft_model)
title('Rango+ICP')
axis off
subplot(1,2,2)
```

```
pcshowpair(f_scene,t_model)
title('Rango')
axis off

figure('units','normalized','outerposition',[0 0 1 1])
subplot(1,2,1)
pcshow(f_scene)
title('K-nearest points')
axis off
subplot(1,2,2)
pcshowpair(scan,t_model)
title('Rango')
axis off

figure('units','normalized','outerposition',[0 0 1 1])
subplot(1,2,1)
pcshow(scan)
title('Scan')
axis off
subplot(1,2,2)
pcshow(model)
title('Model')
axis off
```

Appendix B

MATLAB code: for resampling using weighed octree (Chapter 3)

```
classdef OcTree < handle
% OcTree point decomposition in 3D
%   OcTree is used to create a tree data structure of bins containing 3D
%   points. Each bin may be recursively decomposed into 8 child bins.
%
%   OT = OcTree(PTS) creates an OcTree from an N-by-3 matrix of point
%   coordinates.
%
%   OT = OcTree(...,'PropertyName',VALUE,...) takes any of the following
%   property values:
%
%    binCapacity - Maximum number of points a bin may contain. If more
%                  points exist, the bin will be recursively subdivided.
%                  Defaults to ceil(numPts/10).
%    maxDepth    - Maximum number of times a bin may be subdivided.
%                  Defaults to INF.
%    maxSize     - Maximum size of a bin edge. If any dimension of a bin
%                  exceeds maxSize, it will be recursively subdivided.
%                  Defaults to INF.
%    minSize     - Minimum size of a bin edge. Subdivision will stop after
%                  any dimension of a bin gets smaller than minSize.
%                  Defaults to 1000*eps.
%    style       - Either 'equal' (default) or 'weighted'. 'equal'
%                  subdivision splits bins at their central coordinate
%                  (ie, one bin subdivides into 8 equally sized bins).
%                  'weighted' subdivision divides bins based on the mean
%                  of all points they contain. Weighted subdivision is
%                  slightly slower than equal subdivision for a large
%                  number of points, but it can produce a more efficient
%                  decomposition with fewer subdivisions.
%
%   Example 1: Decompose 200 random points into bins of 20 points or less,
%          then display each bin with its points in a separate colour.
%


%
%   Example 2: Decompose 200 random points into bins of 10 points or less,
%         shrunk to minimallly encompass their points, then display.
%      pts = rand(200,3);
%      OT = OcTree(pts,'binCapacity',10,'style','weighted');
%      OT.shrink
%      figure
%      boxH = OT.plot;
%      cols = lines(OT.BinCount);
%      doplot3 = @(p,varargin)plot3(p(:,1),p(:,2),p(:,3),varargin{:});
%      for i = 1:OT.BinCount
%         set(boxH(i),'Color',cols(i,:),'LineWidth', 1+OT.BinDepths(i))
%         doplot3(pts(OT.PointBins==i,:),'.','Color',cols(i,:))
%      end
%      axis image, view(3)
```

```
%
%
% OcTree methods:
%    shrink          - Shrink each bin to tightly encompass its children
%    query           - Ask which bins a new set of points belong to.
%    plot, plot3      - Plots bin bounding boxes to the current axes.
%
% OcTree properties:
%    Points          - The coordinate of points in the decomposition.
%    PointBins        - Indices of the bin that each point belongs to.
%    BinCount         - Total number of bins created.
%    BinBoundaries     - BinCount-by-6 [MIN MAX] coordinates of bin edges.
%    BinDepths        - The # of subdivisions to reach each bin.
%    BinParents       - Indices of the bin that each bin belongs to.
%    Properties       - Name/Val pairs used for creation (see help above)
%
% See also qtdecomp.

%   Created by Sven Holcombe.
%   1.0     - 2013-03 Initial release
%   1.1     - 2013-03 Added shrinking bins and allocate/deallocate space
%
%   Please post comments to the FEX page for this entry if you have any
%   bugs or feature requests.

   properties
      Points;
      PointBins;
      BinCount;
      BinBoundaries;
      BinDepths;
      BinParents = zeros(0,1);
      Properties;
   end

   methods

      function this = OcTree(pts,varargin)
         % This is the OcTree header line
         validateattributes(pts,{'numeric'},...
            {'real','finite','nonnan','ncols', 3},...
            mfilename,'PTS')

         % Initialise a single bin surrounding all given points
         numPts = size(pts,1);
         this.BinBoundaries = [min(pts,[],1) max(pts,[],1)];
         this.Points = pts;
         this.PointBins = ones(numPts,1);
         this.BinDepths = 0;
         this.BinParents(1) = 0;
         this.BinCount = 1;

         % Allow custom setting of Properties
         IP = inputParser;
         IP.addParamValue('binCapacity',ceil(numPts)/10);
```

```
    IP.addParamValue('maxDepth',inf);
    IP.addParamValue('maxSize',inf);
    IP.addParamValue('minSize',1000 * eps);
    IP.addParamValue('style','equal');
    IP.parse(varargin{:});
    this.Properties = IP.Results;

    % Return on empty or trivial bins
    if numPts<2, return; end

    % Start dividing!
    this.preallocateSpace;
    this.divide(1);
    this.deallocateSpace;
end

% MATLAB performs better if arrays that grow are initialised,
% rather than grown during a loop. These two functions do just that
% before and after the identification of new beens.
function preallocateSpace(this)
    numPts = size(this.Points,1);
    numBins = numPts;
    if isfinite(this.Properties.binCapacity)
        numBins = ceil(2*numPts/this.Properties.binCapacity);
    end
    this.BinDepths(numBins) = 0;
    this.BinParents(numBins) = 0;
    this.BinBoundaries(numBins,1) = 0;
end
function deallocateSpace(this)
    this.BinDepths(this.BinCount+1:end) = [];
    this.BinParents(this.BinCount+1:end) = [];
    this.BinBoundaries(this.BinCount+1:end,:) = [];
end

function divide(this, startingBins)
    % Loop over each bin we will consider for division
    for i = 1:length(startingBins)
        binNo = startingBins(i);

        % Prevent dividing beyond the maximum depth
        if this.BinDepths(binNo)+1 >= this.Properties.maxDepth
            continue;
        end

        % Prevent dividing beyond a minimum size
        thisBounds = this.BinBoundaries(binNo,:);
        binEdgeSize = diff(thisBounds([1:3;4:6]));
        minEdgeSize = min(binEdgeSize);
        maxEdgeSize = max(binEdgeSize);
        if minEdgeSize < this.Properties.minSize
            continue;
        end
```

```
        % There are two conditions under which we should divide
        % this bin. 1: It's bigger than maxSize. 2: It contains
        % more points than binCapacity.
        oldCount = this.BinCount;
        if nnz(this.PointBins==binNo) > this.Properties.binCapacity
            this.divideBin(binNo);
            this.divide(oldCount+1:this.BinCount);
            continue;
        end
        if maxEdgeSize>this.Properties.maxSize
            this.divideBin(binNo);
            this.divide(oldCount+1:this.BinCount);
            continue;
        end
    end
end

function divideBin(this,binNo)
    % Gather the new points (a bit more efficient to copy once)
    binPtMask = this.PointBins==binNo;
    thisBinsPoints = this.Points(binPtMask,:);

    % Get the old corner points and the new division point
    oldMin = this.BinBoundaries(binNo,1:3);
    oldMax = this.BinBoundaries(binNo,4:6);
    if strcmp('weighted',this.Properties.style) && any(binPtMask)
        newDiv = mean(thisBinsPoints,1);
    else
        newDiv = mean([oldMin; oldMax], 1);
    end

    % Build the new boundaries of our 8 subdivisions
    minMidMax = [oldMin newDiv oldMax];
    newBounds = minMidMax([...
        1 2 3 4 5 6;
        1 2 6 4 5 9;
        1 5 3 4 8 6;
        1 5 6 4 8 9;
        4 2 3 7 5 6;
        4 2 6 7 5 9;
        4 5 3 7 8 6;
        4 5 6 7 8 9]);

    % Determine to which of these 8 bins each current point belongs
    binMap = cat(3,[0 0 0],[0 0 1],[0 1 0],[0 1 1],...
        [1 0 0],[1 0 1],[1 1 0],[1 1 1]);
    gtMask = bsxfun(@gt, thisBinsPoints, newDiv);
    [~,binAssignment] = max(all(bsxfun(@eq,gtMask,binMap),2),[],3);
    % [~, binAssignment] = ismember(gtMask,binMap,'rows'); % A little slower than above.

    % Make the new bins and reassign old points to them
    newBinInds = this.BinCount+1:this.BinCount+8;
    this.BinBoundaries(newBinInds,:) = newBounds;
    this.BinDepths(newBinInds) = this.BinDepths(binNo)+1;
    this.BinParents(newBinInds) = binNo;
```

```
    this.PointBins(binPtMask) = newBinInds(binAssignment);
    this.BinCount = this.BinCount + 8;
end

function shrink(this)
    % Shrink all bins to bound only the points they contain
    % WARNING: this operation creates gaps in the final space not
    % covered by a bin. Only shrink OcTree structures when you only
    % intend to use the points used to create the tree to query the
    % tree space.
    binChildren = arrayfun(@(i)find(this.BinParents==i),1:this.BinCount,'Un',0)';
    binIsLeaf = cellfun(@isempty, binChildren);
    for i = find(binIsLeaf(:))'
        binShrink_recurse(i, true)
    end

    function binShrink_recurse(binNo, isLeafBin)
        % Build a list of all points that fall within one of the
        % bins to be checked, and the list of which point falls in
        % which bin.
        oldBoundaryMin = this.BinBoundaries(binNo,1:3);
        oldBoundaryMax = this.BinBoundaries(binNo,4:6);
        if isLeafBin
            % Shrink bin based on child POINTS
            ptsMask = this.PointBins==binNo;
            if ~any(ptsMask)
                % No points, shrink the bin to infinitely small
                proposedBoundaries = [oldBoundaryMin oldBoundaryMin];
            else
                pts = this.Points(ptsMask,:);
                proposedBoundaries = [...
                    max([oldBoundaryMin; min(pts,[],1)]) ...
                    min([oldBoundaryMax; max(pts,[],1)])];
            end
        else
            % Shrink bin based on child BINS
            childBoundaries = this.BinBoundaries(binChildren{binNo},:);
            proposedBoundaries = [min(childBoundaries(:,1:3),[],1) max(childBoundaries(:,4:6),[],1)];
        end

        if ~isequal(proposedBoundaries, [oldBoundaryMin oldBoundaryMax])
            % We just shrunk the boundary. Make it official and
            % check the parent
            this.BinBoundaries(binNo,:) = proposedBoundaries;
            parentBin = this.BinParents(binNo);
            if parentBin>0
                binShrink_recurse(parentBin, false)
            end
        end
    end
end

function binNos = query(this, newPts, queryDepth)
    % Get the OcTree bins that new query points belong to.
    %
```

```
% BINS = OT.query(NEWPTS) searches the OcTree object OT and
% returns an N-by-1 vector of BINS giving the bin index in
% which each of the N points in NEWPTS is contained. For any
% query points outside all bins in OT, the index -1 is
% returned.
%
% BINS = OT.query(NEWPTS,DEPTH) restricts the search to DEPTH
% levels in the OT bin tree. Note that the first bin
% (containing all other bins in OT) has DEPTH = 1.

if nargin<3
   queryDepth = max(this.BinDepths);
end

numPts = size(newPts,1);
newPts = permute(newPts,[3 2 1]);
binNos = ones(numPts,1)*-1;

binChildren = arrayfun(@(i)find(this.BinParents==i),1:this.BinCount,'Un',0)';
binIsLeaf = cellfun(@isempty, binChildren);
ptQuery_recurse(1:numPts, this.BinParents==0, 0)

function ptQuery_recurse(newIndsToCheck_, binsToCheck, depth)
   % Build a list of all points that fall within one of the
   % bins to be checked, and the list of which point falls in
   % which bin.
   boundsToCheck = this.BinBoundaries(binsToCheck,:);
   [ptInBounds, subBinNo] = max(all(...
      bsxfun(@ge, newPts(:,:,newIndsToCheck_), boundsToCheck(:,1:3)) & ...
      bsxfun(@le, newPts(:,:,newIndsToCheck_), boundsToCheck(:,4:6))...
      ,2),[],1);

   if ~all(ptInBounds)
      % Special case usually when depth=0, where a point may
      % fall outside the bins entirely. This should only
      % happen once so let's fix it once and let subsequent
      % code rely on all points being in bounds
      binNos(newIndsToCheck_(~ptInBounds)) = -1;
      newIndsToCheck_(~ptInBounds) = [];
      subBinNo(~ptInBounds) = [];
   end
   binNosToAssign = binsToCheck(subBinNo);
   newIndsToAssign = newIndsToCheck_;
   binNos(newIndsToAssign) = binNosToAssign;

   % Allow a free exit when we reach a certain depth
   if depth>=queryDepth
      return;
   end

   % Otherwise, for all of the points we just placed into
   % bins, check which of the children of those bins those
   % same points fall into
   [unqBinNos, ~, unqGrpNos] = unique(binNosToAssign);
```

```
            for i = 1:length(unqBinNos)
                thisPtMask = unqGrpNos==i;
                if ~binIsLeaf(unqBinNos(i))
                    ptQuery_recurse(newIndsToCheck_(thisPtMask), binChildren{unqBinNos(i)}, depth+1)
                end
            end

        end
    end

    function h = plot(this,varargin)
        % OcTree.plot plots bin bounding boxes of an OcTree object
        %
        % H = OT.plot('name',value,...) allows you to specify any
        % properties of the bounding box lines that you would normally
        % supply to a plot(...,'name',value) command, and returns plot
        % object handles (one per bin) to H.
        hold on;
        h = zeros(this.BinCount,1);
        for i = 1:this.BinCount
            binMinMax = this.BinBoundaries(i,:);
            pts = cat(1, binMinMax([...
                1 2 3; 4 2 3; 4 5 3; 1 5 3; 1 2 3;...
                1 2 6; 4 2 6; 4 5 6; 1 5 6; 1 2 6; 1 2 3]),...
                nan(1,3), binMinMax([4 2 3; 4 2 6]),...
                nan(1,3), binMinMax([4 5 3; 4 5 6]),...
                nan(1,3), binMinMax([1 5 3; 1 5 6]));
            h(i) = plot3(pts(:,1),pts(:,2),pts(:,3),varargin{:});
        end
    end
    function h = plot3(this,varargin)
        % OcTree.plot plots bin bounding boxes of an OcTree
        %
        % See also OcTree.plot
        h = this.plot(varargin{:});
    end
  end
end
```

Appendix C Enlarged Photos Used in Chapter 2

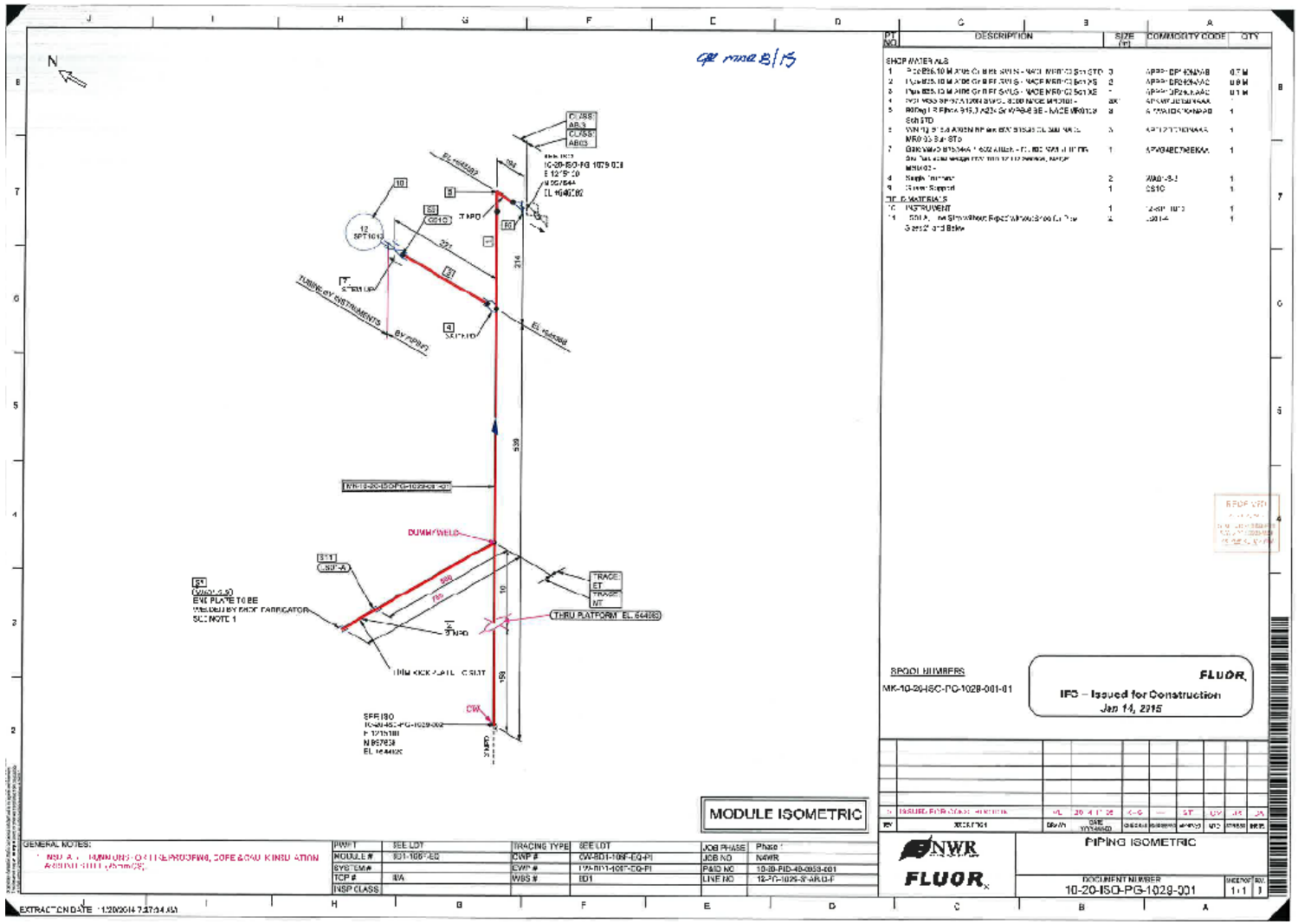
MODULE ISOMETRIC
PIPING ISOMETRIC
FLUOR
NWR
IFC – Issued for Construction
Jan 14, 2015
10-20-ISO-PG-1029-001

Figure 2-3. (a)

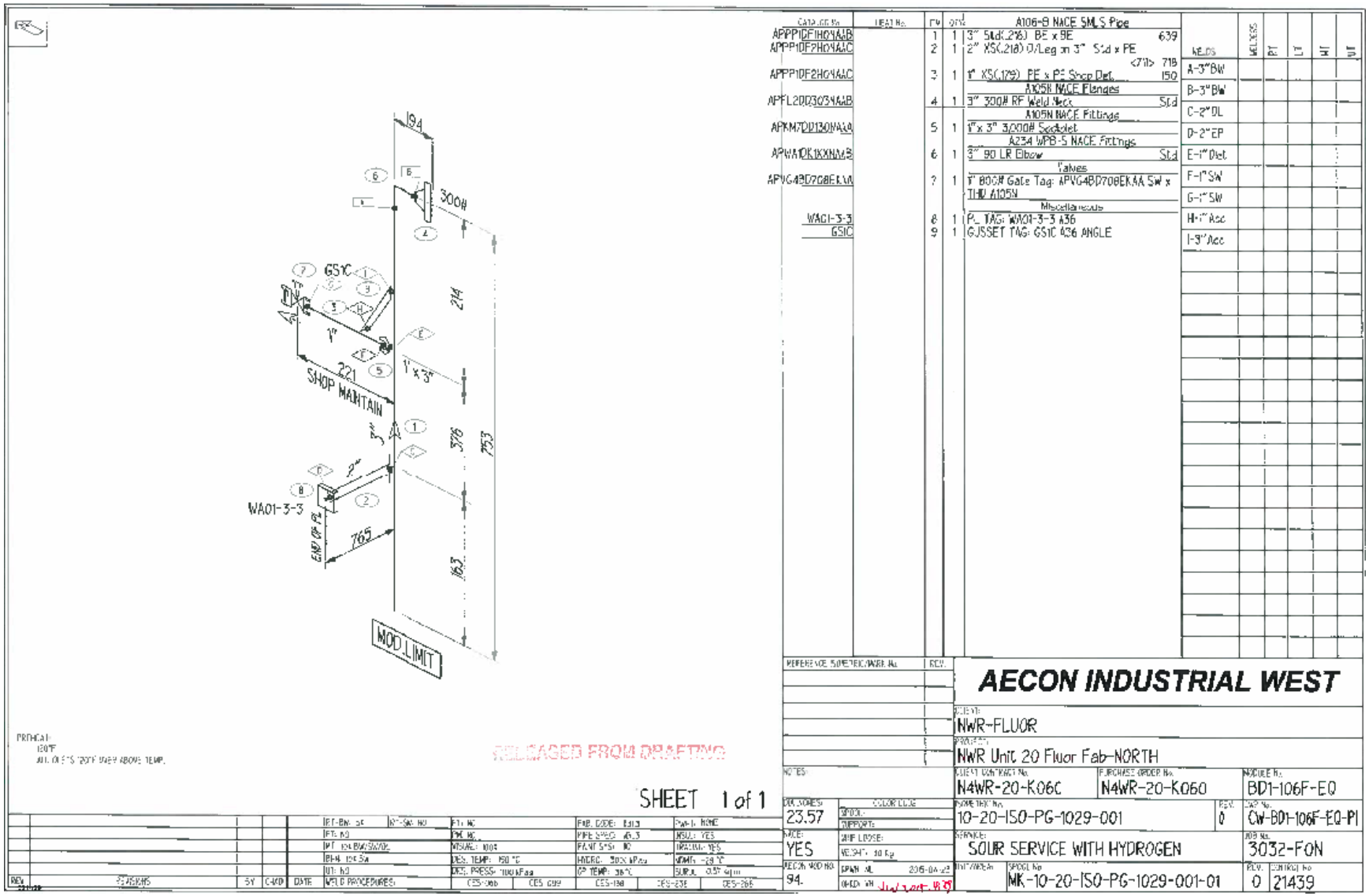
194
300#
GSIC
214
1"
221
SHOP MAINTAIN
1" x 3"
3"
378
753
2"
WA01-3-3
765
END OF PIPE
163
MOD LIMIT
RELEASED FROM DRAFTING
SHEET 1 of 1
AECON INDUSTRIAL WEST
NWR-FLUOR
NWR Unit 20 Fluor Fab-NORTH
N4WR-20-K06C
N4WR-20-K060
BD1-106F-EQ
10-20-ISO-PG-1029-001
CW-BD1-106F-EQ-PI
SOUR SERVICE WITH HYDROGEN
3032-FON
MK-10-20-ISO-PG-1029-001-01
21439

Figure 2-3. (b)

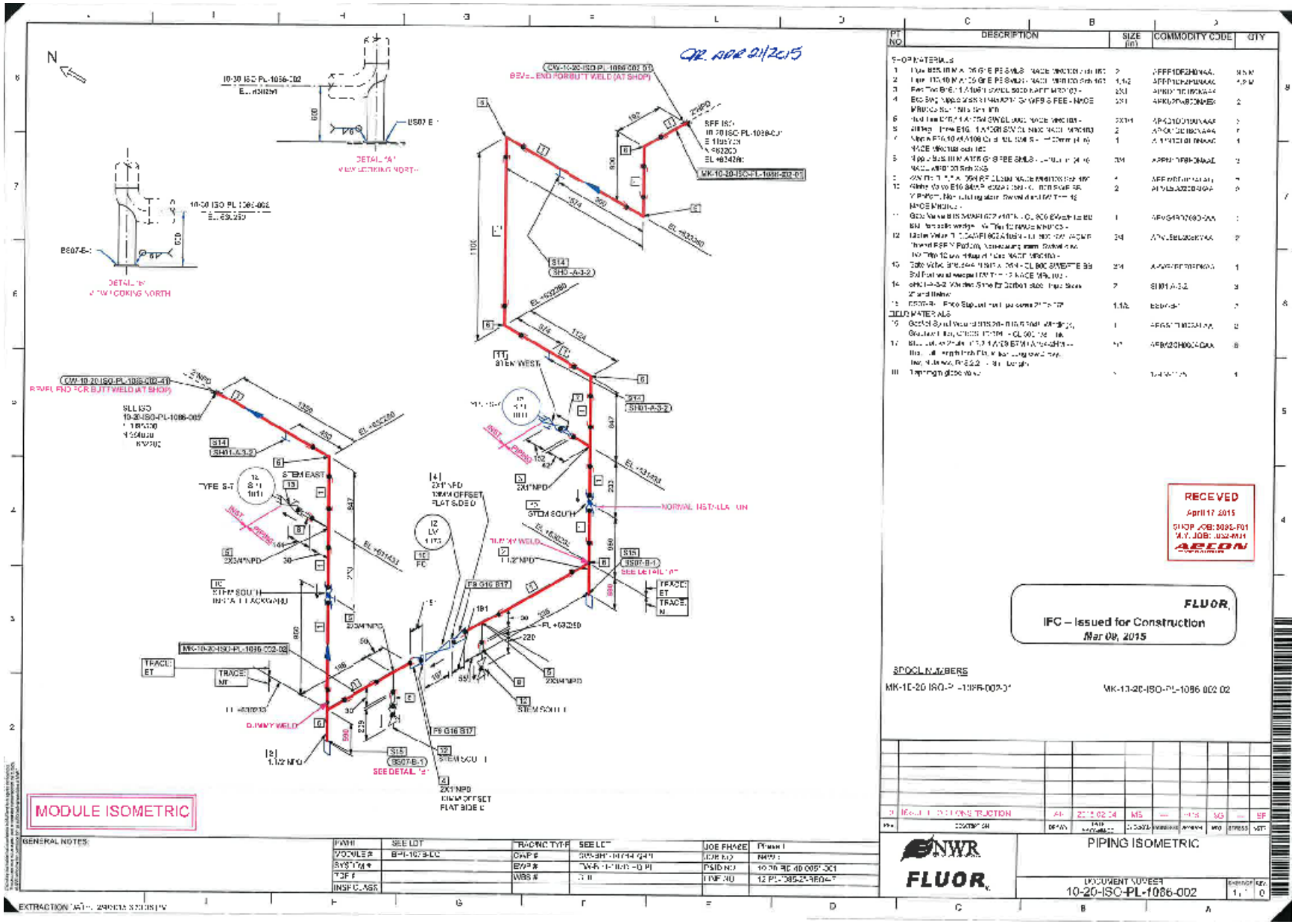
MODULE ISOMETRIC
PIPING ISOMETRIC
FLUOR
IFC – Issued for Construction
Mar 09, 2015
RECEIVED
April 17 2015
10-20-ISC-PL-1086-002

Figure 2-4. (a)

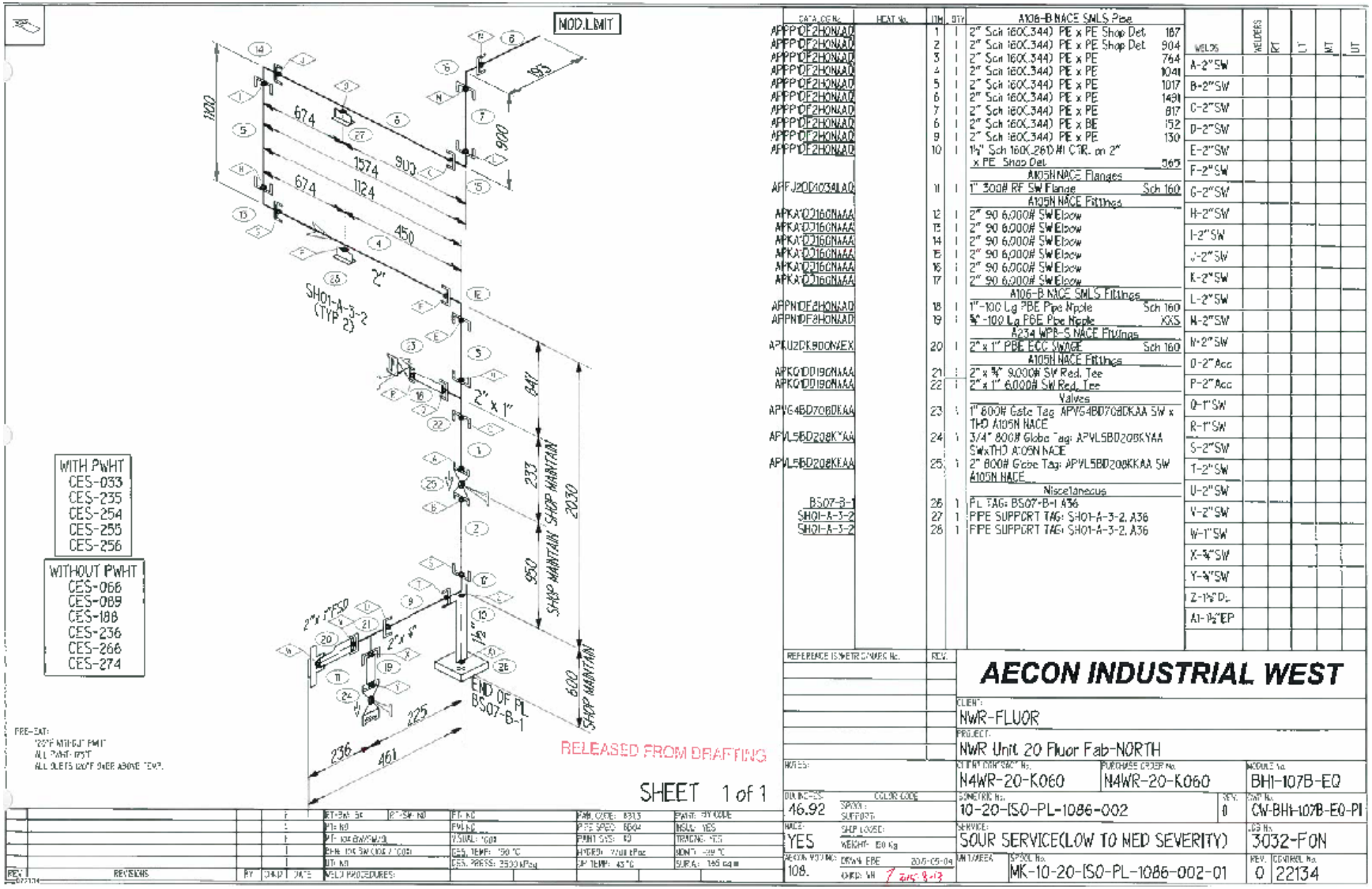
MOD.LIMIT
WITH PWHT
CES-033
CES-235
CES-254
CES-255
CES-256
WITHOUT PWHT
CES-066
CES-089
CES-188
CES-236
CES-266
CES-274
SHO1-A-3-2 (TYP 2)
END OF PL BS07-B-1
SHOP MAINTAIN
RELEASED FROM DRAFTING
SHEET 1 of 1
AECON INDUSTRIAL WEST
NWR-FLUOR
NWR Unit 20 Fluor Fab-NORTH
N4WR-20-K060
10-20-ISO-PL-1086-002
SOUR SERVICE(LOW TO MED SEVERITY)
MK-10-20-ISO-PL-1086-002-01
BH1-107B-EQ
CW-BH1-107B-EQ-PI
3032-FON
22134

Figure 2-4. (b)

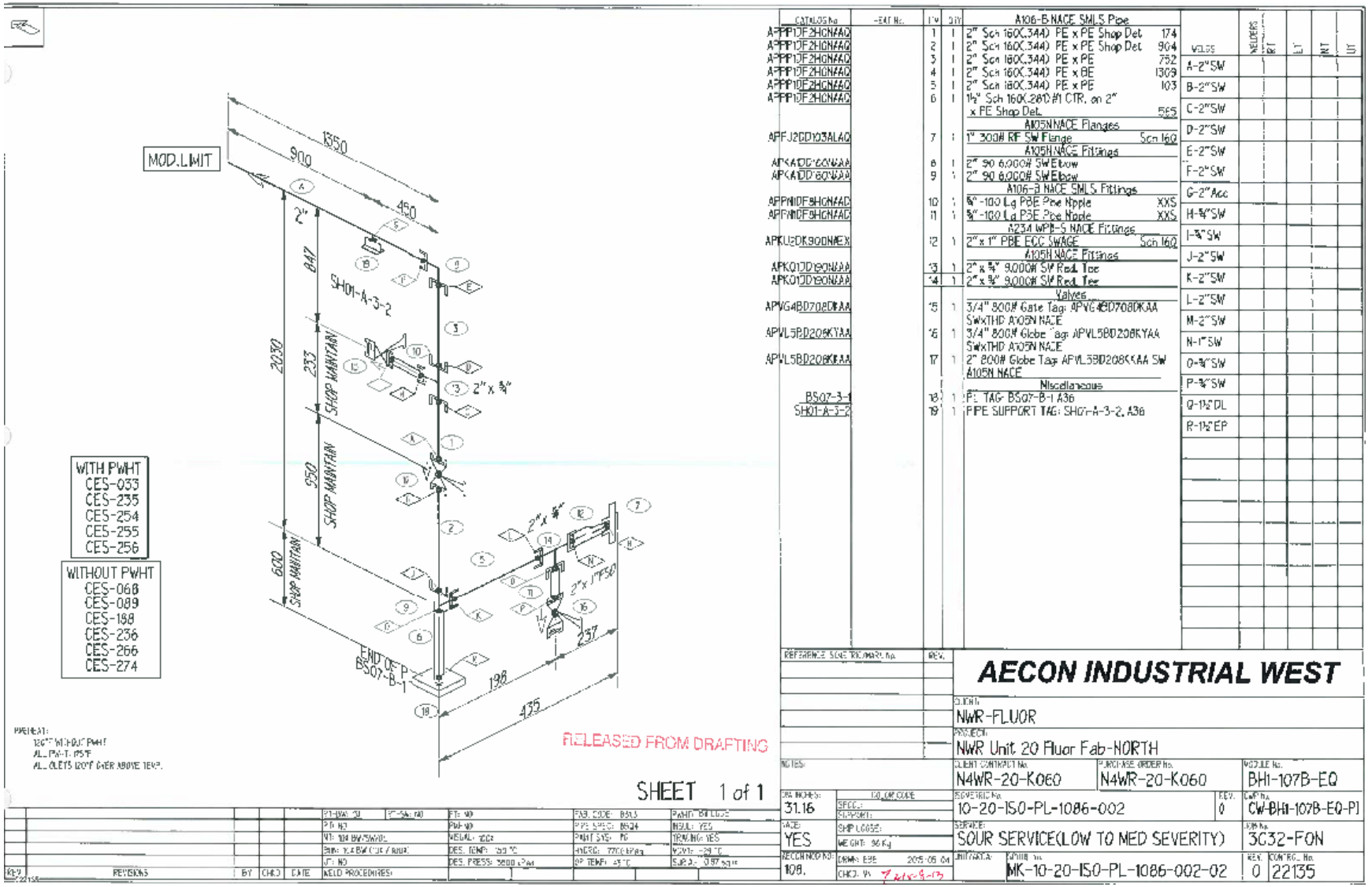
MOD.LWIT
1350
900
450
2"
SHOP MAINTAIN
SHOP MAINTAIN
SHOP MAINTAIN
2030
600
950
255
847
SH01-A-3-2
2" x ¾"
END OF P
BS07-B-1
198
435
237
WITH PWHT
CES-033
CES-235
CES-254
CES-255
CES-256
WITHOUT PWHT
CES-068
CES-089
CES-188
CES-236
CES-266
CES-274
RELEASED FROM DRAFTING
SHEET 1 of 1
AECON INDUSTRIAL WEST
NWR-FLUOR
NWR Unit 20 Fluor Fab-NORTH
N4WR-20-K060
N4WR-20-K060
BH1-107B-EQ
10-20-ISO-PL-1086-002
CW-BH1-107B-EQ-P1
SOUR SERVICE(LOW TO MED SEVERITY)
3C32-FON
MK-10-20-ISO-PL-1086-002-02
22135

Figure 2-4. (c)

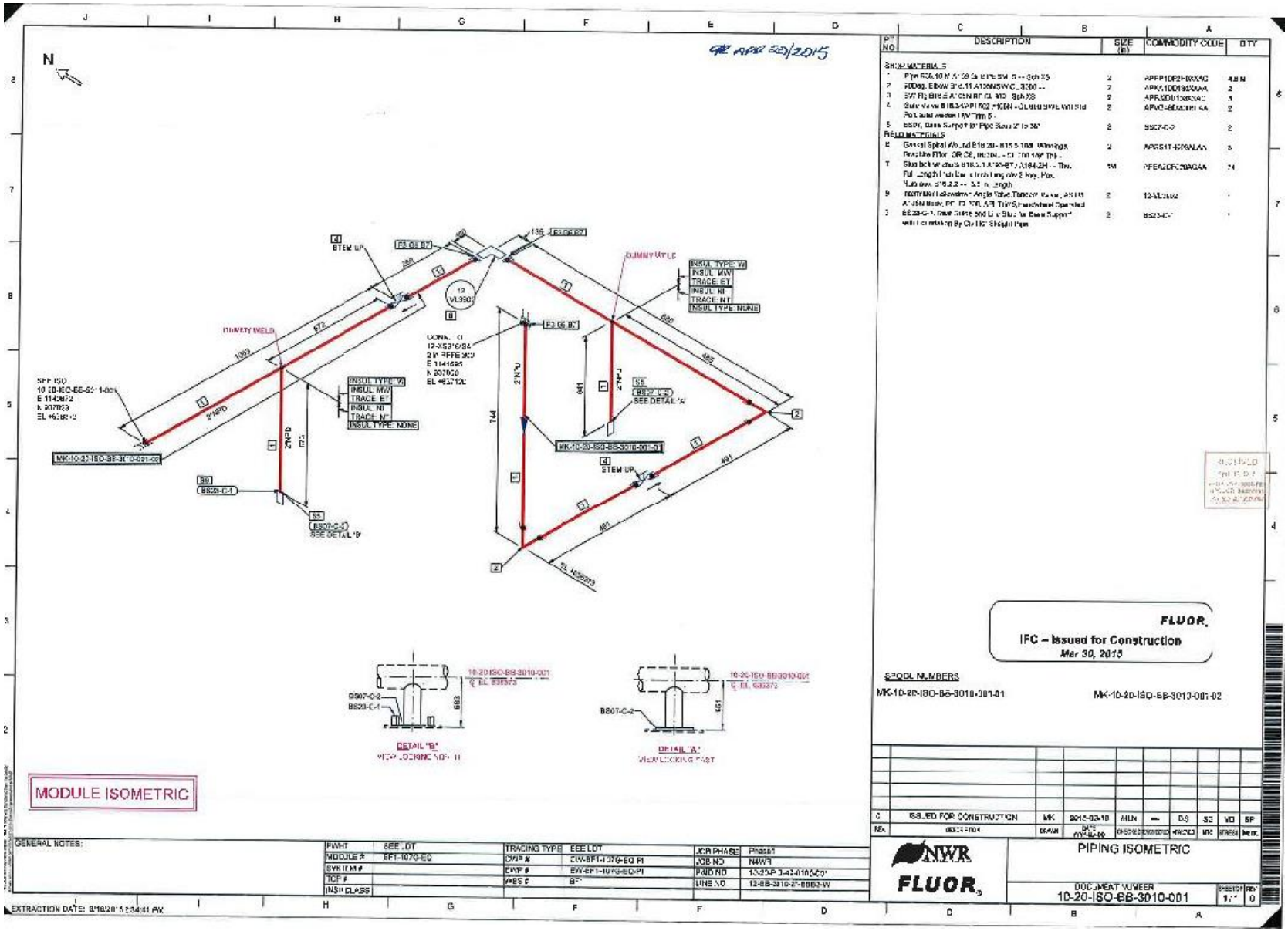
MODULE ISOMETRIC
PIPING ISOMETRIC
FLUOR
IFC – Issued for Construction
Mar 30, 2015
SPOOL NUMBERS
MK-10-20-ISO-BB-3010-001-01
MK-10-20-ISO-BB-3010-001-02
10-20-ISO-BB-3010-001
GENERAL NOTES:
EXTRACTION DATE: 3/18/2015 2:34:41 PM

Figure 2-5. (a)

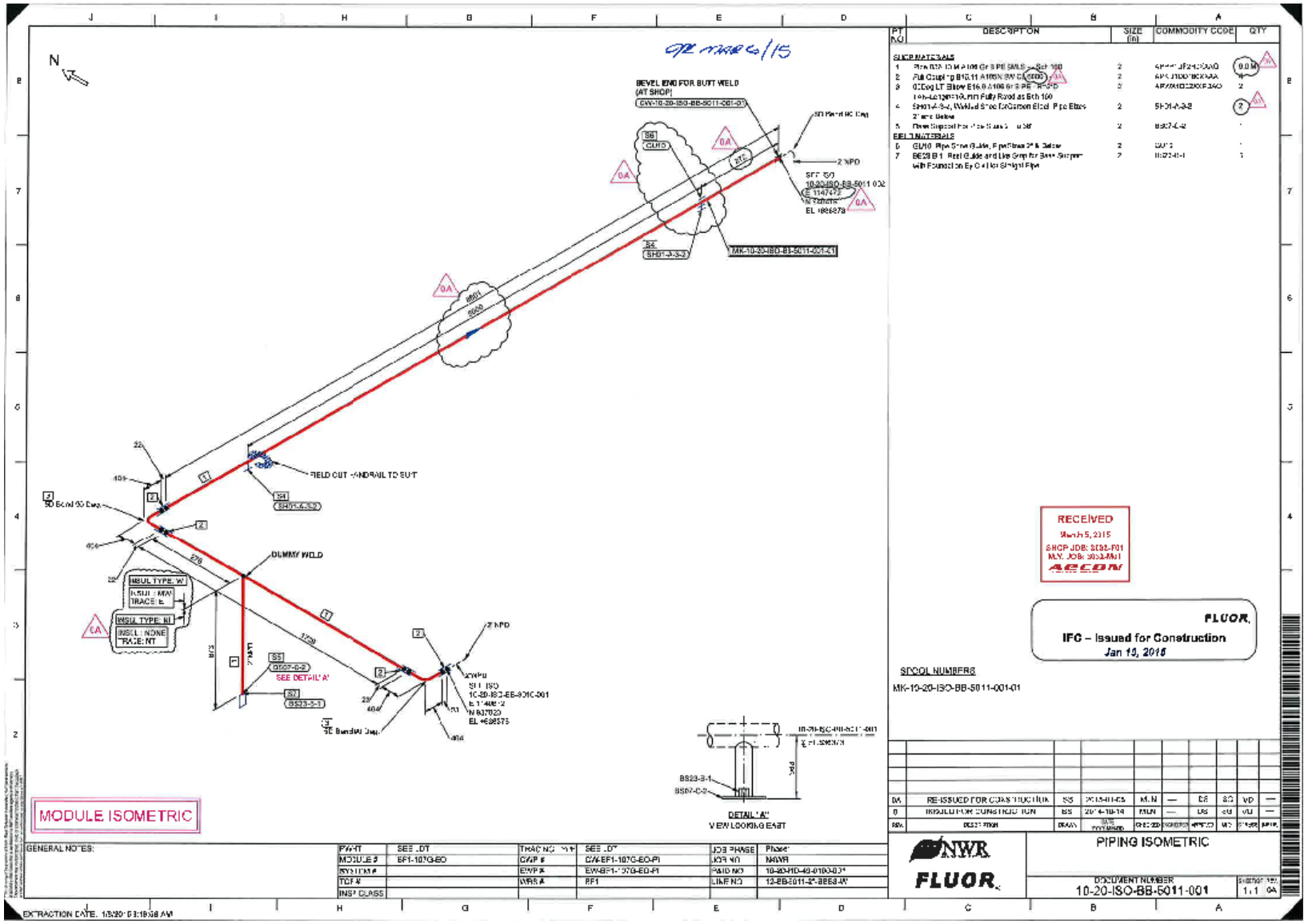
MODULE ISOMETRIC
PIPING ISOMETRIC
FLUOR
NWR
RECEIVED
IFC – Issued for Construction
Jan 15, 2015
10-20-ISO-BB-5011-001
DUMMY WELD
FIELD CUT +ANDRAIL TO SUIT
DETAIL 'A'
VIEW LOOKING EAST

Figure 2-5 (b)

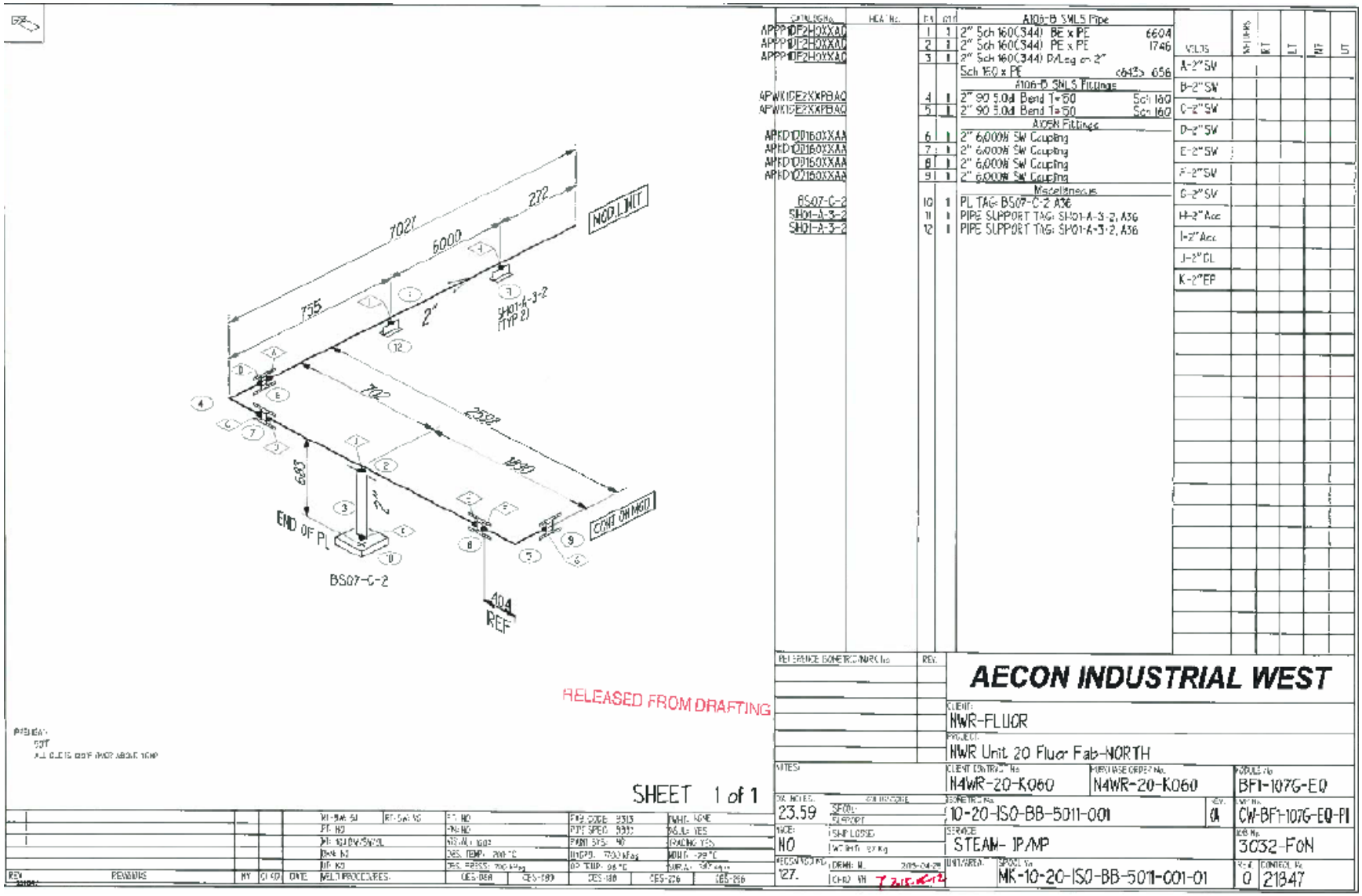
AECON INDUSTRIAL WEST
RELEASED FROM DRAFTING
SHEET 1 of 1
END OF PL
BS07-C-2
CONT ON M60
NOD LIMIT
A106-B SMLS Pipe
A105N Fittings
Miscellaneous
CLIENT: NWR-FLUOR
PROJECT: NWR Unit 20 Fluor Fab-NORTH
STEAM- IP/MP

Figure 2-5. (c)

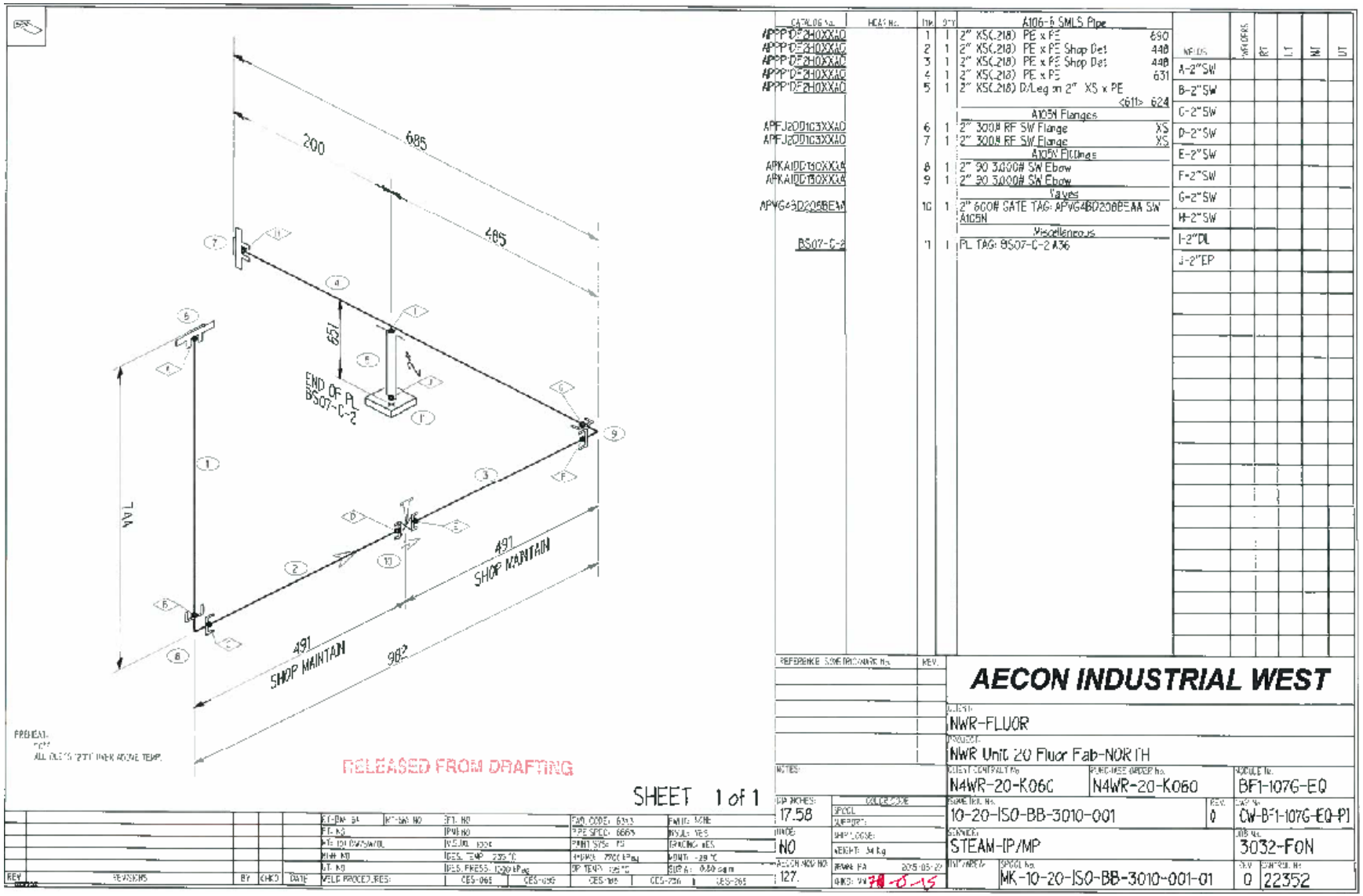
200
685
485
651
END OF PL BS07-C-2
744
491
SHOP MAINTAIN
491
SHOP MAINTAIN
982
RELEASED FROM DRAFTING
SHEET 1 of 1
A106-B SMLS Pipe
A105N Flanges
A105N Fittings
Valves
Miscellaneous
AECON INDUSTRIAL WEST
NWR-FLUOR
NWR Unit 20 Fluor Fab-NORTH
N4WR-20-K06C
N4WR-20-K060
BF1-107G-EQ
10-20-ISO-BB-3010-001
CW-BF1-107G-EQ-P1
STEAM-IP/MP
3032-FON
MK-10-20-ISO-BB-3010-001-01
22352

Figure 2-5 (d)

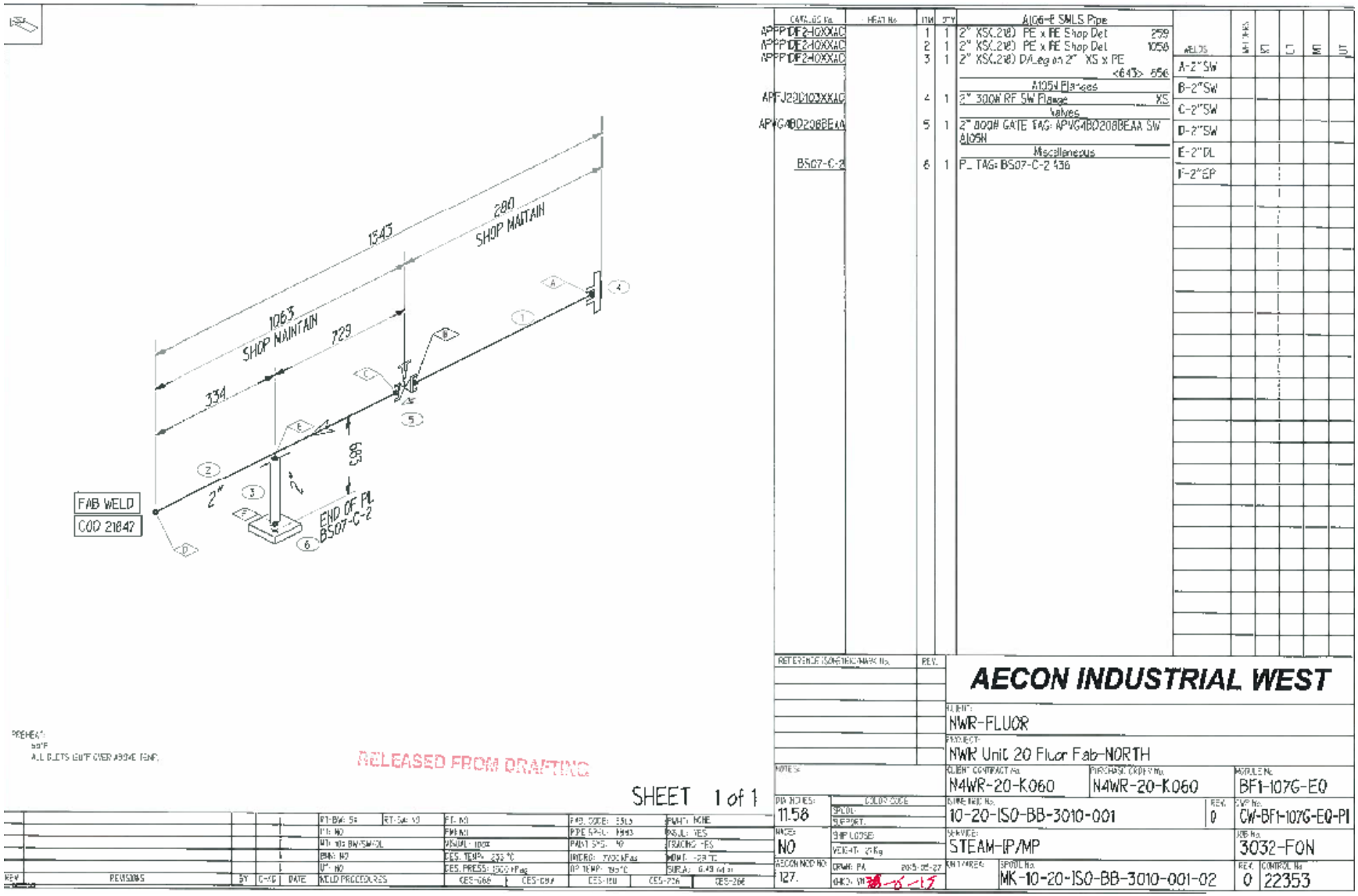
1543
280
SHOP MAINTAIN
1063
SHOP MAINTAIN
729
334
85
2"
FAB WELD
COD 21847
END OF PL
BS07-C-2
RELEASED FROM DRAFTING
SHEET 1 of 1
AECON INDUSTRIAL WEST
NWR-FLUOR
NWR Unit 20 Fluor Fab-NORTH
N4WR-20-K060
N4WR-20-K060
BF1-107G-EQ
10-20-ISO-BB-3010-001
CW-BF1-107G-EQ-PI
STEAM-IP/MP
3032-FON
MK-10-20-ISO-BB-3010-001-02
22353

Figure 2-5. (e)

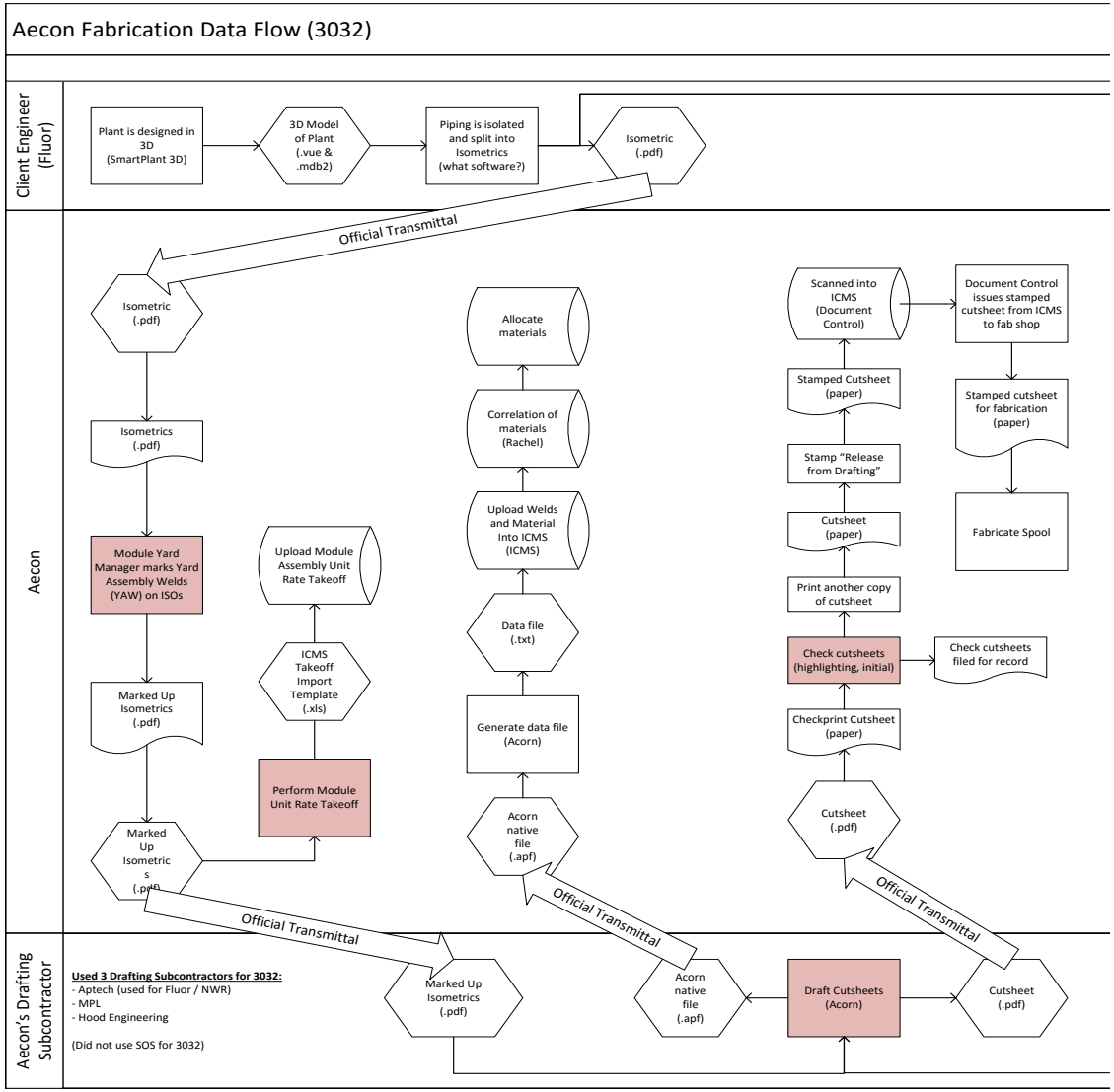
Aecon Fabrication Data Flow (3032)
Client Engineer (Fluor)
Plant is designed in 3D (SmartPlant 3D)
3D Model of Plant (.vue & .mdb2)
Piping is isolated and split into Isometrics (what software?)
Isometric (.pdf)
Official Transmittal
Aecon
Isometric (.pdf)
Isometrics (.pdf)
Module Yard Manager marks Yard Assembly Welds (YAW) on ISOs
Marked Up Isometrics (.pdf)
Marked Up Isometrics (.pdf)
Upload Module Assembly Unit Rate Takeoff
ICMS Takeoff Import Template (.xls)
Perform Module Unit Rate Takeoff
Allocate materials
Correlation of materials (Rachel)
Upload Welds and Material Into ICMS (ICMS)
Data file (.txt)
Generate data file (Acorn)
Acorn native file (.apf)
Scanned into ICMS (Document Control)
Document Control issues stamped cutsheet from ICMS to fab shop
Stamped Cutsheet (paper)
Stamped cutsheet for fabrication (paper)
Stamp "Release from Drafting"
Fabricate Spool
Cutsheet (paper)
Print another copy of cutsheet
Check cutsheets (highlighting, initial)
Check cutsheets filed for record
Checkprint Cutsheet (paper)
Cutsheet (.pdf)
Official Transmittal
Official Transmittal
Official Transmittal
Aecon's Drafting Subcontractor
Used 3 Drafting Subcontractors for 3032:
- Aptech (used for Fluor / NWR)
- MPL
- Hood Engineering
(Did not use SOS for 3032)
Marked Up Isometrics (.pdf)
Acorn native file (.apf)
Draft Cutsheets (Acorn)
Cutsheet (.pdf)

Figure 2-6.

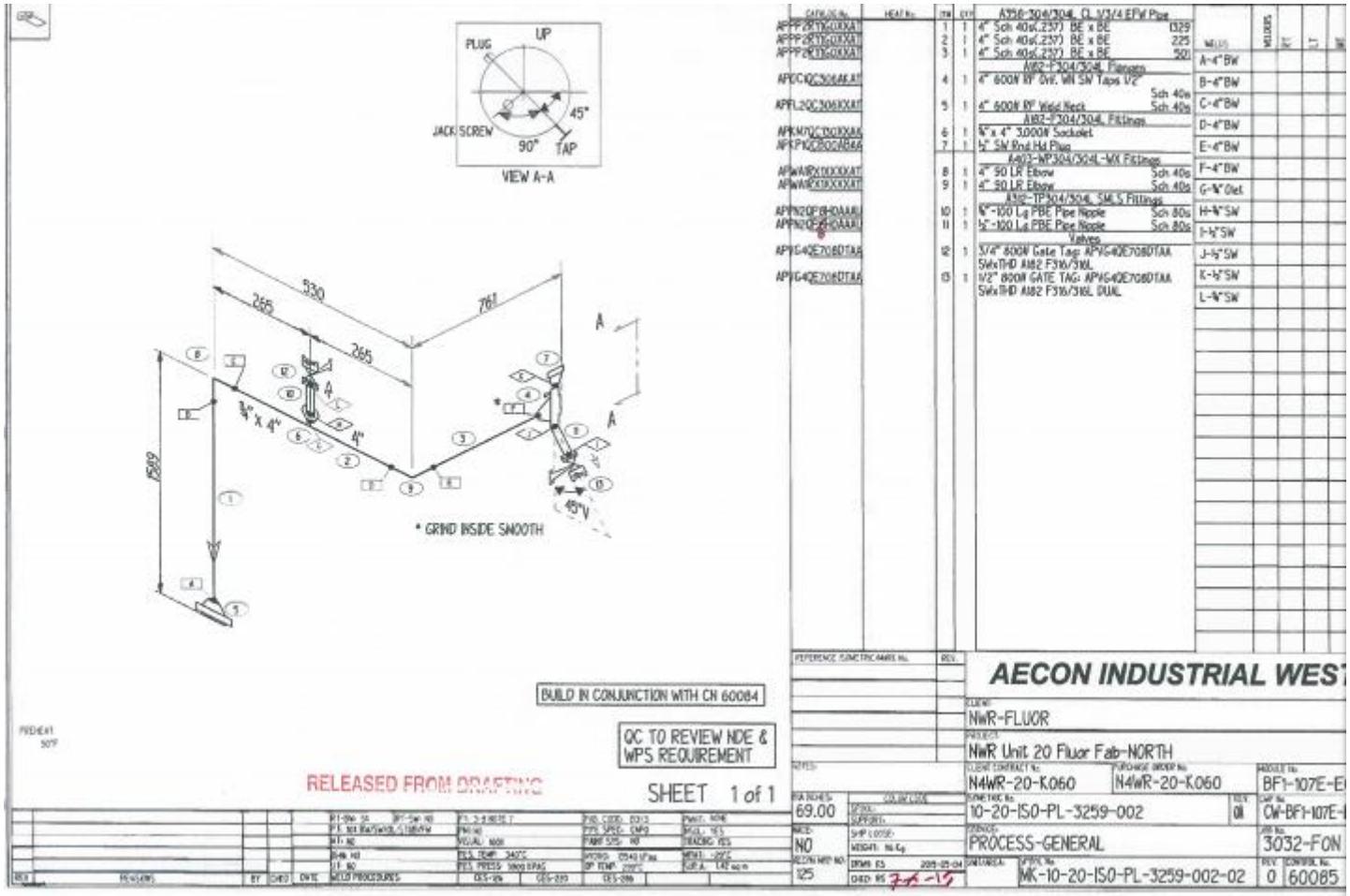
PLUG
UP
45°
JACK SCREW
90°
TAP
VIEW A-A
530
265
265
761
A
A
¾" x 4"
4"
1569
45°
* GRIND INSIDE SMOOTH
BUILD IN CONJUNCTION WITH CN 60084
QC TO REVIEW NDE & WPS REQUIREMENT
RELEASED FROM DRAFTING
SHEET 1 of 1
AECON INDUSTRIAL WEST
NWR-FLUOR
NwR Unit 20 Fluor Fab-NORTH
N4WR-20-K060
N4WR-20-K060
10-20-ISO-PL-3259-002
PROCESS-GENERAL
MK-10-20-ISO-PL-3259-002-02
69.00
NO
325
3032-FON
60085

Figure 2-19.

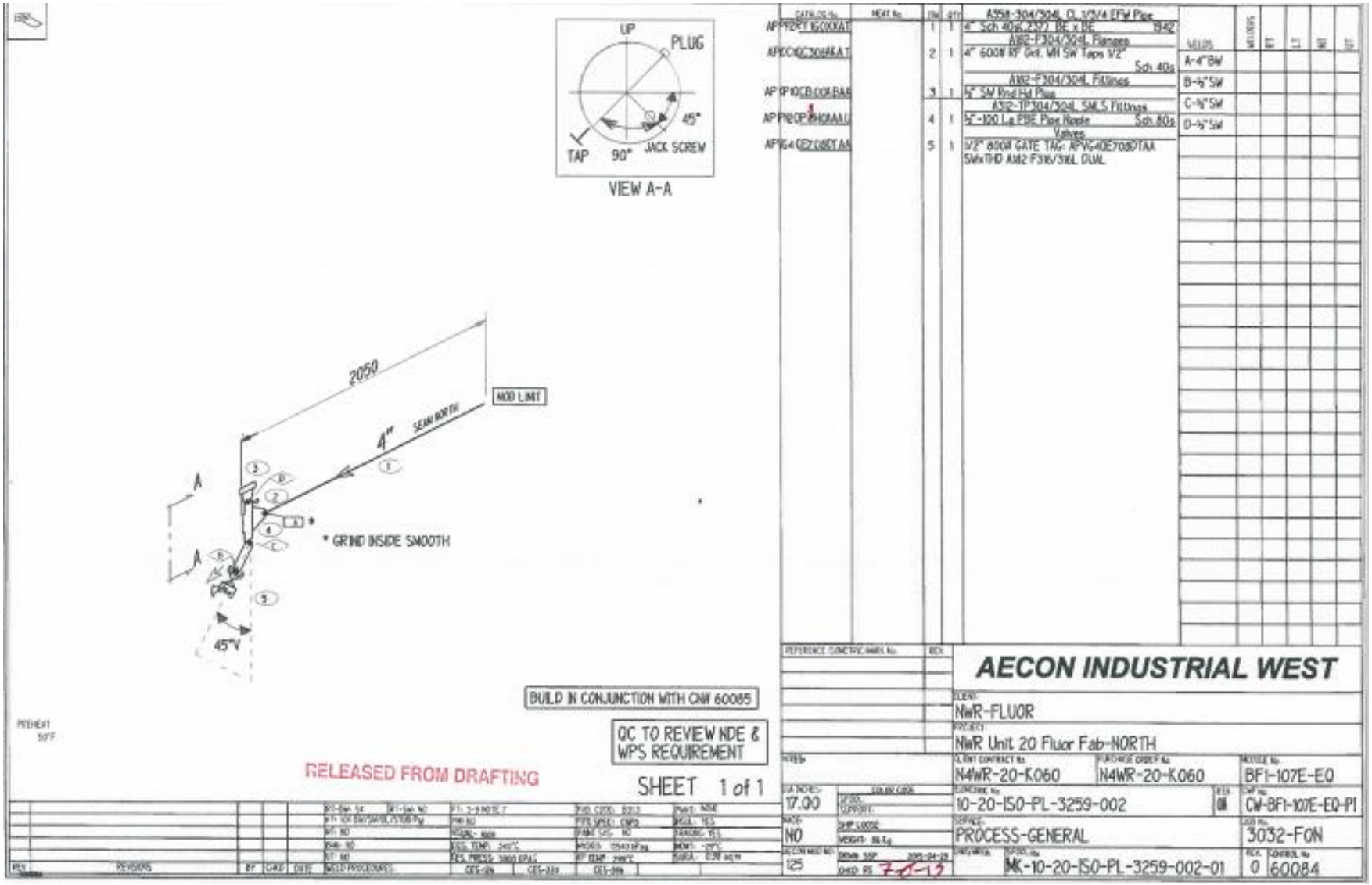
UP
PLUG
45°
TAP
90°
JACK SCREW
VIEW A-A
2050
4"
SEAM WELD
MOD LIMIT
A
A
* GRIND INSIDE SMOOTH
45°V
BUILD IN CONJUNCTION WITH CW# 60085
QC TO REVIEW NDE & WPS REQUIREMENT
RELEASED FROM DRAFTING
SHEET 1 of 1
AECON INDUSTRIAL WEST
NWR-FLUOR
NWR Unit 20 Fluor Fab-NORTH
N4WR-20-K060
N4WR-20-K060
BF1-107E-EQ
10-20-ISO-PL-3259-002
CW-BF1-107E-EQ-P1
PROCESS-GENERAL
3032-FON
MK-10-20-ISO-PL-3259-002-01
0
60084

Figure 2-20.

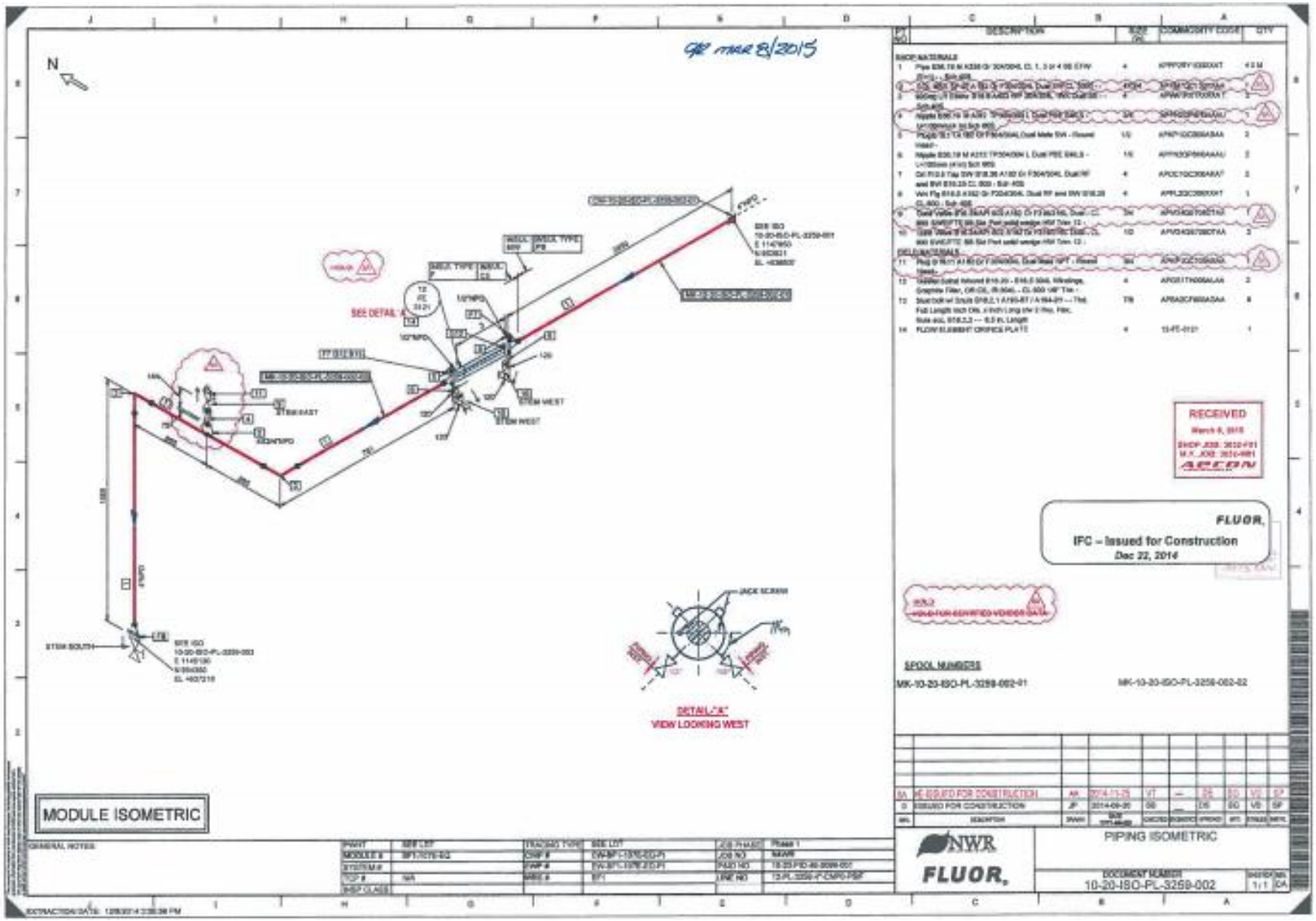
MODULE ISOMETRIC
PIPING ISOMETRIC
FLUOR
NWR
RECEIVED
IFC – Issued for Construction
Dec 22, 2014
SPOOL NUMBERS
MK-10-20-ISO-PL-3259-002-01
MK-10-20-ISO-PL-3259-002-02
DETAIL "A"
VIEW LOOKING WEST
10-20-ISO-PL-3259-002

Figure 2-21.